Institute of Thermoelectricity, Academy of Sciences and Ministry of Education and Science of Ukraine

Journal of THERMOELECTRICITY

International Research

Founded in December, 1993

published 4 times a year

No. 2 *2023*

Editorial Board

International Editorial Board

Founders – National Academy of Sciences, Ukraine
Institute of Thermoelectricity of National Academy of Sciences and Ministry of Education and Science of Ukraine

Certificate of state registration № КВ 15496-4068 ПР

Address of editorial office:
Ukraine, 58002, Chernivtsi, General Post Office, P.O. Box 86.
Phone: +(380-372) 90 31 65.
Fax: +(380-3722) 4 19 17.
E-mail: jt@inst.cv.ua
http://www.jt.inst.cv.ua

Signed for publication 23.06.2023. Format 70×108/16. Offset paper №1. Offset printing.
Printer's sheet 11.5. Publisher's signature 9.2. Circulation 400 copies. Order 4.

Printed from the layout original made by "Journal of Thermoelectricity" editorial board
in the printing house of "Bukrek" publishers,
10, Radischev Str., Chernivtsi, 58000, Ukraine

CONTENTS

L. I. Anatychuk *acad. of the NAS of Ukraine* [1,2]
R. R. Kobylianskyi *cand. phys.-math. sciences*[1,2]
R. V. Fedoriv [1,2]
I. A. Konstantinovych, *Ph.D (Phys and Math)*[1,2]

[1]Institute of Thermoelectricity of the NAS and MES of Ukraine,
1 Nauky str., Chernivtsi, 58029, Ukraine;
e-mail: anatych@gmail.com
[2]Yuriy Fedkovych Chernivtsi National University,
2 Kotsiubynsky str., Chernivtsi, 58012, Ukraine

ON THE PROSPECTS OF USING THERMOELECTRIC COOLING FOR THE TREATMENT OF CARDIAC ARRHYTHMIA

The paper presents the results of an analysis of various methods of treating cardiac arrhythmia. Among them, special attention is drawn to the ablation method, which boils down to the elimination of additional electrical stimuli of cardiac muscle contraction. The latter is achieved by surgical methods, high-frequency irradiation and cryodestruction with liquid nitrogen or the use of the Joule-Thomson effect. Cryotechniques have certain advantages over others, but their implementation is somewhat more complicated, which limits their clinical use. In recent decades, cooling by the Peltier effect has been increasingly used in medicine. It has proven itself to be simple, reliable and accurate in reproducing the required temperature conditions for treatment. This work is devoted to studying the possibility of using the Peltier effect for cryoablation. Bibl. 39, Fig. 2.

Key words: cardiac arrhythmia, atrial fibrillation, cryoablation, thermoelectric cooling.

Introduction

Arrhythmia is a fairly common cardiovascular disease, which is caused by various heart defects, toxic effects of harmful substances, nervous system disorders or thyroid gland diseases, etc. However, the most common cause is the ability of certain heart cells to generate electrical signals in an untimely manner. In doing so, the cardiac muscle tissue of the atria with altered electrical properties supports and conducts these pathological signals, which can lead to arrhythmia [1].

Many methods of combating heart arrhythmia are known. Among them, the treatment of open heart arrhythmia is important.

The first surgical procedures were based on the principle of reducing the mass of the pathological myocardium, this is the so-called left atrial isolation (LA) operation [2 – 3]. In 1981, one of the first successful operations of this type was performed in the treatment of left atrial flutter.

Guiraudon G.M. with co-authors in 1985 proposed the "corridor" procedure. This technique actually involved the creation of a corridor that should connect the sinus and atrioventricular nodes with the area of the atrial septum, which created surgical isolation of the left and right atria [4]. However, in the postoperative period, the transport function of the LA was disturbed, the tachyarrhythmia persisted, and there was a high need for electrocardiostimulation.

Due to the low efficiency, the "LA isolation" and "corridor" operations gave way to the more effective "labyrinth" procedure, which was proposed by Cox J. in 1987. The "labyrinth" operation became a classic in the surgical treatment of arrhythmia, and was subsequently improved and received a number of modifications : "labyrinth I - II - III" [5 – 8]. The operation includes the following actions:

- isolation of pulmonary veins as a single block;
- removal of the appendages of both atria;
- incision connection of the left atrial appendage suture with the collector of the pulmonary veins;
- incision connection of the right atrial appendage suture with the fibrous ring of the triscupid valve;
- connection of the collector of pulmonary veins with the posterior semicircle of the fibrous ring of the mitral valve;
- T-shaped section of the right atrium (vertical atriotomy from the atrioventricular groove + longitudinal section between the superior vena cava and the inferior vena cava);
- incision of the interatrial septum from the atriotomy to the coronary sinus; the atriotomy incisions are connected to each other.

It should be noted that Cox J. and co-authors identified five main conditions that are mandatory for complete elimination of arrhythmia and restoration of sinus rhythm (SR): 1) elimination of atrial fibrillation (AF); 2) restoration of SR; 3) restoration of atrioventricular synchronization and 4) atrial transport function; 5) reducing the risk of thromboembolism. Only the "labyrinth III" operation meets all these requirements and has become the standard of surgical treatment of arrhythmia [9 – 12].

However, despite its high efficiency, the "labyrinth" procedure is very rarely used by surgeons in open-heart surgery due to technical difficulties, significant duration and high risk of bleeding.

The introduction of new technologies into medicine made it possible to significantly facilitate such an operation. It was proposed to replace the traditional scalpel with linear ablation using different energy sources: radiofrequency ablation, cryoablation, etc. [13 – 17].

During radiofrequency ablation, heat is generated using an alternating electric current of medium frequency (in the range of 300 kHz - 1 MHz). Unmodulated monopolar or bipolar current is used for ablation of heart structures, since it is this that leads to coagulation necrosis, which is achieved in more than 90% of cases. To destroy biological tissue, it must be heated to temperatures above 50 °C, since at such temperatures irreversible cell death occurs. At temperatures above 100 C, evaporation of cell fluid occurs and damage to the cell membrane of myocytes, sarcoplasmic reticulum and mitochondria. If the temperature exceeds 140 C, carbonization of the tissue may occur. To ensure softer tissue coagulation, its temperature should be maintained in the range of $50 \div 100$ °C. The duration of radiofrequency ablation ranges from 10 to 20 minutes, which is several times less than the time of aortic cross-clamping during the original operation [5, 13, 18, 19]. The original operation "Maze III" lasts about 1 hour [11, 20].

Cryoablation is performed with the help of a hermetically isolated refrigerant (usually liquid nitrogen), which is delivered to the pathological area of the heart that is responsible for the irregular rhythm, with the aim of neutralizing it [21]. Cryoablation together with radiofrequency ablation gives approximately the same reduction in the time of surgery, clamping of the aorta, and artificial blood circulation compared to the classical option of "Labyrinth III" surgery [22]. The advantage over radiofrequency ablation is that due to transmural freezing of the atrium wall, the efficiency of the cryoablation procedure is higher. This is explained by the fact that freezing does not damage the collagen matrix; body tissues tolerate ultra-low temperatures (-120 -150 oC) better than a burn [25]. Therefore, cryoablation is devoid of the disadvantages of all methods of destruction based on the

influence of high temperature and leading to charring of tissues with subsequent thrombus formation or serious collateral damage to the heart and surrounding organs [23]. Another positive factor of cryodestruction is the often delayed restoration of sinus rhythm within a year after the intervention [24, 25, 26].

The main disadvantage of operations using cryodestruction is the high price of the equipment used to perform such operations. The use of such devices does not make it possible to ensure cooling with the necessary accuracy of temperature maintenance, it is necessary to use hoses and special conditions for the storage and transportation of refrigerants. They are dangerous and toxic substances, so work with them is carried out in a separate special room, away from explosive and flammable objects. If such substances get on the skin, there is a danger of getting all four degrees of frostbite and other complications [27].

However, among the sources of cold there is thermoelectric cooling, which has many advantages: a simple design, high reliability, precise control of temperature regimes, and the absence of dangerous refrigerants [27, 28]. Therefore, *the purpose of this paper* is to study the possibility of using thermoelectric cooling for the treatment of open-heart arrhythmia.

About temperature conditions and known methods of open heart cryodestruction

Cryomodification of the Labyrinth III operation has become widely used in modern medical practice for the treatment of arrhythmia. A number of companies that manufacture special equipment for such operations are known, and the results of clinical applications of this procedure have also been published.

One of the first devices for cryoablation was the cryoprobe from Medtronic (USA). This surgical ablation system consists of a control console that regulates time and temperature conditions, and disposable sterile probes containing a built-in thermocouple to monitor the temperature at the ablation site. The probes are made of specially heat-treated stainless steel and are designed to be flexible enough to be molded while maintaining sufficient rigidity to ensure stability during surgery. The dimensions of the working part of the probe are 60 mm. This device uses an argon-based cryogen for fast, controlled freezing. It is able to freeze biological tissue in the temperature range of -120 ÷ -160 oC and block electrical pathways, creating an inflammatory reaction and cryonecrosis. Ablation is carried out 1 minute after the probe has cooled to – 40 °C. The average time for a complete operation is about 17 minutes. With the help of such a device, 10 operations of the “Labyrinth III” type were performed using cryodestruction [24, 26, 27]. According to the results of this series of operations, there were no deaths or serious complications in patients. Sinus rhythm was restored on the operating table in all. As a result, when these patients were discharged, sinus rhythm was observed in 6 patients, others were on maintenance therapy due to repeated paroxysms of fibrillation. It should be noted that in 2 of them, the correct rhythm was restored after 3 and 6 months of treatment.

Another device actively used in medicine is the Atricure CryoFlex cryoprobe, developed by AtriCure (USA) and intended for cryosurgical treatment of cardiac arrhythmias by freezing tissues to block the passage of pathological electrical impulses. The device is a disposable sterile probe, the working part of which is corrugated and flexible, 10 cm long. N2O is used as a refrigerant. The device works together with the cryoICE BOX V6 control unit, with which you can adjust the temperature and ablation time. The work [32] provides data on the regular use of such a device for ablation of the left atrium during minimally invasive mitral valve procedures. A standard mini-maze procedure is performed, including bilateral pulmonary vein isolation, superior and inferior connecting lesions, mitral annulus lesions, and left atrial appendage lesions. The temperature of the cryoprobe during cryoablation is -140 oC, and the time to create each lesion is ¬ 2 minutes.

Reusable devices are also known. One of these is the "Cryo-01" device of the Russian company Elamed LPU. The principle of operation of the device is as follows. With excessive vapor pressure of the cryoagent (liquid nitrogen) in the Dewar vessel, which, together with the hermetically connected cryogenic block, form the cryostat, a regulated pulsed flow of the cryoagent from the cryostat through the pipeline to the cryoinstrument is formed. All cryotools are built according to the same principle and include a cylindrical working part with a threaded surface for attaching interchangeable nozzles and a docking unit with a connector and a ball seal of the liquid and gas channel of the cryoagent. The working part of cryoinstruments is made of thin-walled tubes and has vacuum thermal insulation, which protects the doctor's hands and the surface of the patient's body adjacent to the area of cryo action from hypothermia during the operation. The work [4] presents the result of using such a device for cryodestruction "Cryo-01". The patient was operated on in 6 stages: 1) local cryoaction between the inferior vena cava and the fibrous ring of tricuspid valve in the right atrium; 2) local cryoaction between the stump of the right atrium appendage and the fibrous ring of the tricuspid valve; 3) linear cryoimpact on the base of the left atrial stump; 4) linear cryoisolation of the mouths of the pulmonary veins; 5) local cryoaction between the line of ablation of the mouths of the pulmonary veins and the stump of the left atrium appendage; 6) local cryoimpact between the stump of the right atrium appendage and the Giradon incision. In this case, the time of artificial circulation was 210 minutes, and the time of aortic compression was 127 minutes. As a result, throughout the entire postoperative period the patient maintained a normal heart rhythm and after 10 days she was discharged in satisfactory condition.

Mechanism of cryodestruction

In modern medical practice, devices based on carbon dioxide, argon, or nitrogen are used for cryoablation to achieve ultralow temperatures in the range (–60 ÷ –200) °C. However, studies [29, 33 – 45] have confirmed that the use of such low temperatures is not necessary to achieve the necessary destruction of biological tissue. For the destruction of biological tissue, more moderate temperatures (-20 ÷ -50) °C can be used [30, 31].

A decrease in the temperature of biological tissue to (–5 ÷ –10) °C leads to the beginning of the process of crystal formation in the extracellular space, and with a decrease in temperature to (-15 ÷ -20) °C and below, the formation of ice crystals inside cells begins, which leads to death of biological tissue [30]. Cryonecrosis (destruction of biological tissue) occurs gradually, while cells and intracellular membranes are damaged by ice crystals. Blood circulation, supply of oxygen, nutrients, tissue respiration and all biochemical processes are completely stopped during freezing. As a result, the death of cells occurs in which all vital processes have been paralyzed for a long time. At the moment of ice crystal formation, a sharp increase in osmotic pressure in the cells occurs, since the extracellular fluid freezes faster and salt cations rush through the membranes into the cells. Biological cells cannot survive such an osmotic shock. The maximum damaging effect is achieved when biological tissue is cooled to -50 °C, and a further decrease in temperature does not increase the lethality of cells [30].

In addition, the intensity of cell destruction in the area of freezing depends not only on the minimum temperature, but also on the rate of cooling of biological tissue. Relatively fast freezing is optimal - (40–50) °C/min. The efficiency of cell cryodestruction is high, if it does not have time to displace the intracellular fluid through the membranes in the process of cooling the tissue before freezing [30]. Slower freezing (3–5) °C/min is impractical, since intracellular ice formation processes do not occur. It is also not rational to use ultra-fast freezing (more than 100 °C/min), since this forms amorphous ice that does not damage the structure of biological tissue [30].

It should be noted that the destruction of biological tissue occurs not only during cooling, but also during heating of the cooled tissue, and its effectiveness increases significantly during cyclic cooling-heating of biological tissue [27, 31].

Thus, the above research results indicate the following:

1. For cryodestruction, it is sufficient to reduce tissue temperatures to -20 ÷ -50 °C.
2. The optimal tissue cooling rate is 40–50 °C/min.

3. To increase the effectiveness of tissue cryodestruction, it is rational to use cyclic cooling and heating.

These conditions can be achieved through the use of thermoelectric cooling and heating method. Moreover, based on the capabilities of this method, its use may have advantages over others in terms of ease of use, accuracy of reproducing the required temperature conditions, cost of equipment, etc.

The principle of cryodestruction for arrhythmia and the method of its implementation

In order to achieve complete destruction of the pathological heart tissue, it is necessary that the lesion of the complete block of the conduction of pathological impulses be transmural, otherwise the electrical activity can cross the lesion line. For example, if a linear lesion is located on the endocardial side of the atrium and is not transmural, electrical activity may cross the lesion line on its epicardial side. Conversely, if a linear lesion is located on the epicardial side of the atrium and is not transmural, electrical activity may cross the lesion line on its endocardial side [32, 33].

The size of the lesion by cryoablation is proportional to the temperature of the probe, the area of he contact surface of the probe, the duration of energy supply and the number of freeze-thaw cycles [34 – 36].

Myocardial thickness varies considerably between different regions of the heart and between individuals (distal: range 1.4 – 7.7 mm, middle: range 1.2 – 4.4 mm, proximal: range 0 – 3.2 mm) [37]. However, from a clinical point of view, deep lesions are necessary only in a minority of cases. Currently, the majority of cryoablations are performed in atria with a typical muscle thickness of less than 3 mm [37].

For the treatment of open-heart arrhythmia using cryodestruction, a modification of the "Cox-Maze III" operation (Fig. 1) or a modification of the "Kosakai-Maze" operation (Fig. 2) is usually used [30, 38, 39].

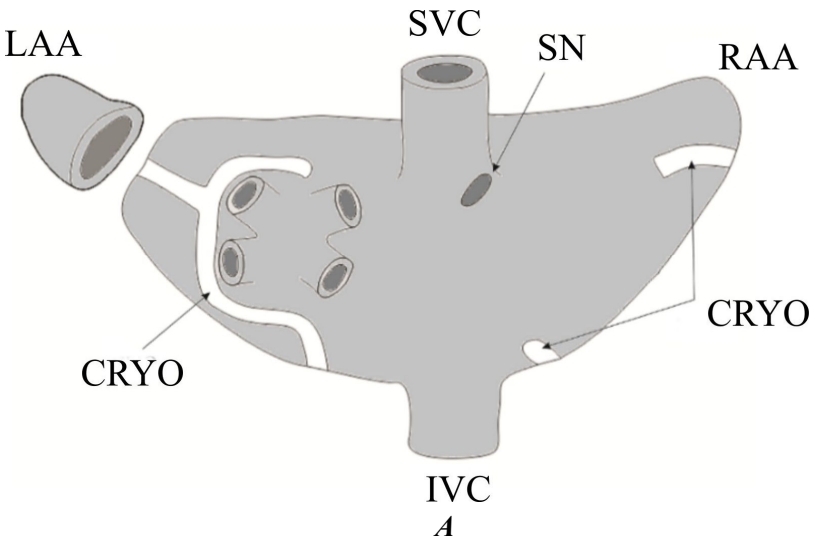

A

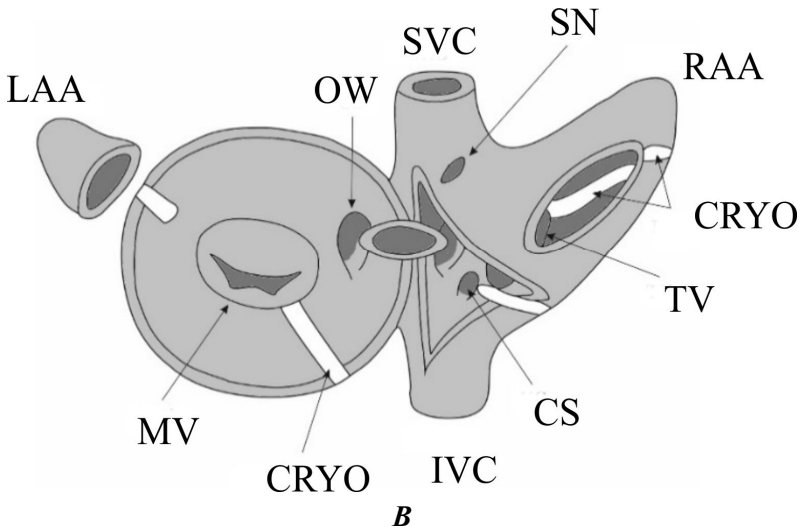

Fig. 1 Scheme of the "Cox-Maze III" operation (A - epicardial view, B - endocardial view).
LAA - left atrial appendage, SVC - superior vena cava, SN - sinus node,
RAA - right atrial appendage, IVC - inferior vena cava, OW - oval window,
TV - tricuspid valve, CS - coronary sinus, MV - mitral valve, CRYO - areas subject to cryodestruction

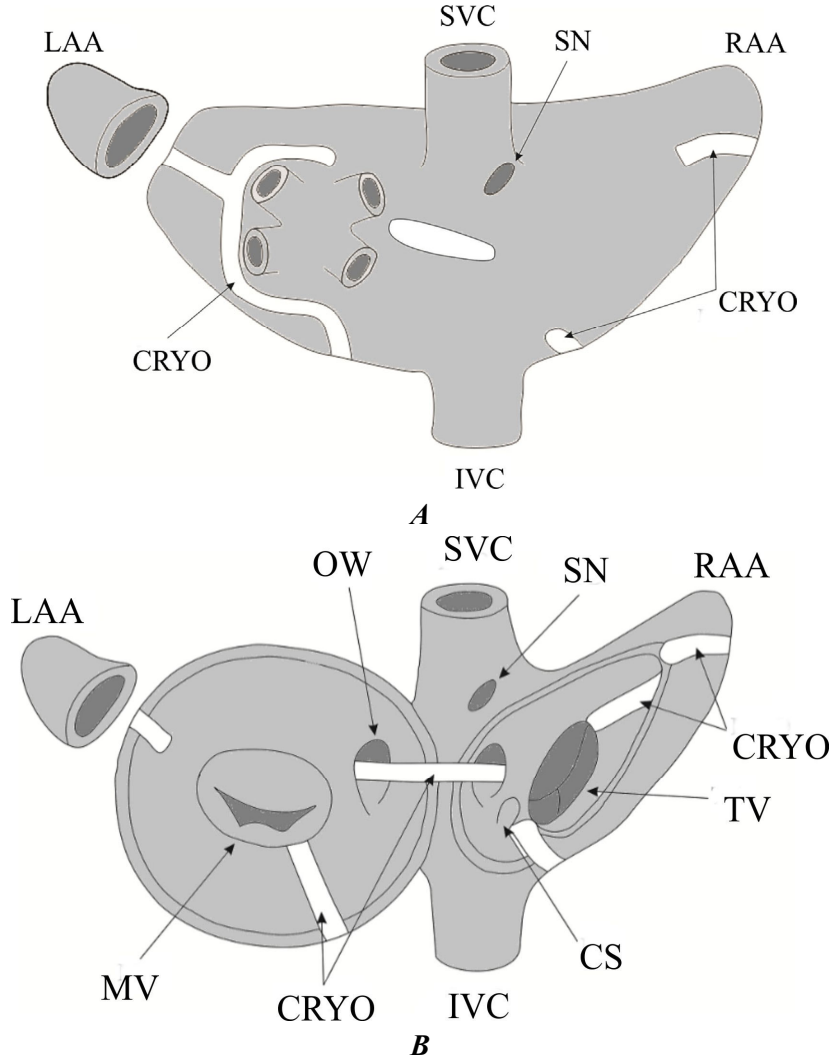

Fig.2. Scheme of the "Kosakai-Maze" operation (A – epicardial view, B – endocardial view).
LAA - left atrial appendage, SVC - superior vena cava, SN - sinus node, RAA - right atrium appendage,
IVC - inferior vena cava, OW - oval window, TV - tricuspid valve, CS - coronary sinus,
MV - mitral valve- sections subject to cryodestruction

Such procedures are carried out with special flexible probes, 4 to 10 cm long and 4 - 5 mm in diameter. They are able to provide cooling to (-60 ÷ -160)°C by using liquid nitrogen or argon. The duration of one cryo-lesion is 1 - 2 minutes [71 – 75].

Method of implementation of the "Cox-Maze III" operation

First, a cryo-lesion is performed on the inferior aspect of the pulmonary vestibule along the atrial ridge that separates the pulmonary vestibule from the mitral valve. The next cryo-lesion is created around the lateral aspect of the left pulmonary vein, between the left atrial appendage opening and the left superior pulmonary vein so as to cross the first lesion to form a connection between them. Next, the lesion is made on the upper aspect of the pulmonary vein, which connects to the left atriotomy incision, which is the only non-cryo lesion. After that, an endocardial lesion is created, which joins the previous lesions around the pulmonary veins to the mitral valve annulus. Next, an epicardial lesion is made, passing through the coronary sinus and the oblique sinus. And at the end, two lesions of the endocardium are created, 1 - to the tricuspid ring at the 2 o'clock position, and the other - between the right atrial appendage and the tricuspid ring at the 10 o'clock position [38].

Method of implementation of the "Kosakai-Maze" operation

At the first stage, cryoablation of the left atrial appendage is performed. Next, a cryo lesion is created on the back wall of the left atrium between the edge of the left atrial incision and the mitral annulus. The next lesion is made on the left side of the interatrial septum between the edge of the left atrium incision and the dorsum of the oval window, directed from the right atrium using forceps. Next, they move to the right atrium and perform cryoablation on the right side of the interatrial septum between the right atrium and the oval window. Cryoablation is then performed between the end of the right atriotomy and the tricuspid annulus. Finally, cryoablation is performed between the posterior edge of the right atrium incision and the junction with the fan [39].

Prospects for implementing temperature conditions of cryodestruction using thermoelectricity

From the above information, it can be concluded that the necessary conditions for the destruction of biological tissue can be achieved by using the thermoelectric method of cooling and heating. At the same time, based on the capabilities of this method, its use may have advantages over others in terms of ease of operation, accuracy of reproduction of the required temperature regimes, cost of equipment, etc.

In addition, the ability to reproduce multiple freezing-thawing makes it possible to reduce the temperature lethal for pathological tissue, to find a kind of compromise between the desire to freeze the pathogenic tissue as much as possible and the need to preserve healthy surrounding biological tissue [30].

It should be noted that in recent years research has been conducted on the use of thermoelectric cooling in medicine [27]. Many thermoelectric devices for cryodestruction have been created in the world, designed for the treatment of various diseases in various fields of medicine. Such devices are increasingly becoming widely used due to their advantages: simple design, high reliability, precise control of temperature regimes, and the absence of dangerous refrigerants [27, 28].

Conclusions

1. A review of the literature on open heart arrhythmia treatment methods has been made. It has been established that the promising method is the use of cryoablation.

2. The mechanism of cryodestruction was determined from the analysis of the literature and data was obtained that the use of excessive cooling is not necessary. It has been established that for cryodestruction, it is sufficient to reduce tissue temperatures to -20 ÷ -50 °C, and the optimal cooling rate of tissues should be 40–50 °C/min. To increase the efficiency of tissue cryodestruction, it is rational to use cyclic cooling and heating to (+39 ÷ +45) ºC, which indicates the prospects of using thermoelectric cooling in medical practice, since such conditions can be achieved by using the thermoelectric method of cooling and heating.
3. The most effective methods of treating arrhythmia using cryodestruction were studied and it was found that the depth of the lesion should be around 3 mm (the wall thickness is different in different parts of the heart). To create transmural damage to heart tissue, it is necessary to use the temperature of the working instrument T = -60 ºC, exposure time t = 2 minutes.
4. It was established that the use of the thermoelectric method of cooling is promising, as it provides the necessary conditions for the destruction of biological tissue, and its use may have advantages over other methods in terms of ease of operation, accuracy of reproduction of the required temperature regimes, cost of equipment, etc.

References

1. *What Is Arrhythmia?* National Heart, Lung, and Blood Institute. July 1, 2011. Archived from the original on March 2, 2015. Retrieved March 7, 2015.
2. Vigano M., Graffinga A., Reissa L. et al. (1996). Surgery for atrial fibrillation. *Eur J Cardiothore Surg*. 10, 490 – 497.
3. Williams J. M., Ungerleider R. M., Lofland G.K., Cox J. L. (1980). Left atrial isolation: new technique for the treatment of supraventricular arrhythmias. *J. Thorac Cardiovasc Surg*., 80(3), 373 – 380.
4. Guiraudon G. M., Campbell C. S., Jones D. L. et al. (1985). Combined sinoatrial node atrioventricular isolation: A surgical alternative to His bundle ablation in patients with atrial fibrillation. *Circulation*, 72, 111 – 220.
5. Cox J. L., Boineau J. P., Schuessler R. B., et al. (1993). Five-year experience with the Maze procedure for atrial fibrillation. *Ann Thorac Surg*., 56(4), 814 – 823. 79.
6. Cox J. L., Canavan T. E., Schuessler R. B., et al. (1991). The surgical treatment of atrial fibrillation. II. Intraoperative electrophysiologic mapping and description of the electrophysiologic basis of atrial flutter and atrial fibrillation. *J Thorac Cardiovasc Surg*., 101(3), 406 – 426.
7. Cox J. L., Schuessler R. B., D'Agostino H. J., Jr., et al. (1991). The surgical treatment of atrial fibrillation. III. Development of a definitive surgical procedure. *J Thorac Cardiovasc Surg*., 101(4), 569 – 583.
8. Ferguson T. V., Sox J. L. (1995). Surgery for atrial fibrillation. *Cardiac eleclrophysiology*, 2, 1563 – 1576.
9. McCarthy P. M., Gillinov A. M., Castle L., Chung M., Cosgrove D., 3rd. (2000). The Cox-Maze procedure: the Cleveland Clinic experience. *Semin Thorac Cardiovasc Surg*.,12 (1), 25 – 29.
10. Prasad S. M., Maniar H. S., Camillo C. J., et al. (2003). The Cox maze III procedure for atrial fibrillation: long-term efficacy in patients undergoing single versus concomitant procedures. *J. Thorac Cardiovasc Surg*., 126 (6), 1822 – 1828.
11. Raanani E., Albage A., David T. E., Yau T. M., Armstrong S. (2001). The efficacy of the Cox/maze procedure combined with mitral valve surgery: a matched control study. *Eur J. Cardiothorac Surg*., 19(4), 438 – 442.

12. Schaff H. V., Dearani J. A., Daly R. C., Orszulak T. A., Danielson G. K. (2000). CoxMaze procedure for atrial fibrillation: Mayo Clinic experience Semin. *Thorac Cardiovasc Surg*., 12 (1), 30 – 37.
13. Chen M. C., Quo G. B. F., Chang J. P. et al. (1998). Radiofrequency and cryoablation of atrial fibrillation in patients undergoing valvular operations. *Ann Thorac Surg*., 65, 1666 – 1672.
14. Schuetz A., Schulze C. J., Sarvanakis K. K., et al. (2003). Surgical treatment of permanent atrial fibrillation using microwave energy ablation: a prospective randomized clinical trial. *Eur J Cardiothorac Surg*., 24 (4), 475 – 480.
15. Sie H. T., Beukema W. P., Ramdat Misier A. R. et al. (2001). Radiofrequency modified Maze in patients with atrial fibrillation undergoing concomitant cardiac surgery. *J Thorac Cardiovasc Surg*., 122, 249 – 256.
16. Szalay Z. A., Skwara W., Pitschner H.-F. et al. (1999). Midterm results after the mini-maze procedure. *Eur. J. Cardiothorac Surg*., 16, 306 – 311.
17. Tang C. W., Scheinman M. M., Van Hare G. F. et al. (1995). Use of P-wave configuration during atrial tachycardia to predict site of origin. *J Am Coll Cardiol*., 26, 1315 – 1324.
18. Cox J. L., Jaquiss R. D. B., Schuessler R. B., Boineau J. P. (1995). Modification of the Maze procedure for alrial flutter and alrial fibrillation. II. Surgical technique of the Maze III procedure. *Thorac Cardiovasc Surg*., 110, 485 – 495.
19. Kosakai Y., Kawaguchi A. T., Isobe F. et al. (1994). Cox Maze procedure for chronic atrial fibrillation associated with mitral valve disease. *J Thorac Cardiovasc Surg*., 108, 1049 – 1055.
20. Handa N., Schaff H. V., Morris J. J. et al. (1999). Outcome of valve repair and the Cox Maze procedure for mitral regurgitation and associated atrial fibrillation. *J Thorac Cardiovasc Surg*., 118 (4), 626 – 635.
21. Jourda F., Providencia R., Marijon E., et al. (2015). Contact-force guided radiofrequency vs. second-generation balloon cryotherapy for pulmonary vein isolation in patients with paroxysmal atrial fibrillation - a prospective evaluation. *Europace*, 17, 225 – 31.
22. Mack M., et al. (2005). Surgical treatment of atrial fibrillation using argonbased cryoablation during concomitant cardiac procedures. *Circulation*, 112, 11 – 16.
23. Lustgarten D., Keane D., Ruskin J. (1999). Cryothermal ablation: mechanism of tissue injury and current experience in the treatment of tachyarrhythmias. *Prog Cardiovasc*, 41, 481 – 498.
24. Cox J. L. (2000). Cryoablation is an effective choice. *Seminars J Thorac Cardiovasc Surg*. 12, 15 – 19.
25. Hebeler R. F. (2004). *Surgical treatment of atrial fibrillation*. San Antonio, 260.
26. Benussi S. (2004). Treatment of atrial fibrillation. *J Cardiothoracic Surg*, 26, 539 – 541.
27. Moskalik I. A., Manik O. M. (2013). About the development of thermoelectric cooling in the practice of cryodestruction. *J.Thermoelectricity*, 6, 84 – 92.
28. Anatychuk L. I. (2003). *Termoelektrichestvo. T. 2. Termoelektricheskiie preobrazovatelu energii [Thermoelectricity. Vol. 2. Thermoelectric energy converters]*. Kyiv, Chernivtsi: Naukova Dumka.
29. Vishal N. Shah, Oleg I. Orlov, Cinthia Orlov, Manabu Takebe, Matthew Thomas, and Konstadinos Plestis. Combined cryo-maze procedure and mitral valve repair through a ministernotomy. Multimed Man Cardiothorac Surg. 2018. doi: 10.1510/mmcts.2018.022.
30. Yiu W., Basco M. T., Aruny J. E., Sumpio B. E. (2007). Cryosurgery:A review. *Int J Angiol*; 16 (1):1 – 6. 19.
31. How can temperature help in the fight against cancer [Electronic resource] // Oncology clinic “K-test” – Retrieved from: https://www.k-test.ru/index.php?rid=4.

32. Cox James L. (2001). Intraoperative options for treating atrial fibrillation associated with mitral valve disease. *The Journal of Thoracic and Cardiovascular Surgery*, 122 (2), 212 – 215.
33. Thomas S. P., Wallace E. M., Ross D. L. (2000). The effect of a residual isthmus of surviving tissue on conduction after linear ablation in atrial myocardium. *J Intervent Card Electrophysiol*, 4, 273 – 281.
34. Tse H.-F., Ripley K. L., Lee K. L. E., C.-W., Van Vleet J. F., Pelkey W. L., Lau C. P. (2005). Effects of temporal application parameters on lesion dimensions during transvenous catheter cryoablation. *J Cardiovasc Electrophysiol,* 16, 201 – 204.
35. Wadhwa M. K., Rahme M. M., Dobak J., Li P., Wolf P., Chen P., Feld G. K. (2000). Transcatheter cryoablation of ventricular myocardium in dogs. *J Intervent Card Electrophysiol*, 4, 537 – 545.
36. Reek S., Geller J. C., Schildhaus H.-U., Ripley K. L., Klein H. U. (2004). Feasibility of catheter cryoablation in normal ventricular myocardium and healed myocardial infarction. *PACE*, 27, 1530 – 1539.
37. Becker A. E. (2004). Left atrial isthmus: anatomic aspects relevant for linear catheter ablation procedures in humans. *Journal of Cardiovascular Electrophysiology*, 15 (7),809 – 12.
38. Cox J. L., Boineau J. P., Schuessler R. B., Jaquiss R. D., Lappas D. G. (1995). Modification of the maze procedure for atrial flutter and atrial fibrillation. I. Rationale and surgical results. *J Thorac Cardiovasc Surg*, 110, 473 – 484.
39. Kosakai Y. (2000). How I perform the maze procedure. Operative techniques in Thoracic and *Cardiovascular Surgery*, 5, 23 – 45.

Submitted: 13.02.2023

Анатичук Л. І., *акад. НАН України* [1,2]
Кобилянський Р. Р., *канд. фіз.-мат. наук* [1,2]
Федорів Р. В. [1,2]
Константинович І. А., *канд. фіз.-мат. наук* [1,2]

[1] Інститут термоелектрики НАН та МОН України,
вул. Науки, 1, Чернівці, 58029, Україна;
[2] Чернівецький національний університет імені Юрія Федьковича,
вул. Коцюбинського 2, Чернівці, 58012, Україна
e-mail: anatych@gmail.com

ПРО ПЕРСПЕКТИВИ ВИКОРИСТАННЯ ТЕРМОЕЛЕКТРИЧНОГО ОХОЛОДЖЕННЯ ДЛЯ ЛІКУВАННЯ АРИТМІЇ СЕРЦЯ

У роботі наводяться результати аналізу різноманітних методів лікування аритмії серця. Серед них особливу увагу привертає метод абляції, що зводиться до ліквідації додаткових електричних подразників скорочення серцевих м'язів. Останнє досягається хірургічними методами, високочастотним опроміненням та кріодеструкцією рідким азотом або шляхом використання ефекту Джоуля-Томсона. Кріометоди мають певні переваги перед іншими, однак їх реалізація є дещо складнішою, що обмежує їх клінічні використання. В

останні десятиріччя у медицині все ширше використовується охолодження ефектом Пельтьє. Він зарекомендував себе як простий, надійний і точний у відтворенні необхідних температурних умов лікування. Дана робота присвячена дослідженню можливості використання ефекту Пельтьє для кріоабляції. Бібл. 39, рис. 2.

Ключові слова: аритмія серця, фібриляція передсердь, кріоабляція, термоелектричне охолодження.

References

1. *What Is Arrhythmia?* National Heart, Lung, and Blood Institute. July 1, 2011. Archived from the original on March 2, 2015. Retrieved March 7, 2015.
2. Vigano M., Graffinga A., Reissa L. et al. (1996). Surgery for atrial fibrillation. *Eur J Cardiothore Surg*. 10, 490 – 497.
3. Williams J. M., Ungerleider R. M., Lofland G.K., Cox J. L. (1980). Left atrial isolation: new technique for the treatment of supraventricular arrhythmias. *J. Thorac Cardiovasc Surg*., 80(3), 373 – 380.
4. Guiraudon G. M., Campbell C. S., Jones D. L. et al. (1985). Combined sinoatrial node atrioventricular isolation: A surgical alternative to His bundle ablation in patients with atrial fibrillation. *Circulation*, 72, 111 – 220.
5. Cox J. L., Boineau J. P., Schuessler R. B., et al. (1993). Five-year experience with the Maze procedure for atrial fibrillation. *Ann Thorac Surg*., 56(4), 814 – 823. 79.
6. Cox J. L., Canavan T. E., Schuessler R. B., et al. (1991). The surgical treatment of atrial fibrillation. II. Intraoperative electrophysiologic mapping and description of the electrophysiologic basis of atrial flutter and atrial fibrillation. *J Thorac Cardiovasc Surg*., 101(3), 406 – 426.
7. Cox J. L., Schuessler R. B., D'Agostino H. J., Jr., et al. (1991). The surgical treatment of atrial fibrillation. III. Development of a definitive surgical procedure. *J Thorac Cardiovasc Surg*., 101(4), 569 – 583.
8. Ferguson T. V., Sox J. L. (1995). Surgery for atrial fibrillation. *Cardiac eleclrophysiology*, 2, 1563 – 1576.
9. McCarthy P. M., Gillinov A. M., Castle L., Chung M., Cosgrove D., 3rd. (2000). The Cox-Maze procedure: the Cleveland Clinic experience. *Semin Thorac Cardiovasc Surg*.,12 (1), 25 – 29.
10. Prasad S. M., Maniar H. S., Camillo C. J., et al. (2003). The Cox maze III procedure for atrial fibrillation: long-term efficacy in patients undergoing single versus concomitant procedures. *J. Thorac Cardiovasc Surg*., 126 (6), 1822 – 1828.
11. Raanani E., Albage A., David T. E., Yau T. M., Armstrong S. (2001). The efficacy of the Cox/maze procedure combined with mitral valve surgery: a matched control study. *Eur J. Cardiothorac Surg*., 19(4), 438 – 442.
12. Schaff H. V., Dearani J. A., Daly R. C., Orszulak T. A., Danielson G. K. (2000). CoxMaze procedure for atrial fibrillation: Mayo Clinic experience Semin. *Thorac Cardiovasc Surg*., 12 (1), 30 – 37.
13. Chen M. C., Quo G. B. F., Chang J. P. et al. (1998). Radiofrequency and cryoablation of atrial fibrillation in patients undergoing valvular operations. *Ann Thorac Surg*., 65, 1666 – 1672.
14. Schuetz A., Schulze C. J., Sarvanakis K. K., et al. (2003). Surgical treatment of permanent atrial fibrillation using microwave energy ablation: a prospective randomized clinical trial. *Eur J Cardiothorac Surg*., 24 (4), 475 – 480.

15. Sie H. T., Beukema W. P., Ramdat Misier A. R. et al. (2001). Radiofrequency modified Maze in patients with atrial fibrillation undergoing concomitant cardiac surgery. *J Thorac Cardiovasc Surg*., 122, 249 – 256.
16. Szalay Z. A., Skwara W., Pitschner H.-F. et al. (1999). Midterm results after the mini-maze procedure. *Eur. J. Cardiothorac Surg*., 16, 306 – 311.
17. Tang C. W., Scheinman M. M., Van Hare G. F. et al. (1995). Use of P-wave configuration during atrial tachycardia to predict site of origin. *J Am Coll Cardiol*., 26, 1315 – 1324.
18. Cox J. L., Jaquiss R. D. B., Schuessler R. B., Boineau J. P. (1995). Modification of the Maze procedure for alrial flutter and alrial fibrillation. II. Surgical technique of the Maze III procedure. *Thorac Cardiovasc Surg*., 110, 485 – 495.
19. Kosakai Y., Kawaguchi A. T., Isobe F. et al. (1994). Cox Maze procedure for chronic atrial fibrillation associated with mitral valve disease. *J Thorac Cardiovasc Surg*., 108, 1049 – 1055.
20. Handa N., Schaff H. V., Morris J. J. et al. (1999). Outcome of valve repair and the Cox Maze procedure for mitral regurgitation and associated atrial fibrillation. *J Thorac Cardiovasc Surg*., 118 (4), 626 – 635.
21. Jourda F., Providencia R., Marijon E., et al. (2015). Contact-force guided radiofrequency vs. second-generation balloon cryotherapy for pulmonary vein isolation in patients with paroxysmal atrial fibrillation - a prospective evaluation. *Europace*, 17, 225 – 31.
22. Mack M., et al. (2005). Surgical treatment of atrial fibrillation using argonbased cryoablation during concomitant cardiac procedures. *Circulation*, 112, 11 – 16.
23. Lustgarten D., Keane D., Ruskin J. (1999). Cryothermal ablation: mechanism of tissue injury and current experience in the treatment of tachyarrhythmias. *Prog Cardiovasc*, 41, 481 – 498.
24. Cox J. L. (2000). Cryoablation is an effective choice. *Seminars J Thorac Cardiovasc Surg*. 12, 15 – 19.
25. Hebeler R. F. (2004). *Surgical treatment of atrial fibrillation*. San Antonio, 260.
26. Benussi S. (2004). Treatment of atrial fibrillation. *J Cardiothoracic Surg*, 26, 539 – 541.
27. Moskalik I. A., Manik O. M. (2013). About the development of thermoelectric cooling in the practice of cryodestruction. *J.Thermoelectricity*, 6, 84 – 92.
28. Anatychuk L. I. (2003). *Termoelektrichestvo. T. 2. Termoelektricheskiie preobrazovatelu energii [Thermoelectricity. Vol. 2. Thermoelectric energy converters]*. Kyiv, Chernivtsi: Naukova Dumka.
29. Vishal N. Shah, Oleg I. Orlov, Cinthia Orlov, Manabu Takebe, Matthew Thomas, and Konstadinos Plestis. Combined cryo-maze procedure and mitral valve repair through a ministernotomy. Multimed Man Cardiothorac Surg. 2018. doi: 10.1510/mmcts.2018.022.
30. Yiu W., Basco M. T., Aruny J. E., Sumpio B. E. (2007). Cryosurgery:A review. *Int J Angiol*; 16 (1):1 – 6. 19.
31. How can temperature help in the fight against cancer [Electronic resource] // Oncology clinic “K-test” – Retrieved from: https://www.k-test.ru/index.php?rid=4.
32. Cox James L. (2001). Intraoperative options for treating atrial fibrillation associated with mitral valve disease. *The Journal of Thoracic and Cardiovascular Surgery*, 122 (2), 212 – 215.
33. Thomas S. P., Wallace E. M., Ross D. L. (2000). The effect of a residual isthmus of surviving tissue on conduction after linear ablation in atrial myocardium. *J Intervent Card Electrophysiol*, 4, 273 – 281.
34. Tse H.-F., Ripley K. L., Lee K. L. E., C.-W., Van Vleet J. F., Pelkey W. L., Lau C. P. (2005). Effects of temporal application parameters on lesion dimensions during transvenous catheter cryoablation. *J Cardiovasc Electrophysiol,* 16, 201 – 204.
35. Wadhwa M. K., Rahme M. M., Dobak J., Li P., Wolf P., Chen P., Feld G. K. (2000).

Transcatheter cryoablation of ventricular myocardium in dogs. *J Intervent Card Electrophysiol*, 4, 537 – 545.

36. Reek S., Geller J. C., Schildhaus H.-U., Ripley K. L., Klein H. U. (2004). Feasibility of catheter cryoablation in normal ventricular myocardium and healed myocardial infarction. *PACE*, 27, 1530 – 1539.
37. Becker A. E. (2004). Left atrial isthmus: anatomic aspects relevant for linear catheter ablation procedures in humans. *Journal of Cardiovascular Electrophysiology*, 15 (7),809 – 12.
38. Cox J. L., Boineau J. P., Schuessler R. B., Jaquiss R. D., Lappas D. G. (1995). Modification of the maze procedure for atrial flutter and atrial fibrillation. I. Rationale and surgical results. *J Thorac Cardiovasc Surg*, 110, 473 – 484.
39. Kosakai Y. (2000). How I perform the maze procedure. Operative techniques in Thoracic and *Cardiovascular Surgery*, 5, 23 – 45.

Submitted: 13.02.2023

L. I. Anatychuk, *acad. National Academy of Sciences of Ukraine*[1,2]
L. M. Vikhor, *doc. phys-math sciences*[1]
I. D. Matsenko [2]

1, Nauky str., Chernivtsi, 58029, Ukraine,
e–mail: anatych@gmail.com
[2]Yu.Fedkovych Chernivtsi National University,
2, Kotsiubynskyi str., Chernivtsi, 58012, Ukraine

PHYSICAL MODELS OF OPTICAL-ELECTRONIC SYSTEMS OF THE IR SPECTRUM RANGE WITH THERMOELECTRIC COOLING (REVIEW)

The paper considers the main physical models of optical-electronic systems in the IR spectrum range with thermoelectric cooling. The features and advantages of these models are analyzed. It was established that the simplest and the one that is practically used in industrial samples of IR devices is a model of a thermoelectric module built into a metal case with photosensitive elements that are cooled. Such a model with cascade thermoelectric coolers (TEC) made of materials based on Bi_2 Te_3 ensures the level of operating temperatures of IR devices up to 195 K. It has been shown that expanding the cooling range to temperatures of 140-150 K is possible by using functionally graded materials and additional stages of low-temperature thermoelectric materials, for example BiSb-based materials, for TEC. It has been established that the energy efficiency of a TEC significantly depends on the optimization of its design, which should take into account the electrical and thermal resistance of contacts, interconnect and insulation plates, as well as the influence of the thermal resistance of the IR detector case, its connections with the TEC, heat sinks and heat exchangers used in the system for heat removal from TEC. Therefore, the TEC design must take into account all system components, and the choice of the physical model of the optical-electronic system with TEC is important. Bibl. 32, Fig. 11, Tabl. 2.
Key words: optical-electronic system, IR device, thermoelectric cooler, physical model.

General information about optical-electronic systems of the IR range

Optical-electronic systems are widely used for recording IR radiation and forming IR images in modern ground-based and space-based equipment. But the leading place among the many uses of infrared optical-electronic technology is occupied by its application in military affairs. IR systems are used to detect and track ground, surface and underwater targets, in night vision and thermal reconnaissance devices, in forward inspection systems for aircraft, combat vehicles, in mine detectors, range finders, in weapon and projectile control systems and many other military instruments equipment necessary for protection and safety.

The main element of IR systems and devices is a photodetector, that is, a radiation detector with an internal photoelectric effect. In general, the simplest photodetector is a photosensitive element located in a sealed protective housing with an input window made of transparent material for radiation. As a photosensitive element, photoresistor, photodiode, phototransistor and photothyristor structures made of semiconductor material sensitive to radiation in the operating (for a given device) spectrum range are

used. Modern photodetectors, as a rule, are multi-element, that is, they contain a number of photosensitive elements.

The problem is that the photosensitive element needs to be cooled in order for IR photodetectors to work. In order to increase the detection ability, it is necessary to suppress the own radiation of the sensitive element. This is achieved by cooling to temperatures at which self-radiation noise becomes negligible. In addition, the cooling of small sensitive elements with a low heat capacity makes it impossible for them to heat up too much under the influence of intense radiation. Cooling is also necessary to reduce the thermal generation of charge carriers in the semiconductor photosensitive element. The heat spreaders of the carriers compete with the optical transitions, which leads to a large amount of dark noise in uncooled devices.

The operating temperature of the photodetector is related to the operating wavelength range of the IR detector and depends on the material and technology of the photosensitive element. Photocells made of different semiconductor materials will also have different operating temperatures which can reach the cryogenic level [1]. Four cooling methods are used:

- liquefied gases;
- due to the Joule-Thomson effect;
- cryogenic machines;
- thermoelectric cooling.

The choice of method depends on the requirements for the operating temperature of the receiver and on the surrounding conditions. In particular, the method of liquefied gases is used in the conditions of laboratory research, in industry, medicine, but it is absolutely not suitable for military equipment. Other methods, on the contrary, are mainly developed for military affairs, but are also used in other fields.

To cool the IR detectors to cryogenic temperatures, micro cryogenic systems based on the Stirling gas machine [2], which is connected to the photodetector in a single structure, are specially developed and used. They ensure the cooling temperature of the photodetector at the level of 75 - 150 K. These are energy-efficient coolers. With a cooling capacity in the range of 100 - 600 mW, their coefficient of performance reaches the values of 10^{-2} – 3 10^{-2}. The main disadvantage of such systems is their high cost. Such mechanical cooling systems make optoelectronic devices bulky, expensive, and unreliable, which prevents the widespread practical use of IR devices.

However, not all IR devices need such deep cooling. For example, medium-wave (3 – 5 μm) and long-wave (5 – 30 μm) IR detectors, which are required for many important practical applications, usually work without cryocooling [1]. Scientific studies have shown that sufficiently high characteristics of sensors in the medium and long-wave IR range are provided at operating temperatures of photodetectors significantly higher than cryogenic ones [3, 4]. These temperatures are achieved using thermoelectric cooling [5, 6], which in this case is more rational compared to the machine method of cold generation.

Thermoelectric cooling is widely used to ensure the required operating temperature of IR detectors [1]. Operating temperatures of IR detectors up to 190 K are achieved using thermoelectric coolers [1, 5, 6], which have no moving parts, are compact, reliable, and have a long service life. The operating temperature of such devices is related to the operating range of the IR detector and depends on the material and manufacturing technology of the photosensitive element. The most common elements for IR detectors are photoresistors based on *PbS* and *PbSe*, photodiodes made of InGaAs, photodiodes and photoresistors based on *InSb* and *HgCdTe*. Modern materials for IR detectors are, for example, *GaAs*/*AlGaAs* quantum well materials [7] and *InAs*/*GaSb* superlattices [8], which serve as an

alternative to *HgCdTe*, because the use of *Hg* and *Cd* toxic elements in electronic devices is limited by European Union directives. The operating temperatures of photosensitive elements made of all these materials are compatible with the temperature range provided by thermoelectric cooling. Single-stage thermoelectric modules are used for temperature stabilization and shallow cooling of IR detectors. Two-stage modules are used for IR detectors with an operating temperature of 230 K, three-stage modules are cooled to an operating temperature of 210 K, and four-stage modules are cooled to 195 K. The industrial manufacturer of IR detectors based on *HgCdTe* with built-in 2-, 3- and 4-stage thermoelectric modules is the European company Vigo Photonics [6].

Main physical models of optical-electronic systems with thermoelectric cooling

Let us consider the physical models of optical-electronic systems with thermoelectric cooling. The simplest model contains a photo-receiving device placed on the heat-absorbing face of a thermoelectric cooling module, which is usually mounted in a sealed case, the base of which is in thermal contact with the heat exchanger.

This simplest model was used in the period 1973 – 1975 for airborne infrared technology [9]. An IR detector with a *PbSe*-based photosensitive element and a single-stage thermoelectric cooler (TEC) was installed in the device case with a lens pumped at a given solid angle. The physical model of the device is shown in Fig. 1.

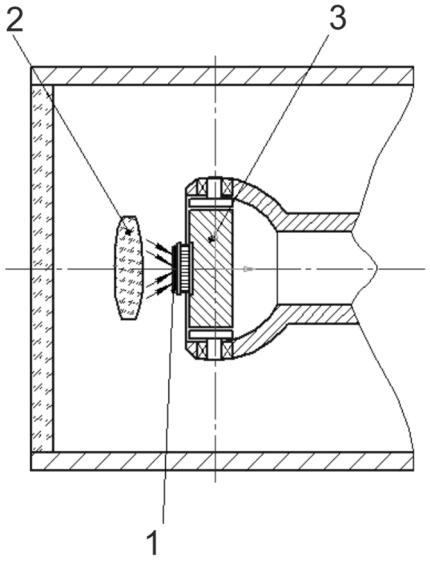

Fig. 1. The simplest model of IR device with TEC [9].
1 – IR detector with TEC, 2 – lens, 3 – hear-receiving base

The cooler consumed less than 0.6 W of power and lowered the temperature of the sensitive element by 35-45 K. The necessary sensitivity and heat resistance of the device was ensured both in the barrage mode and under the conditions of the peak temperature value of the air flow approaching the device. The device was used in the former USSR until the 90s.

In the simplest model of optoelectronic systems, cascade coolers are often used. The technology for developing a 4-stage TEC for cooling an IR receiver based on a 2D focal array of sensitive elements with *HgCdTe* to a temperature of 200 K is described in [10]. Materials based on Bi_2Te_3 with a quality factor of $2.95 \cdot 10^{-3}$ K^{-1} in *n*-type and $2.9 \cdot 10^{-3}$ K^{-1} in *p*-type were used. Experimental samples of a cooler were manufactured, containing in stages, respectively, 2-5-12-31 thermocouples with crystals measuring 1.5 1.5 1.8 mm. At a heat exchanger temperature of 333 K, the average value of the maximum

temperature difference was 147 K. In operating mode with a cooling capacity of 100 mW, the TEC provided cooling to 200 K. The average value of power consumption was 10.5 W, and the coefficient of performance in operating mode reached 0.0093.

In [11], Marlow Industries proposed a physical model of a TEC integrated into the body of an IR detector array to stabilize its temperature. Thermoelectric temperature stabilization is often used in cooling-free infrared imaging systems due to the temperature sensitivity of the detector array. These infrared systems operate under changing ambient temperatures. The TEC is used to heat or cool the detector array to an optimal temperature.

Infrared detector arrays must operate in a hermetically sealed enclosure. Typically, the TEC is mounted in a metal case, and the detector array is mounted directly on top of the TEC. The metal case has several input/output contacts, through which the signal received from the detector is transmitted to the electronic components of the system. The window is attached to the top of the case. With this approach, the TEC, which has two ceramic plates, is soldered into the case or filled with epoxy resin. The leads from the TEC are attached to the power contacts on the case.

The concept of built-in TEC facilitates the installation method. Instead of a metal case, the TEC is built into a case made of multilayer ceramics (Fig. 2). Metallization platforms are located at the base of the case, which allow p- and n-elements to be soldered directly to the base of the case. The power supply wires of the TEC are attached to the pins on the outside of the case with metallized transition holes and tracks that eliminate the additional process of soldering the wires.

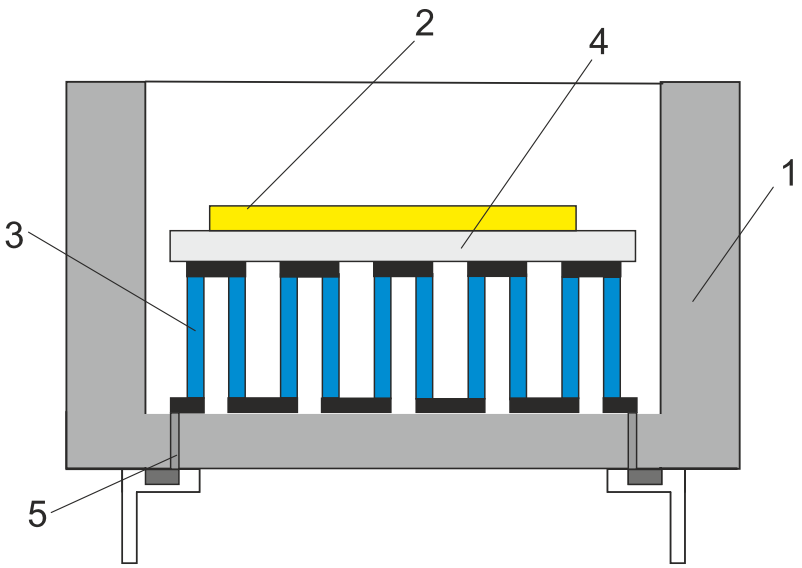

Fig. 2. Model of TEC embedded into a ceramic case [11]. 1 – ceramic case, 2 – cooling object, 3 – thermoelements, 4 – ceramic plate, 5 – metallized holes for power wires

Thus, the concept of embedded TEC involves soldering individual thermoelements directly into the base of the ceramic base with built-in electric wires for both TEC and the detector array. Integrating the cooler directly into the case offers many advantages. This reduces the number of component parts in the system, the number of soldering and connection operations, eliminates the TEC assembly operation for detector manufacturers.

[11] provides an overview of the thermal, electrical, and dimensional requirements needed to effectively design an integrated cooler for an uncooled infrared system. The embedded TEC must be designed based on operating parameters such as power, temperature difference, size and reliability.

An example of the characteristics of the built-in TEC for cooling to 25 C an array of detectors with an active heat release of 0.5 W at an ambient temperature of 75 C and a thermal resistance of the heat sink of 2 C/W is given. The TEC power in this mode is 1.89 W [11].

In [12], a physical model of a cascade TEC with a separate supply of stages is proposed (Fig. 3). Such a model is advisable to use for so-called planar microcoolers, which are located in the same plane as a miniature optical-electronic device that is cooled. As a rule, specially developed microelectronics technologies, namely MEMS technologies, are used for the manufacture of such TECs. A feature of the physical model is that thermal matching in the stages is carried out due to the ratio of the areas of the stages and the length of the thermoelements in the stages.

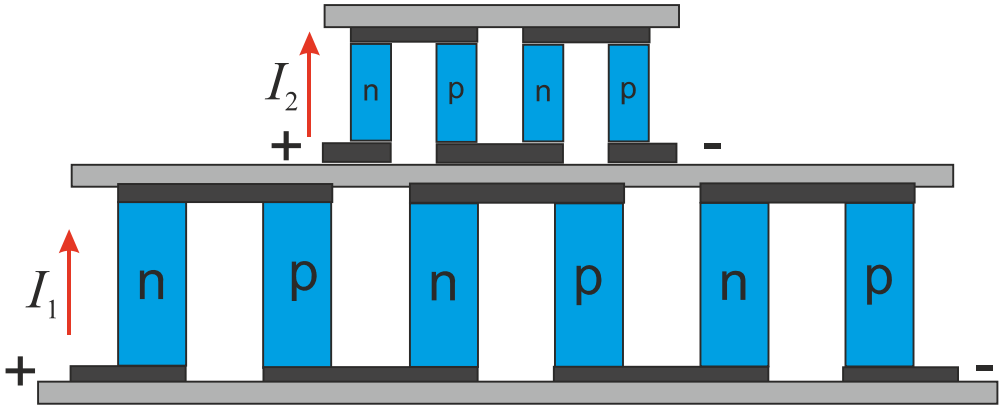

Fig. 3. Model of TEC with a separate power supply to stages

In [12], the principle of calculating the maximum temperature difference for a given refrigerating capacity of a two-stage TEC with separate power supply of the stages is proposed. An example of designing and calculating the characteristics of a planar two-stage TEC for an IR laser with a heat output of 10 mW is given. The problem of heat loss is also discussed as the most important mechanism of deterioration of the characteristics of miniature TECs. In particular, to reduce heat losses caused by the presence of interstage thermal resistance and heat removal through wires, instead of the TEC model shown in Fig. 3, a physical model with parallel power supply of stages is proposed, the configuration of which is illustrated in Fig. 4. In this model, there is no interstage insulating plate and only one pair of electrical wires is used, but both stages can operate at optimal current as a result of adapting the areas of the stages to the height of the thermoelectric legs.

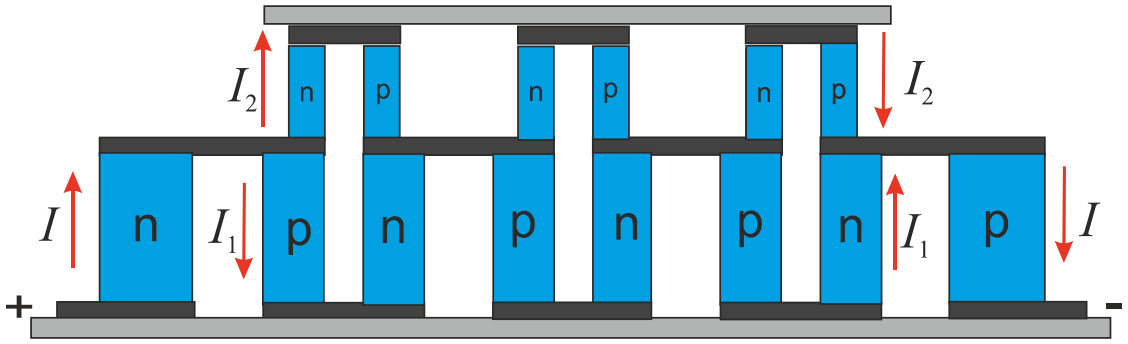

Fig.4. Model of TEC with a parallel power supply to stages

In [13], a three-dimensional (3D) physical model of the system is considered, which consists of an optical-electronic object, an array of thermoelements with ceramics on the cold and hot sides, and a heat sink (Fig. 5).

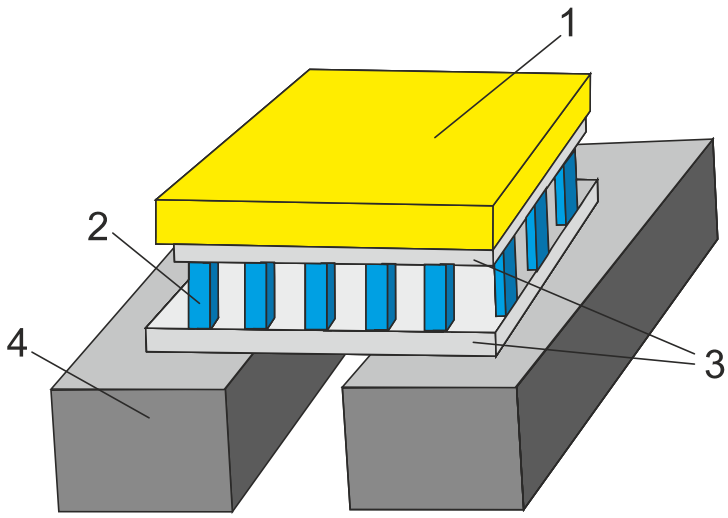

Fig. 5. Structure of a 3D physical model of a thermoelectric cooling system for an optical-electronic object. 1 – optical-electronic object, 2 – thermoelements, 3 – ceramics, 4 – heat sink with a hole

One-dimensional models do not provide information in directions perpendicular to thermoelements. Therefore, they are not suitable for systems with heat sinks with uneven temperature distribution over the surface, or in the case of incomplete contact of ceramics with the heat sink. In such cases, 3D models are used. In [13], the model takes into account transient and three-dimensional effects, the temperature dependence of the characteristics of the model materials, as well as convective and radiative heat exchange between ceramics and is used to determine the following values: time and electric power of the TEC to reach the required temperature of the object, power in steady-state mode to maintain the set temperature, the maximum TEC power, at which the maximum temperature difference between ceramics, temperature gradients on the object and other components of the system is achieved. The computer simulation uses a finite element method with a feedback control loop to correlate the power supply to the TEC in order to regulate the temperature of the object. An example of using the model to calculate the parameters of a thermoelectric temperature stabilization system for an IR detector, which is used in uncooled night vision cameras with a heat sink that is not completely in contact with the hot ceramics of the TEC due to the large hole for electrical wires, is described.

A series of works [14 – 18] are devoted to the problems of cooling optical-electronic devices. As heat sources, optical-electronic components can be divided into three groups. Devices of the first group have low heat generation power and small dimensions. Traditional TEC configurations successfully solve the problem of their thermal regulation.

The second group includes optoelectronics devices with intense heat generation (powerful diodes, infrared lasers, etc.). To ensure their reliable operation, miniature TECs with high cooling capacity are required. It is known that reducing the length of thermoelements leads to an increase in the cooling capacity of TECs. However, there are physical limitations that hinder the miniaturization of TEC. Such limitations are irreversible losses caused by the electrical contact resistance, as well as the electrical and thermal resistance of the interconnects and ceramic plates of TEC. Therefore, the physical model of TEC (Fig. 6) for such optical-electronic devices must take into account these factors, which cannot be eliminated in principle.

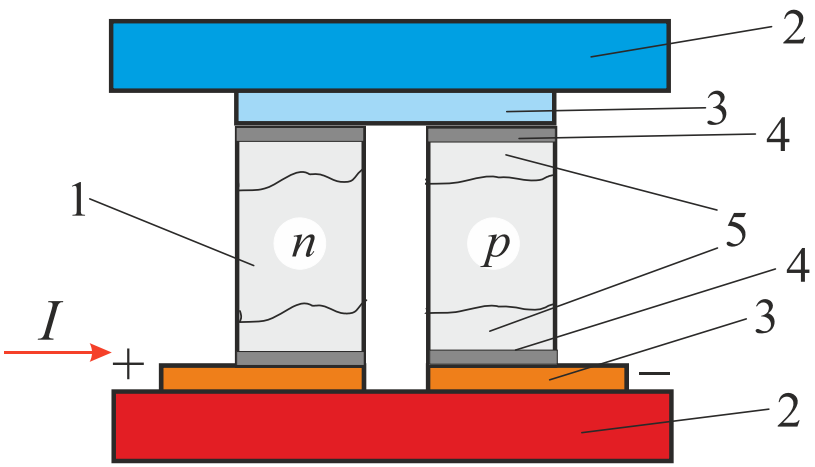

Fig. 6. Physical model of a thermoelectric miniature converter. 1 – thermoelectric material, 2 – insulation ceramic plate, 3 – interconnect plate, 4 – anti-diffusion metal layer, 5 – contact zone

The quality of electrical contacts is the most important factor that significantly affects the operation of cascade TECs. In [18], the characteristics of low-temperature cascade TECs were analyzed depending on the value of the electrical contact resistance. Two key characteristics are considered: the maximum coefficient of performance at a given temperature difference and the maximum cooling achieved for a TEC with a fixed configuration. To maintain the coefficient of performance at an acceptable level, it is necessary to provide a contact resistance r_c in the range from 10^{-7} Ohm см^2 to 10^{-6} Ohm cm^2, while with higher resistance the coefficient of performance of the TEC sharply decreases, especially for TEC with thermoelectric legs with a height of 0.5 mm or less. Irreversible losses caused by the electrical resistance of the interconnect metal plates were also analyzed, and their thicknesses were determined, which should provide an acceptable low level of resistance for various cascade TECs with typical sizes of thermoelectric legs and the distance between them.

In [17], the influence of the thermal properties of insulating ceramic plates on the operation of cascade TECs was studied. A mathematical model has been developed for the analytical calculation of the thermal resistance of interstage ceramics associated with three-dimensional heat transfer from a smaller cascade to a larger cascade. The model is used to determine the maximum temperature difference for standard multi-stage TECs with different ceramics. The TEC with the length of thermoelectric legs in the range from 0.3 mm to 2 mm was considered. A comparative analysis of the obtained results was carried out and recommendations were formulated for choosing the appropriate material for insulation plates.

The third group includes large-sized planar optical-electronic devices, for example, multi-element arrays of IR detectors and imagers, charge-coupled devices (CCDs), etc. These are typically low-intensity distributed heat sources that require low operating temperatures, typically 200 K and below. Here the problem arises: how to provide the necessary deep cooling in conditions of minimum cooling capacity. Typically, a few thermocouples are usually sufficient in the upper stage. Therefore, its surface area is small compared to the object being cooled. As a result, it is difficult to meet the requirements of temperature uniformity and mechanical strength. A low-temperature, multi-stage TEC is needed, in which the increased dimensions of the cold stage are combined with minimum power and mechanical strength. Traditional pyramidal stages are not suitable here. Special low-temperature cascade TECs with increased dimensions of the cold surface, but with a small cooling capacity, are needed.

Two physical TEC models are used to solve the problem. The first model, the traditional one, consists in the uniform distribution of thermoelectric legs in cold stages to increase the area. This model is used only if the total required number of thermoelectric legs in the cold stage is sufficient to withstand the applied mechanical and thermal loads. The second model is the use of an increased number of legs in cold stages with their mixed series-parallel connection. Thus, two or more legs are arranged in parallel, forming a separate thermoelectric leg, the height of which increases proportionally to maintain the optimal geometry of the legs. In this way, it is possible to significantly increase the number of legs and obtain TEC with almost the same area of stages. This model has the advantages of increased packing density of legs, which means increased mechanical strength. The results of testing such modules are given in [15, 16]. Despite the greatly increased dimensions of the upper stages, these TECs provide ΔT_{max} values at the level of the best pyramid modules.

In [15, 16], a physical model of an optical-electronic device with TEC, which is placed in a small-sized metal case, whose own thermal characteristics affect the operation of TEC, is considered. The case made of kovar has a significant thermal resistance and affects the temperature of the hot surface of the TEC. In addition, additional heat enters through the case cover. As a result, the actual characteristics of the TEC may differ significantly from the expected ones.

Fig. 7 shows a physical model of a device with thermoelectric cooling. A substrate with an optical-electronic element on top is installed on the cold surface of the TEC. The structure is located inside a metal case on a base plate which is fixed on the heat sink. The entire system is closed with a lid thermally connected to the base.

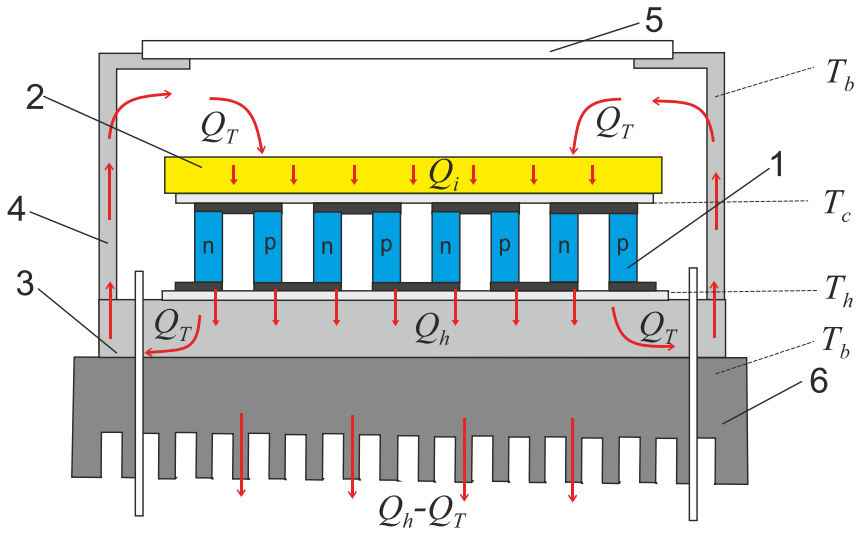

Fig. 7. Physical model of an optical-electronic device with TEC in a metal case [16]. 1 – TEC, 2 – optical-electronic element, 3 – case base plate, 4 – case cover, 5 – window, 6 – heat exchanger base

The stationary thermal model of the system is described by the following equations:

$$Q_c = A(\alpha T_c i - 0.5 i^2 (\rho + 2r_c / L)L - \frac{\kappa}{L}(T_h - T_c)), \quad (2.1)$$

$$Q_h = A(\alpha T_c i + 0.5 i^2 (\rho + 2r_c / L)L - \frac{\kappa}{L}(T_h - T_c)), \quad (2.2)$$

$$Q_c = Q_i + Q_T\,, \tag{2.3}$$

$$T_h - T_b = R_h Q_h\,, \tag{2.4}$$

$$T_b - T_a = R_{hs}(Q_h - Q_T)\,, \tag{2.5}$$

where A is the total cross-sectional area of all thermoelectric legs, L is the length of thermoelectric legs, α, ρ, κ are the Seebeck coefficient, resistivity and thermal conductivity of thermoelectric material, r_c is the value of contact resistance, i is density of TEC supply current, Q_c is cooling capacity of the cooler, Q_h is heat power on the heat-releasing surface of TEC, Q_i is heat generated by optical-electronic object, T_b is temperature of heat sink base, T_a is ambient temperature, R_h and R_{hs} are thermal resistances of the base and heat sink. Q_T is entering the cold surface of TEC from the environment which in the first approximation can be calculated by the formula

$$Q_T = K_c(T_b - T_c)\,, \tag{2.6}$$

where K_c is the coefficient of the combined effect of convection, radiation and thermal conductivity of the wires connected to the optical-electronic object. For a known Q_i and a given value of the current density i the system of equations (2.1) - (2.6) makes it possible to find the unknown temperatures T_c, T_h, T_b and heat capacities Q_c, Q_h, Q_T. However, the system is solved, if the thermal parameters of the case, namely K_c, R_h and R_{hs} are known values that can be determined experimentally.

Work [16] shows the influence of the thermal resistance R_h of the base on the characteristics of TECs with different lengths of thermoelectric legs. The maximum temperature drop loss is 2.4 K for a TEC with a leg length of 1.5 mm, and for a TEC with a leg length of 0.5 mm, the loss increases to 8 K. Thus, the intuitive desire to use a TEC with a larger cooling capacity to achieve better cooling may lead to the opposite result. On the other hand, it may turn out that the TEC with excessively long legs does not have sufficient cooling capacity to maintain the required value of the cooling temperature T_c. Therefore, the optimal TEC configuration should be based on the analysis of all system components taking into account their thermal connection, and the choice of the correct physical model of optical-electronic systems with TEC plays a significant role in the design of the cooler.

The physical model shown in Fig. 7, was used in [19] to develop and study the design of an IR detector with thermoelectric cooling for operation in the spectral range of 3 – 5 μm. A 3-stage cooler is used to col the $Cd_{1-x}Hg_xTe$ photosensitive element to 200 K. A photosensitive element on a leucosapphire substrate is glued to the heat-absorbing surface of the TEC. The cover, sealing the volume of the photodetector, is welded to the kovar base with sealed glass-metal terminals for the photocell and TEC. The cover includes an entrance window. To absorb the remaining gases after evacuation and sealing of the photodetector, a gas absorber (getter) is used in the design, which allows maintaining the pressure of residual gases in the working volume of the photodetector below 10^{-3} Pa throughout its entire service life. The photoelectric characteristics of the photodetector were measured. It was established that the value of the specific detectable power of the photodetector at a temperature of ~ 200 K at a wavelength of $\lambda = 4.5$ μm is equal to $D^*_{\lambda max} \geq 1 \cdot 10^{10}$ cm $Hz^{1/2}W^{-1}$, the time to enter the operating mode is 70 s, the supply current of TEC is 1 A, TEC power consumption - 5.5 - 6.0 W, cooling capacity 120 - 100 mW, dimensions of the cooled area – 4 × 7 mm^2. It was also established that after conducting tests on vibration

resistance, shock resistance, heat resistance and cold resistance, the photodetector maintained its main parameters within 3000 hours.

Screens in physical TEC models for IR detectors

To reduce the heat load on the coldest stage of the TEC, back in 1980 it was proposed in [20] to use a screen. An example of a physical model with a screen in a thermoelectric cooling system for an IR detector given in [20] is shown in Fig.8. Made of metal with high thermal conductivity, the screen is easily cooled by the TEC stage to which it is attached. Its main function is to shield the detector and the upper cold stages of TEC from the flow of heat coming due to convection and radiation from the inner walls of the IR device case, as well as from the hot surface of the TEC base. In addition to the screen, this physical model has another feature, namely, the wires from the detector before exiting the device case are first connected to the surface of one of the lower stages. This reduces the component of the thermal load on the upper TEC stage, caused by the thermal conductivity of the wires.

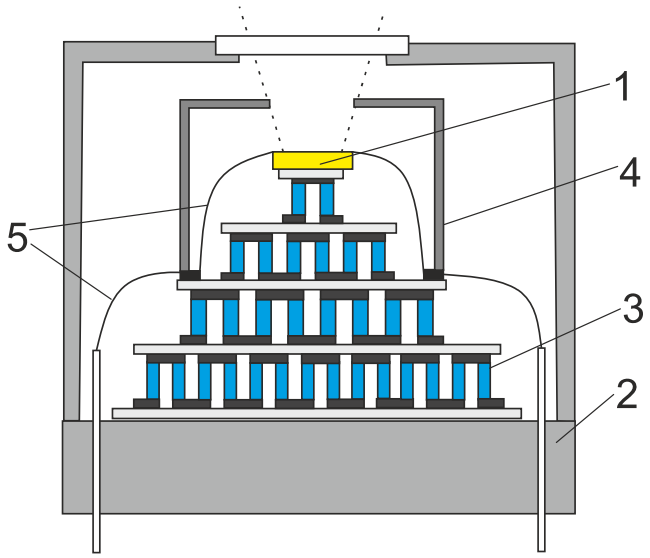

Fig. 8. Physical model of an optical-electronic device with a 4-stage TEC with a screen on the second stage [20].
1 – IR detector, 2 – device case, 3 – TEC, 4 – screen, 5 – IR detector wires

Physical models of thermoelectric cooling systems for IR detectors containing thermal screens are protected by patents [21, 22]. In [21], a system with screens on each TEC stage was proposed. The screens are cup-shaped, attached to the interstage plates and nested within each other, with each thermal screen covering all successive screens and stages. Each screen has an opening to provide an optical path for the optical radiation detector, which is installed on the coldest stage. Part of the thermal energy is absorbed by each screen and removed through the lower stage of the cooler. Screens are made of material with high thermal conductivity such as silver, copper, aluminum and polished to minimize heat absorption. It is noted that the use of screens on all stages provides maximum cooling. However, approximately 90 % of the maximum cooling capacity is achieved with only two screens mounted on the lower and upper interstage plates, eliminating all intermediate screens. This physical model also proposes installing an optical window on the outer screen, connected to the hottest surface, namely the base of the cooler. This arrangement eliminates the need for electrical window heating to minimize the formation of dew on the window.

Patent [22] describes the physical model of the cooling system of IR detectors with a screen that is installed in the base of the detector case and, accordingly, is not cooled. But it surrounds the TEC and the detector (Fig. 9).

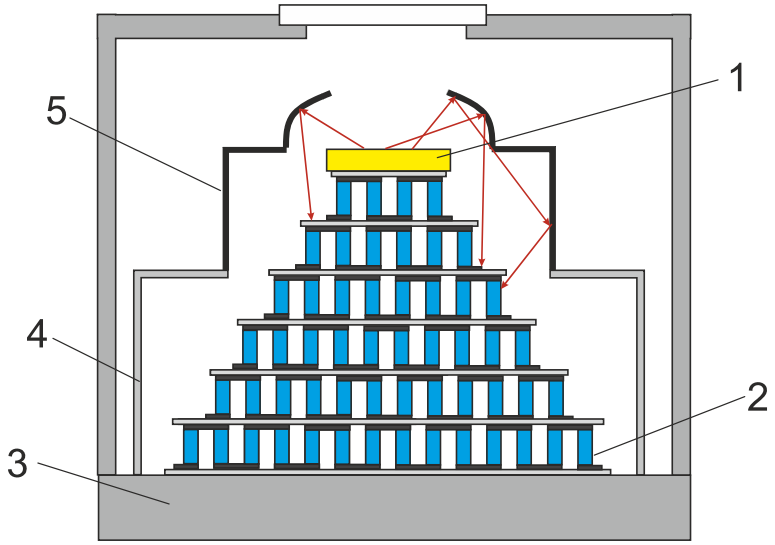

Fig. 9. Physical model of TEC with a screen for IR detectors [22].
1 – IR detector, 2 – cascade TEC, 3 – case, 4 – screen holder,
5 – screen with a curved surface

The screen has a curved reflective surface and reflective side walls that absorb and eliminate the thermal energy of radiation. This reduces the heat load on the coldest TEC stage.

Modern ideas in the physical models of optical-electronic systems with thermoelectric cooling

The introduction of modern advanced technologies for IR detectors allows a shift in the operating temperature of the IR detector from the cryogenic region to the range of 150 – 200 K [4, 23 – 25]. At the same time, its characteristics do not deteriorate. Such temperatures can be achieved by thermoelectric cooling by using new modern approaches in physical models of optical electronic devices with cascade thermoelectric coolers.

One of these approaches is the use of functionally graded thermoelectric materials (FGTM) for thermoelement legs [26]. These are heterogeneous materials with an optimal distribution of the main thermoelectric properties: thermoEMF, electrical conductivity and thermal conductivity along the height of the thermoelectric leg.

Another approach is the use of materials with increased efficiency in the low temperature region. An example of such materials are *Bi-Sb* alloys of n-type conductivity. These alloys have a high thermoelectric figure of merit at temperatures below 160 K, which also increases in a magnetic field. The use of an optimally non-uniform magnetic field further increases the cooling efficiency of modules made of such materials [26].

In [27], the results of calculating the energy parameters of low-temperature cascade thermoelectric modules that provide cooling to temperatures below 200 K at a heat-generating surface temperature of 300 K are presented (Table 1). The maximum coefficient of performance was calculated taking into account the above approaches.

Table 1

Estimated values of energy parameters of low-temperature TEC

Cooling temperature *Tc*, K	Number of stages	Coefficient of performance, ε_{max}	Power at thermal load Q_0 = 10 mW, W, W	TEC material
200	3	$4 \cdot 10^{-2}$	0.25	FGTM based on *Bi-Te*
190	3	$2.5 \cdot 10^{-2}$	0.4	FGTM based on *Bi-Te*
180	4	$1.2 \cdot 10^{-2}$	0.83	FGTM based on *Bi-Te*
170	4	$5 \cdot 10^{-3}$	2.0	FGTM based on *Bi-Te*
160	4	$2 \cdot 10^{-3}$	5.0	FGTM based on *Bi-Te*
150	5	$8 \cdot 10^{-4}$	12.0	4 stages – FGTM based on *Bi-Te*, 1 upper stage – *n-BiSb* in the inhomogeneous magnetic field, *p-BiTe* FGTM
140	6	$3 \cdot 10^{-4}$	33.5	4 stages – FGTM based on *Bi-Te*, 2 upper stages – *n-BiSb* in the inhomogeneous magnetic field, *p-BiTe* FGTM

It was established that to reach temperatures of 160 - 200 K it is enough to use three-, four-cascade modules, the thermoelements of which are made of FGTM on the basis of *Bi-Te*. Such FGTM can be formed by the formation of a corresponding inhomogeneous distribution of impurities in the material or by changing its composition. To cool to temperatures of 150 – 140 K, a four-stage module with a Bi-*Te*-based FGTM must be supplemented with low-temperature stages. In these stages, it is advisable to use alloys based on *Bi-Sb* for the n-type conductivity legs. At room temperature, the figure of merit *Z* in *n-BiSb* is approximately $0.8 \cdot 10^{-3}$ K^{-1}, at low temperatures, *Z* increases, reaching $5 \cdot 10^{-3}$ K^{-1} per 100 K. A magnetic field further increases this value to $8 – 9 \cdot 10^{-3}$ K^{-1} [26]. In this case, FGTM of *n*-type conductivity based on *Bi-Sb*, i.e. a material with variable basic thermoelectric characteristics α, σ, κ, can be obtained by optimally changing the induction of the magnetic field in which this material is placed. Until now, in the arsenal of thermoelectricity there are no materials of p-type conductivity with a similar dependence of the figure of merit on the magnetic field. Therefore, for *p*-type legs, it is possible to use FGTM based on the traditional *Bi-Te* composition.

The results of these studies indicate that the practical use of modern technologies in the manufacture of modules makes it possible to expand the temperature range of the thermoelectric method of cooling IR detectors and can ensure their operating temperatures up to 150 – 140 K with sufficient energy efficiency.

In [28] it is shown that the so-called SWaP-C (size, weight, power and cost) characteristics of thermoelectric deep cooling systems for IR sensors can be significantly improved by using FGTM thermoelements. Based on a comparison of the results of experimental studies of homogeneous and

FGTM thermoelements, an increase in the maximum temperature difference by 35 %, an increase in the coefficient of performance by 150 % and a cooling capacity by 200 % is predicted in a single-cascade TEC design, and in multi-cascade designs the maximum difference SWaP-C is expected.

An example of the development and manufacture of a prototype mid-wave IR sensor based on an *In*-doped *PbTe* photodiode with thermoelectric cooling is described in [29, 30]. The advantage of *PbTe* photodiodes is the ability to use them with cooling to temperatures significantly higher than the cryogenic level, namely up to 180 K. The optimal temperature range is 140 – 150 K. Therefore, multi-cascade coolers can be used for them. The physical model of the TEC photodiode system prototype is shown in Fig. 10. The TEC consists of two parts. The low-temperature part is a two-stage module that provides the operating temperature of cooling the photodiode to the level of 140 – 150 K from a temperature of 180 – 200 K. The high-temperature part is a 4-stage module with a cooling temperature of up to 180 K from 300 K.

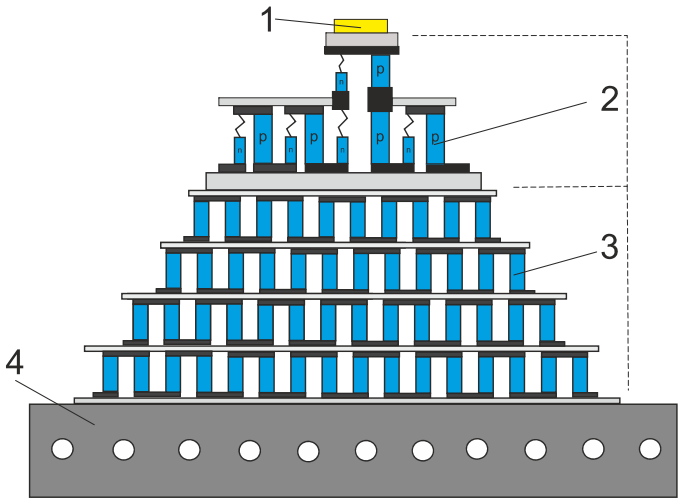

Fig.10. Physical model of the prototype photodiode system with a multi-stage TEC [30].
1- an IR range sensor based on a PbTe photodiode doped with In,
2 – low-temperature two-stage module, 3 – 4-stage module,
4 – heat-exchanger

For the low-temperature module, extruded $Bi_{0.91}Sb_{0.09}$ n-type crystals were used, which demonstrate a high figure of merit $Z \approx 3.5\ 10^{-3}\ K^{-1}$ in the temperature range of 80 – 200 K [31]. The figure of merit of *p*-type *Bi-Sb* alloys is much lower [32], and they cannot be used for thermoelectric coolers in this temperature range. Therefore, *p*-type $(Bi, Sb)_2Te_3$ solid solutions of optimized composition are used.

Due to the large difference in thermal expansion of the p- and n-legs, the rigid design of the two-stage low-temperature module would lead to destruction of the device. Large mechanical stresses of the n-legs are eliminated by their flexible connection with the p-legs. The thermocouple legs have different lengths and cross sections, optimized to achieve maximum figure of merit *Z* of thermocouples at the operating temperatures of each stage. Legs of both types of conductivity are hard soldered to the hot side of each module stage. The cold side of the *p*-type legs is also hard soldered, and the n-legs are connected to the base through a mechanical stress damper, made in the form of a flexible copper bus. The first stage of the TE module consists of four thermocouples with leg sizes: n-leg: 0.7 mm ×1. 4 mm × 2.7 mm; p-leg: 2.4 mm × 1.4 mm × 3.3 mm. The second stage consists of one thermocouple with leg sizes: n-leg: 0.7 mm × 1.4 mm × 2.7 mm; p-leg: 1.8 mm × 1.4 mm × 3.3 mm.

In this design, the length and cross-section of the legs were optimized to obtain thermal and electrical matching of the legs in the module and achieve the maximum coefficient of performance of the device. At the hot temperature of the low-temperature module T_{hot}=180 – 200 K the maximum temperature difference ΔT_{max} = 45 – 50 K and the maximum cooling capacity Q_{max} = 85 – 90 mW are achieved. The electrical power consumption of such a module is 1 – 1.3 W.

For the high-temperature part of the TEC, a standard 4-stage module made of Bi_2Te_3-based materials was used. The module is designed to provide cooling temperatures in the range of 180 – 200 K with a cooling capacity of 1 – 1.3 W. Under these conditions, the power consumption of the 4-stage module is 60 – 90 W.

Thus, in general, such a 6-stage TEC structure can provide cooling of a *PbTe*-based IR detector, the heat release of which does not exceed 10 mW, to a temperature of 140 – 150 K. In this case, the system must be equipped with a heat exchanger with a heat release power of 100 W. In [30], it is proposed to ensure the efficiency of the heat exchanger by using a heat pipe in the design.

Heat removal from TEC for optical-electronic devices plays an important role. Therefore, research is directed towards improving and developing new heat removal systems for cascade TEC. In particular, combined cooling systems for optical-electronic equipment, which include thermoelectric coolers and heat pipes, are common. Work [9] describes a version of such a system developed for aviation infrared technology. The physical model of the system is shown in Fig. 11.

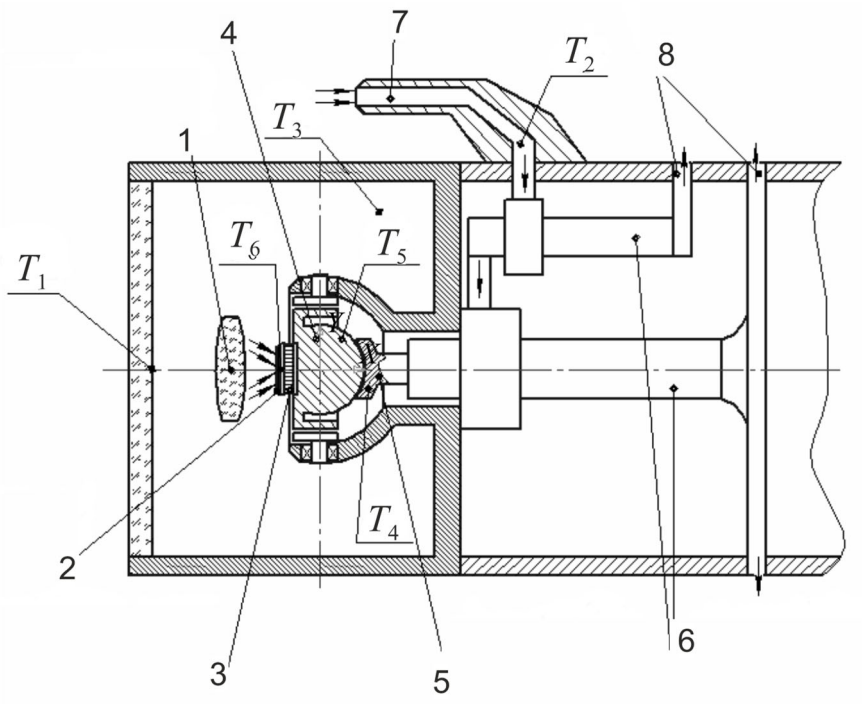

Fig.11. Physical model of the IR detector cooling system based on TEC and heat pipes [9].
1 – lens, 2 – IR detector, 3 – TEC, 4 –base, 5 – heat-dissipating rod,
6- system of vortex tubes, 7 -air intake,
8 – exhaust air outlets

The system includes a 4-stage TEC for the IR detector and vortex tubes. The optical system with an IR detector and a TEC is housed in a sealed case. Heat is transferred to the case base, which, using special thermal bridges, is connected to an unsealed block in which thermal bridge heat sinks are located, blown by atmospheric air cooled in a vortex tube. Such a system stabilizes the sensitive thermoelements

of the IR detector at a level of 200 – 210 K. At the same time, the vortex tube maintains the base temperature at a level of 310 – 330 K.

One of the industrial manufacturers in Europe of IR detectors based on *HgCdTe* with thermoelectric cooling is the company VigoPhotonics[6]. For cooling, small-sized 2, 3 and 4-stage standard thermoelectric modules produced by many companies around the world are used. A traditional physical model is used, namely, the detectors, together with the TEC, are mounted in a special sealed metal case with a window for the entry of IR radiation. The case is filled with a dry mixture of krypton and xenon inert gases, which has low thermal conductivity. To prevent condensation of water vapor, a moisture absorber container is installed in the case. To reduce temperature fluctuations in a detector with a 3- or 4-stage TEC, a screen is installed on the surface between the two lower stages. The TEC parameters (maximum temperature difference Tmax, cooling capacity Qmax, voltage Umax, supply current Imax), which are equipped with IR detectors from VigoPhotonics, are given in Table 2 [6].

Table 2

Parameters of cascade TEC for cooling IR detectors [6]

Parameter	2-stage TEC	3-stage TEC	4-stage TEC
$T_{detector}$, K	~ 230 K	~ 210 K	~ 195 K
Q_{max}, W	0.36	0.27	0.28
ΔT_{max}, K	92	114	125
U_{max}, V	1.3	3.6	8.3
I_{max}, A	1.2	0.45	0.4

To remove the heat generated by a thermoelectric cooler, the use of metal case walls and a screw securing the case to the detector in an IR device is usually not enough. Therefore, the base of the case is fixed to a conventional heat sink. To improve the thermal contact of the base with the heat sink, layers of thermally conductive glue or silicone paste are used. For 2- and 3-stage TECs, it is recommended to use heat sinks with a thermal resistance of ~ 2 K/W; for 4-stage TECs, heat exchangers with a resistance of ~ 1 K/W are advised.

Conclusions

A review of scientific information regarding thermoelectric cooling of optical-electronic devices in the IR spectrum range has shown that despite the variety of physical models of such devices, the most common and used in industrial designs of IR detectors, is the simplest model of a TEC built into a sealed metal case with photosensitive elements that are cooled. 1-, 2-, 3-, and 4-stage TECs made of materials based on Bi_2Te_3, are used, which ensure the operating temperature level of IR devices up to 195 K. Screens can be used to reduce convective and radiative heat load in cascade TECs. Conventional heat sinks are usually used to remove the thermal power generated by the TEC.

The main disadvantage of TEC for optical-electronic devices in the IR range is their low coefficient of performance compared to mechanical cooling methods. Increasing the coefficient of performance and expanding the temperature range of the TEC is an urgent task, the implementation of which is possible with the development and use of new promising thermoelectric materials with increased figure of merit in the low temperature region (up to 140 K).

The energy efficiency of TECs, especially their miniature dimensions with the height of thermoelectric legs less than 0.5 mm, significantly depends on the optimization of its design, which should take into account the electrical and thermal resistances of the contacts, interconnect and insulation plates of the module. These resistances lead to electrical and thermal losses in the efficiency of thermoelectric energy conversion, reduce the coefficient of performance, and are one of the main reasons for the fact that in thermoelectric coolers the properties of materials are not fully realized.

Also, the energy efficiency of the TEC is influenced by the thermal resistance of the IR detector case, its connections to the TEC, heat sinks and heat exchangers, which are used in the system to remove the heat generated by the TEC.

Therefore, the design and optimization of the TEC configuration should be based on the analysis of all system components, taking into account their thermal connection, and the selection of the correct physical model of the optical-electronic system with the TEC is essential in the design of the cooler.

References

1. Rogalski A. (2012). Progress in focal plane arrays technologies. *Progress in Quantum Electronics*, 36, 2 – 3, 342 – 473.
2. Veprik A., Zehtzer S., Vilenchik H. and Pundak N. (2010) Micro-miniature split Stirling linear cryocooler. *AIP Conf. Proc*. 1218, p. 363 – 370.
3. Kinch M.A. (2000). Fundamental physics of infrared detector materials. *J. of Electronic Materials*, 29 (6), 809 – 817.
4. Shtrichman Itay, Aronov Daniel, ben Ezra Michael, et al. (2012). High operating temperature *InSb* and *XBn-InAsSb* photodetectors. *Proceedings of SPIE* Volume 8353, Infrared Technology and Applications XXXVIII, 83532Y, May 1, 2012.
5. Piotrowski A., Piotrowski J., Gawron W., Pawluczyk J. and Pedzinska M. (2009). Extension of usable spectral range of Peltier cooled photodetectors. *ACTA Physica Polonica A*, 116, s-52 – s-55.
6. Vigo Photonics https://vigophotonics.com/ (25 August 2023).
7. Crane D., Madigan B., Bell L. (2022). Path to higher SWaP-C for cooled IR through thermoelectrics with distributed transport properties*, Proc. SPIE 11982 (2022).*
8. Müller R., Gramich V, Wauro M., Niemasz J. et al. (2019). High operating temperature *InAs*/*GaSb* type-II superlattice detectors on GaAs substrate for the long wavelength infrared, *Infrared Physics & Technology* 96, 141 – 144.
9. Molodyk A. V., Smolyar G. A., Lobzin D. V. (2012). Combination of energy transformers as a method for solving the problems of modern instrument making. *J. Thermoelectricity*, 3, 55 – 64.
10. Mongellaz Francois, Fillot A., Griot R., De Lallee J. (1994). Thermoelectric cooler for infrared detectors. *Proc. SPIE 2227, Cryogenic Optical Systems and Instruments VI, (23 June 1994),* p. 156 – 165.
11. Zamboni John M. (2003). Integrated thermoelectric cooler/package for infrared detector array temperature stabilization*. Proc. SPIE 5209, Materials for Infrared Detectors III, (8 December 2003),* p. 173 – 181.
12. Yang R., Chen G., Snyder G.J., Fleurial J.-P. (2002). Multistage thermoelectric micro coolers. *IEEE Proc. of Inter Society Conference on Thermal Phenomena, 2002*, p. 323 – 329.
13. Salinas M. A. (2000). 3-D thermoelectric cooler analysis. *IEEE Proc. of Sixteenth IEEE SEMI-THERM™ Symposium,* p. 10 – 18.

14. Semenyuk V. A. (2003). Advances in development of thermoelectric modules for cooling electro-optic components. *IEEE Proc. of XXII International Conference on Thermoelectrics, 2003*, p. 631 – 636.
15. Semenyuk V. A. (2005). Novel thermoelectric microcoolers compatible with electro-optic components. *Proc. of 3rd International Energy Conversion Engineering Conference, 15 – 18 August 2005, San Francisco, California*.
16. Semenyuk V. A. (2006). Thermoelectric cooling of electro-optic components, in *Thermoelectrics Handbook, Macro to Nano. Edited by D.M. Rowe, CRC Taylor&Francis, 2006,* p. 58-1 – 58-20.
17. Semenyuk. V. A. (2014). Comparison of performance characteristics of multistage thermoelectric coolers based on different ceramic substrates. *J. of Electronic Materials*, 43, 1539 – 1547.
18. Semenyuk V. (2019). Effect of electrical contact resistance on the performance of cascade thermoelectric coolers. *J. of Electronic Materials*, 48 (4), 1870 – 1876.
19. Agaev Z. F., Abdinov D. Sh. (2007). Photodetector with thermoelectric cooler. *Proc. of SPIE, 6636, p. 66360F-1 – 66360F-7.*
20. Wurtz H.P. (1980). Design guidelines for thermoelectrically cooled infrared detectors*, Proc. SPIE 0246, Contemporary Infrared Sensors and Instruments, (3 December 1980)*, p. 15 – 21.
21. Patent US 4 833 889. Thermoelectric refrigeration apparatus. R.W. Harwell, W.M. Simon, 1989.
22. Patent US 4 990 782. Radiation shield for thermoelectrically cooled infrared detectors. W.H. Wellman, R.D. Granneman, 1991.
23. Vuillermet M., Tribolet P. (2010). Operating temperature: a challenge for cooled IR technologies. *Proc. of SPIE, Vol. 7660, 2010.*
24. Klipstein P., Klin O., Grossman S., Snapi N. et al. (2012). High operating temperature *XBn-InAsSb* bariode detectors. *Proc. of SPIE, Vol. 8268, 2012.*
25. Tsao S., Lim H., Zhang W., and Razeghi M. (2007). High operating temperature 320x256 middle-wavelength infrared focal plane array imaging based on an *InAs/InGaAs/InAlAs/InP* quantum dot infrared photodetector. *Applied Physics Letters*, 90, 201109-1 – 201109-3.
26. Anatychuk L. I., Vikhor L. N. (2012). *Thermoelectricity, volume IV. Functionally Graded Thermoelectric Materials.* Institute of Thermoelectricity, Chernivtsi, 2012, 180 p.
27. Anatychuk L. I., Vikhor L. N. (2013). Boundaries of thermoelectric cooling for photodetectors. *J.Thermoelectricity*, 5, 58 – 63.
28. Crane D., Madigan B., Bell L. (2022). Path to higher SWaP-C for cooled IR through thermoelectrics with distributed transport properties. *Proc. SPIE 11982 (2022) Components and Packaging for Laser Systems VIII, p.1198207-1 – 1198207-9.*
29. Gradauskas J., Dzundza B, Chernyak L., Dashevsky Z. (2021). Two-color infrared sensor on the *PbTe*: In *p-n* junction. *Sensors*, 21,1195 1 – 9.
30. Parashchuk T., Sidorenko N., Ivantsov L., et al. (2021). Development of a solid-state multi-stage thermoelectric cooler. *Journal of Power Sources*, 496, 229821-1 – 9.
31. Sidorenko N., Parashchuk T., Maksymuk M., Dashevsky Z. (2020). Development of cryogenic cooler based on n-type Bi-Sb thermoelectric and HTSC. *Cryogenics*, 112 (2020 Dec) p.103197.
32. Sidorenko N.A., Dashevsky Z.M. (2019). Cryogenic thermoelectric cooler for operating temperatures below 90 K. *Semiconductors* 53 (6) (2019 Jun 10), 752 – 755.

Submitted: 15.03.2023

Анатичук Л. І., *акад. НАН України* [1,2]
Вихор Л. М. *док. фіз.-мат. наук* [1]
Маценко І. Д. [2]

[1] Інститут термоелектрики НАН та МОН України,
вул. Науки, 1, Чернівці, 58029, Україна;
[2] Чернівецький національний університет імені Юрія Федьковича,
вул. Коцюбинського 2, Чернівці, 58012, Україна
e-mail: anatych@gmail.com

ФІЗИЧНІ МОДЕЛІ ОПТИКО-ЕЛЕКТРОННИХ СИСТЕМ ІЧ ДІАПАЗОНУ СПЕКТРУ З ТЕРМОЕЛЕКТРИЧНИМ ОХОЛОДЖЕННЯМ
(Огляд)

В роботі розглянуті основні фізичні моделі оптико-електронних систем ІЧ діапазону спектру з термоелектричним охолодженням. Проаналізовані особливості і переваги цих моделей. Встановлено, що найпростішою і такою, що практично застосовується в промислових зразках ІЧ пристроїв, є модель вбудованого в металічний корпус термоелектричного модуля з фоточутливими елементами, які охолоджуються. Така модель з каскадними термоелектричними охолоджувачами (ТЕО) з матеріалів на основі Bi_2Te_3 забезпечує рівень робочих температур ІЧ пристроїв до 195 К. Показано, що розширення діапазону охолодження до температур 140 – 150 К можливе шляхом застосування для ТЕО функціонально-градієнтних матеріалів і додаткових каскадів з низькотемпературних термоелектричних матеріалів, наприклад, з матеріалів на основі BiSb. Встановлено, що енергетична ефективність ТЕО суттєво залежить від оптимізації його конструкції, яка повинна враховувати електричні і теплові опори контактів, комутаційних та ізоляційних пластин, а також вплив теплових опорів корпусу ІЧ приймача, його з'єднань з ТЕО, радіаторів і теплообмінників, які застосовуються в системі для відводу тепла від ТЕО. Отже проєктування ТЕО має враховувати всі компоненти системи і вибір фізичної моделі оптико-електронної системи з ТЕО має важливе значення. Бібл. 32, рис. 11, табл. 2.

Ключові слова: оптико-електронна система, ІЧ пристрій, термоелектричний охолоджувач, фізична модель.

References

1. Rogalski A. (2012). Progress in focal plane arrays technologies. *Progress in Quantum Electronics*, 36, 2 – 3, 342 – 473.
2. Veprik A., Zehtzer S., Vilenchik H. and Pundak N. (2010) Micro-miniature split Stirling linear cryocooler. *AIP Conf. Proc*. 1218, p. 363 – 370.
3. Kinch M.A. (2000). Fundamental physics of infrared detector materials. *J. of Electronic Materials*, 29 (6), 809 – 817.
4. Shtrichman Itay, Aronov Daniel, ben Ezra Michael, et al. (2012). High operating temperature *InSb* and *XBn-InAsSb* photodetectors. *Proceedings of SPIE* Volume 8353, Infrared Technology and Applications XXXVIII, 83532Y, May 1, 2012.

5. Piotrowski A., Piotrowski J., Gawron W., Pawluczyk J. and Pedzinska M. (2009). Extension of usable spectral range of Peltier cooled photodetectors. *ACTA Physica Polonica A*, 116, s-52 – s-55.
6. Vigo Photonics https://vigophotonics.com/ (25 August 2023).
7. Crane D., Madigan B., Bell L. (2022). Path to higher SWaP-C for cooled IR through thermoelectrics with distributed transport properties*, Proc. SPIE 11982 (2022).*
8. Müller R., Gramich V, Wauro M., Niemasz J. et al. (2019). High operating temperature *InAs*/*GaSb* type-II superlattice detectors on GaAs substrate for the long wavelength infrared, *Infrared Physics & Technology* 96, 141 – 144.
9. Molodyk A. V., Smolyar G. A., Lobzin D. V. (2012). Combination of energy transformers as a method for solving the problems of modern instrument making. *J. Thermoelectricity*, 3, 55 – 64.
10. Mongellaz Francois, Fillot A., Griot R., De Lallee J. (1994). Thermoelectric cooler for infrared detectors. *Proc. SPIE 2227, Cryogenic Optical Systems and Instruments VI, (23 June 1994),* p. 156 – 165.
11. Zamboni John M. (2003). Integrated thermoelectric cooler/package for infrared detector array temperature stabilization*. Proc. SPIE 5209, Materials for Infrared Detectors III, (8 December 2003),* p. 173 – 181.
12. Yang R., Chen G., Snyder G.J., Fleurial J.-P. (2002). Multistage thermoelectric micro coolers. *IEEE Proc. of Inter Society Conference on Thermal Phenomena, 2002*, p. 323 – 329.
13. Salinas M. A. (2000). 3-D thermoelectric cooler analysis. *IEEE Proc. of Sixteenth IEEE SEMI-THERM™ Symposium,* p. 10 – 18.
14. Semenyuk V. A. (2003). Advances in development of thermoelectric modules for cooling electro-optic components. *IEEE Proc. of XXII International Conference on Thermoelectrics, 2003*, p. 631 – 636.
15. Semenyuk V. A. (2005). Novel thermoelectric microcoolers compatible with electro-optic components. *Proc. of 3rd International Energy Conversion Engineering Conference, 15 – 18 August 2005, San Francisco, California*.
16. Semenyuk V. A. (2006). Thermoelectric cooling of electro-optic components, in *Thermoelectrics Handbook, Macro to Nano. Edited by D.M. Rowe, CRC Taylor&Francis, 2006,* p. 58-1 – 58-20.
17. Semenyuk. V. A. (2014). Comparison of performance characteristics of multistage thermoelectric coolers based on different ceramic substrates*. J. of Electronic Materials*, 43, 1539 – 1547.
18. Semenyuk V. (2019). Effect of electrical contact resistance on the performance of cascade thermoelectric coolers. *J. of Electronic Materials*, 48 (4), 1870 – 1876.
19. Agaev Z. F., Abdinov D. Sh. (2007). Photodetector with thermoelectric cooler. *Proc. of SPIE, 6636, p. 66360F-1 – 66360F-7.*
20. Wurtz H.P. (1980). Design guidelines for thermoelectrically cooled infrared detectors*, Proc. SPIE 0246, Contemporary Infrared Sensors and Instruments, (3 December 1980)*, p. 15 – 21.
21. Patent US 4 833 889. Thermoelectric refrigeration apparatus. R.W. Harwell, W.M. Simon, 1989.
22. Patent US 4 990 782. Radiation shield for thermoelectrically cooled infrared detectors. W.H. Wellman, R.D. Granneman, 1991.
23. Vuillermet M., Tribolet P. (2010). Operating temperature: a challenge for cooled IR technologies. *Proc. of SPIE, Vol. 7660, 2010.*
24. Klipstein P., Klin O., Grossman S., Snapi N. et al. (2012). High operating temperature *XBn-InAsSb* bariode detectors. *Proc. of SPIE, Vol. 8268, 2012.*

25. Tsao S., Lim H., Zhang W., and Razeghi M. (2007). High operating temperature 320x256 middle-wavelength infrared focal plane array imaging based on an *InAs/InGaAs/InAlAs/InP* quantum dot infrared photodetector. *Applied Physics Letters*, 90, 201109-1 – 201109-3.
26. Anatychuk L. I., Vikhor L. N. (2012). *Thermoelectricity, volume IV. Functionally Graded Thermoelectric Materials.* Institute of Thermoelectricity, Chernivtsi, 2012, 180 p.
27. Anatychuk L. I., Vikhor L. N. (2013). Boundaries of thermoelectric cooling for photodetectors. *J.Thermoelectricity*, 5, 58 – 63.
28. Crane D., Madigan B., Bell L. (2022). Path to higher SWaP-C for cooled IR through thermoelectrics with distributed transport properties. *Proc. SPIE 11982 (2022) Components and Packaging for Laser Systems VIII, p.1198207-1 – 1198207-9.*
29. Gradauskas J., Dzundza B, Chernyak L., Dashevsky Z. (2021). Two-color infrared sensor on the *PbTe*: In *p-n* junction. *Sensors*, 21,1195 1 – 9.
30. Parashchuk T., Sidorenko N., Ivantsov L., et al. (2021). Development of a solid-state multi-stage thermoelectric cooler. *Journal of Power Sources*, 496, 229821-1 – 9.
31. Sidorenko N., Parashchuk T., Maksymuk M., Dashevsky Z. (2020). Development of cryogenic cooler based on n-type Bi-Sb thermoelectric and HTSC. *Cryogenics*, 112 (2020 Dec) p.103197.
32. Sidorenko N. A., Dashevsky Z. M. (2019). Cryogenic thermoelectric cooler for operating temperatures below 90 K. *Semiconductors* 53 (6) (2019 Jun 10), 752 – 755.

Submitted: 15.03.2023

A. O. Snarskii, *doc. phys.– math. science, professor*
I. M. Ivanova, *cand phys – math sciences, assoc. prof.*
V. V. Fedotov, *senior lecturer*

National Technical University of Ukraine
"Ihor Sikorsky Kyiv Polytechnic Institute",
Prospect Beresteiskyi, 37, Kyiv, 03056, Ukraine,
e-mail: *asnarskii@gmail.com*

THERMOELECTRIC COMPOSITES AND RECIPROCITY RELATIONS

The effective kinetic coefficients in macro-inhomogeneous media, their behavior when changing the concentration of component phases and setting the percolation threshold are considered. Combinations of the effective kinetic coefficients were found for which the reciprocity relations are fulfilled. Bibl. 7, Fig. 4, Tabl. 6.
Key words: kinetic coefficients, two-phase medium, single-flow systems, thermoEMF.

Introduction

The main charactreristic of randomly inhomogeneous media are effective kinetic coefficients. When describing, for instance, electrical conductivity - σ_e, when Ohm's law applies

$$\mathbf{j} = \sigma \mathbf{E} . \tag{1}$$

Where $\mathbf{j}$ – electric current density and – $\mathbf{E}$ – electric field strength, and local conductivity $\sigma(\mathbf{r})$, where $\langle ... \rangle = 1/V \int ...dV$ is volume average and in case of a two-phase medium the conductivity in the first phase acquires the value σ_1, and in the second phase σ_2. The effective conductivity σ_e is defined as

$$\langle \mathbf{j} \rangle = \sigma_e \langle \mathbf{E} \rangle , \tag{2}$$

A huge number of articles and monographs [1 – 5] are devoted to the calculation of the effective properties of such media, in particular, the calculation of the effective conductivity, thermoEMF and elastic properties. One of the successful approximate methods that describe the effective conductivity well is the Bruggeman-Landauer approximation [6 – 7], which is often called the mean field approximation - MAE. For effective conductivity, it has the form

$$\frac{\sigma_e - \sigma_1}{2\sigma_e + \sigma_1} p + \frac{\sigma_e - \sigma_2}{2\sigma_e + \sigma_2}(1 - p) = 0 . \tag{3}$$

Where σ_1 and σ_2 are the values of conductivity in the first and second phases.

Now let us turn to thermoelectric phenomena. We shall write down the equations interrelating the electric current density - $\mathbf{j}$, the heat flux - $\mathbf{q}$ and the electric field strength $\mathbf{E}$, as well as the temperature gradient $\mathbf{g} = -gradT$ as follows

$$\mathbf{j} = \sigma\mathbf{E} + \gamma\mathbf{g},$$

$$\mathbf{s} = \gamma\mathbf{E} + \chi\mathbf{g}, \tag{4}$$

where $\gamma = \sigma\alpha$, α is thermoemf, $\chi = \kappa/T$, κ is thermal conductivity and for convenience (symmetry in system (4)) the flux $\mathbf{s} = \mathbf{q}/T$ is introduced.

The effective kinetic coefficients of the thermoelectric system will have the form

$$\langle\mathbf{j}\rangle = \sigma_e\langle\mathbf{E}\rangle + \gamma_e\langle\mathbf{g}\rangle,$$

$$\langle\mathbf{s}\rangle = \gamma_e\langle\mathbf{E}\rangle + \chi_e\langle\mathbf{g}\rangle, \tag{5}$$

As it was shown in [8], the task of calculating effective thermoelectric coefficients can be reduced (in certain cases) to the task of determining the effective electrical conductivity in a system where there are no thermoelectric phenomena. In other words, if we know the solution for the effective coefficient in a single-flow system, we can find out the solution for the effective kinetic coefficients in a two-flow system (for example, with the joint flow of interconnected electric current and heat flux). Later on, this method, called the method of isomorphism, was written in various mathematical versions and generalized to various problems [9 – 11].

Reciprocity relations for single-flow (conductivity) system

There is a special class of two-dimensional two-phase media such that the effective conductivity (1) is isotropic and that when the local conductivities of the phases are interchanged, the effective conductivity remains unchanged. One of the many examples of the deterministic structure of such media is a checkerboard, where black cells are one phase, white cells are another, other examples are given in [12]. Randomly inhomogeneous media with half concentration of phases also belongs to this class of media. As was precisely shown in [13, 14], the effective conductivity of such a medium is equal to

$$\sigma_e = \sqrt{\sigma_1\sigma_2}\ . \tag{6}$$

In the case when in randomly inhomogeneous media the concentration of phases is $p = 1/2$, the reciprocity relation holds [13, 14]

$$\sigma_e(p)\cdot\sigma_e(1-p) = \sigma_1\sigma_2, \tag{7}$$

that is, the product of two functions that depend on the concentration $\sigma_e(p)\cdot\sigma_e(1-p)$ is concentration-independent

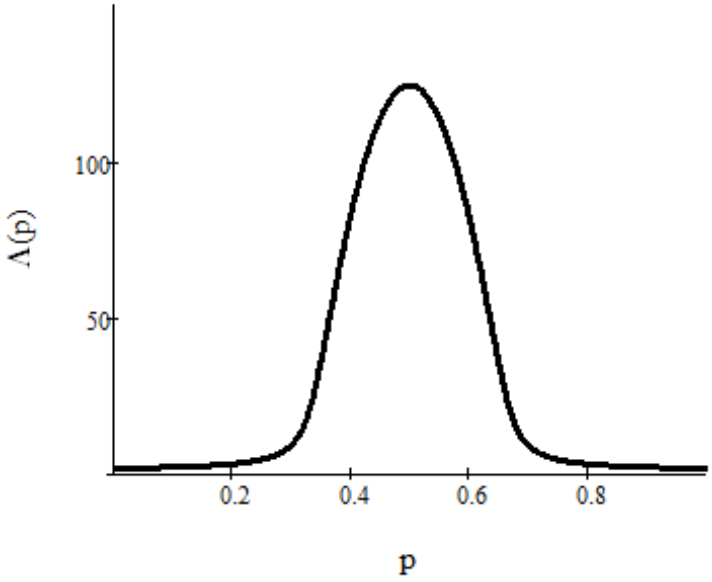

Fig. 1. Concentration dependence of the product of effective conductivities in a three-dimensional random-inhomogeneous medium. For example, $\sigma_1 = 1,\ \sigma_2 = 10^{-2}$ *is selected (in conventional units)*

The analysis of this behavior of randomly inhomogeneous two-phase media by the approximate method of the mean field theory - MAE gives the same result.

Naturally, in randomly inhomogeneous three-dimensional media, as shown in Fig. 1, there is no such behavior.

For the concentration dependence of the effective conductivity, there is a specific parameter - p_c. With great heterogeneity, that is, with a large value of the phase conductance ratio $\sigma_1 / \sigma_2 >> 1$, the effective conductivity experiences a sharp change in behavior during the passage of the concentration through the so-called percolation threshold A sharp change in the behavior of effective conductivity is associated with the appearance in the medium of the so-called infinite cluster, a continuous path along one of the phases through the entire system [1, 5]. In the framework of the mean field approximation - MAE it has the value of the percolation threshold in the three-dimensional case $p_c = 1/3$, and in the two-dimensional case $p_c = 1/2$. At the same time, different values of percolation threshold are observed in different real composites. In this regard, in [15] a modification of MAE was proposed, which allows describing three-dimensional composites with a predetermined percolation threshold $\tilde{p}_c$, not necessarily equal to 1/3.

$$\frac{\frac{\sigma_e - \sigma_1}{2\sigma_e + \sigma_1}}{1 + c(p, \tilde{p}_c)\frac{\sigma_e - \sigma_1}{2\sigma_e + \sigma_1}} p + \frac{\frac{\sigma_e - \sigma_2}{2\sigma_e + \sigma_2}}{1 + c(p, \tilde{p}_c)\frac{\sigma_e - \sigma_2}{2\sigma_e + \sigma_2}} (1 - p) = 0, \tag{8}$$

where $c(p, \tilde{p}_c)$ is the Sarychev-Vinogradov term

$$c(p,\tilde{p}_c)=(1-3\tilde{p}_c)\left(\frac{p}{\tilde{p}_c}\right)^{\tilde{p}_c}\left(\frac{1-p}{1-\tilde{p}_c}\right)^{1-\tilde{p}_c}. \quad (9)$$

Later, this approach, which uses the introduction of some term in the Bruggeman-Landauer equation, was generalized to the two-dimensional case, to anisotropic structures, and to describe elastic phenomena [16 – 19].

In the future, we will explore the possibility of the existence of reciprocity relations between media with different percolation thresholds.

Reciprocity relations for the effective kinetic coefficients of thermoelectric composites

To analyze the behavior of the effective kinetic coefficients in thermoelectric media, we use the isomorphism method [20]. Let us first consider the two-dimensional case. In the absence of thermoelectric phenomena (i.e., at $\alpha_1=0,\ \alpha_2=0$) the system degenerates into two mutually incoherent relations - Ohm's law and Fourier's law, while for each of their effective coefficients (effective conductivity and thermal conductivity) the reciprocity relations are satisfied. In the presence of thermoelectric phenomena, the reciprocity relations are not fulfilled. As can be seen from Fig. 2, the normalized products of effective conductivities and thermoelectric coefficients are no longer constant with a change in concentration

$$\Lambda\sigma(p)=\frac{\sigma_e(p)\sigma_e(1-p)}{\left[\sigma_e(p_c=1/2)\right]^2},\ \Lambda\alpha(p)=\frac{\alpha_e(p)\alpha_e(1-p)}{\left[\alpha_e(p_c=1/2)\right]^2} \quad (10)$$

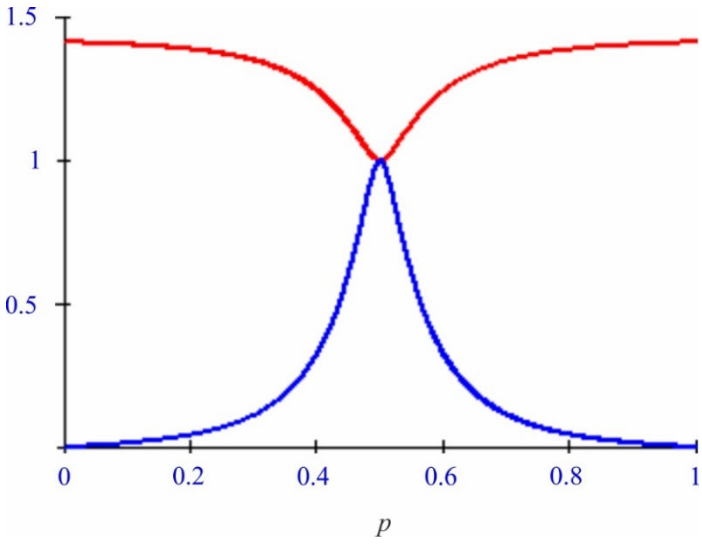

Fig. 2. Two-dimensional case. Concentration dependence of normalized products of conductivity and thermoelectric coefficients - $\Lambda\sigma(p)$ - upper curve and $\Lambda\alpha(p)$ - lower curve. For example, the following values of local kinetic coefficients were chosen: $\sigma_1=5\cdot10^7\,\mathrm{Ohm}^{-1}m^{-1}$, $\chi_1=0.1\,W/m$, $\alpha_1=0\ V/K$, $\sigma_2=3.207\cdot10^4\ Ohm^{-1}m^{-1}$, $\chi_2=3.3\cdot10^{-3}W/m$, $\gamma_2=6.414\ V/K$, $T=300\ K$

Thus, in thermoelectric systems, the effective kinetic coefficients individually do not satisfy the reciprocity relations. However, as the isomorphism method states, the two-flow problem is reduced to a

single-flow problem, with one effective kinetic coefficient for which, naturally, the reciprocity relation must hold. This means that it is possible, using isomorphism “in the opposite direction” (moving from a single-flow system to a two-flow system), to find those combinations of effective kinetic coefficients for which a reciprocity relation will take place in a two-flow system.

Isomorphism method

Here we will turn to the version proposed by A. Dykhne [20] (see [5] for details).

We will reduce the local two-flow system (4) to a single-flow system, for this we will add the first equation (4) to the second multiplied by some constant K

$$\mathbf{j} + K\mathbf{s} = (\sigma + K\gamma)\mathbf{E} + (\gamma + K\chi)\mathbf{g}, \tag{11}$$

where σ, α, γ and χ are coordinate-dependent and acquire the values $\sigma_1, \gamma_1, \chi_1$ – in the first and $\sigma_2, \gamma_2, \chi_2$ – in the second phases.

Rewriting (11) in the form

$$\mathbf{j} + K\mathbf{s} = (\sigma + K\gamma)\left(\mathbf{E} + \frac{\gamma + K\chi}{\sigma + K\gamma}\mathbf{g}\right) \tag{12}$$

we can introduce a new “current” $\mathbf{i}$ and a new field $\boldsymbol{\varepsilon}$

$$\mathbf{i} = \mathbf{j} + K\mathbf{s}, \quad \boldsymbol{\varepsilon} = \mathbf{E} + \frac{\gamma + K\chi}{\sigma + K\gamma}\mathbf{g}. \tag{13}$$

In the stationary case under consideration, for fields and currents the following equations hold

$$div\mathbf{j} = 0, \quad div\mathbf{s} = 0, \quad rot\mathbf{E} = 0, \quad rot\mathbf{g} = 0 \tag{14}$$

The new «field»- $\boldsymbol{\varepsilon}$ and «current»- $\mathbf{i}$ must obey similar equations

$$div\mathbf{i} = 0, \quad rot\boldsymbol{\varepsilon} = 0, \tag{15}$$

which define a single-flow system

$$\mathbf{i} = f \cdot \boldsymbol{\varepsilon}, \tag{16}$$

where $f(\mathbf{r})$ is the kinetic coefficient of a new single-flow system (an analog to conductivity).

To fulfill equations (15), it is necessary that the factor near $\mathbf{g}$ does not depend on the coordinates, that is, that it has the same value in both phases - we denote it by ω. This requirement can be written as follows

$$\frac{\gamma_1 + K\chi_1}{\sigma_1 + K\gamma_1} = \frac{\gamma_2 + K\chi_2}{\sigma_2 + K\gamma_2} = \omega. \tag{17}$$

Equation (17) defines two possible values for the constants K and ω

$$K_{1,2}=\frac{\chi_2\sigma_1-\chi_1\sigma_2\pm\sqrt{\left(\chi_2\sigma_1-\chi_1\sigma_2\right)^2-4\left(\chi_1\gamma_2-\chi_2\gamma_1\right)\left(\gamma_1\sigma_2-\gamma_2\sigma_1\right)}}{2\left(\chi_1\gamma_2-\chi_2\gamma_1\right)} \tag{18}$$

Writing similar (12, 13, 16) equations for averaged fields and currents, we obtain, in particular, the averaged Ohm's law (for a single-flow medium)

$$\langle\mathbf{i}\rangle=f^e\langle\boldsymbol{\varepsilon}\rangle, \tag{19}$$

where now the role of local conductivity in the first and second phases σ_1,σ_2 will be played by conductivities μ_1,μ_2

$$\mu_1=\sigma_1+K\gamma_1,\qquad \mu_2=\sigma_2+K\gamma_2\ . \tag{20}$$

It should be noted that there are two pairs of local effective kinetic coefficients μ_1 and μ_2, that depend on K_1 and one pair μ_1 and μ_2, that depends on K_2.

Thus, given that two values of the constant are possible (18), law (16) can be written as follows

$$\begin{aligned}\langle\mathbf{j}\rangle+K_1\langle\mathbf{s}\rangle&=f_1^e\left(\langle\mathbf{E}\rangle+\omega_1\langle\mathbf{g}\rangle\right),\\ \langle\mathbf{j}\rangle+K_2\langle\mathbf{s}\rangle&=f_2^e\left(\langle\mathbf{E}\rangle+\omega_2\langle\mathbf{g}\rangle\right),\end{aligned} \tag{21}$$

where it is taken into account that constant ω similar to constant K can take on two values and

$$f_1^e=f^e\left(\mu_1,\mu_2,K_1,\omega_1\right),\qquad f_2^e=f^e\left(\mu_1,\mu_2,K_2,\omega_2\right). \tag{22}$$

Now we find from (22) the expressions for $\langle\mathbf{j}\rangle$ and $\langle\mathbf{s}\rangle$

$$\begin{aligned}\langle\mathbf{j}\rangle&=\frac{K_2f_1^e-K_1f_2^e}{K_2-K_2}\langle\mathbf{E}\rangle+\frac{K_2f_1^e\omega_1-K_1f_2^e\omega_2}{K_2-K_2}\langle\mathbf{g}\rangle,\\ \langle\mathbf{s}\rangle&=\frac{f_1^e-f_2^e}{K_2-K_2}\langle\mathbf{E}\rangle+\frac{f_1^e\omega_1-f_2^e\omega_2}{K_2-K_2}\langle\mathbf{g}\rangle\end{aligned} \tag{23}$$

Thus, knowing the dependence of the effective kinetic coefficients of a single-flow system on the local kinetic coefficients and concentration, it is possible to obtain similar dependences for the effective kinetic coefficients of a thermoelectric (two-flow) system from (23). Indeed, comparing (23) and (5), σ_e,α_e and χ_e can be written as

$$\sigma_e=\frac{K_2f_1^e-K_1f_2^e}{K_2-K_2},\qquad \alpha_e=\frac{K_2f_1^e\omega_1-K_1f_2^e\omega_2}{K_2f_1^e-K_1f_2^e},\qquad \chi_e=\frac{f_1^e\omega_1-f_2^e\omega_2}{K_2-K_2}\ . \tag{24}$$

Reciprocity relations of thermoelectric composites

The isomorphism method described above explains why the effective kinetic coefficients do not directly give the reciprocity relation. According to [14], the reciprocity relations hold for single-flow two-dimensional randomly heterogeneous media. In this case, for the single-flow system (16), they must be present for the effective coefficients f_1^e and f_2^e and we write them in the form

$$\begin{aligned} f^e\left(\mu_1,\mu_2,K_1,p\right)\cdot f^e\left(\mu_1,\mu_2,K_1,1-p\right)&=f^e\left(\mu_1,\mu_2,K_1,1/2\right)^2,\\ f^e\left(\mu_1,\mu_2,K_2,p\right)\cdot f^e\left(\mu_1,\mu_2,K_2,1-p\right)&=f^e\left(\mu_1,\mu_2,K_2,1/2\right)^2 \end{aligned} \tag{25}$$

or in abbreviated notations

$$f_1^e\left(p\right)\cdot f_1^e\left(1-p\right)=f_1^e\left(1/2\right)^2,\qquad f_2^e\left(p\right)\cdot f_2^e\left(1-p\right)=f_2^e\left(1/2\right)^2. \tag{26}$$

Thus, the effective kinetic coefficients of thermoelectric systems are a function of local kinetic coefficients, found constants (18), effective coefficients of single-flow systems $f_1^e\left(p\right),\quad f_2^e\left(p\right)$.

Let us now use (24) and find the expressions for $f_1^e\left(p\right),\quad f_2^e\left(p\right)$ through the effective kinetic coefficients of thermoelectric systems, for instance, in the form

$$f_1^e\left(p\right)=\sigma_e+K_1\sigma_e\alpha_e,\qquad f_2^e\left(p\right)=\sigma_e+K_2\sigma_e\alpha_e. \tag{27}$$

According to (26) and (27) we can write the reciprocity relations for the effective kinetic coefficients of thermoelectric system for K_1

$$\sigma_e\left(p\right)\left[1+K_1\alpha_e\left(p\right)\right]\cdot\sigma_e\left(1-p\right)\left[1+K_1\alpha_e\left(1-p\right)\right]=const \tag{28}$$

And similarly for the second case of constant K_2

$$\sigma_e\left(p\right)\left[1+K_2\alpha_e\left(p\right)\right]\cdot\sigma_e\left(1-p\right)\left[1+K_2\alpha_e\left(1-p\right)\right]=const \tag{29}$$

Numerical analysis for two-dimensional thermoelectric systems

Let us consider several specific examples of the behavior of the effective kinetic coefficients and reciprocity relations. To do this, we normalize expressions (27 - 28) (recall that for the two-dimensional case in the standard MAE approximation the percolation threshold is equal to $p_c=1/2$)

$$\begin{aligned} \Lambda_1\left(p\right)&=\frac{\sigma_e\left(p\right)\left[1+K_1\alpha_e\left(p\right)\right]\cdot\sigma_e\left(1-p\right)\left[1+K_1\alpha_e\left(1-p\right)\right]}{\left\{\sigma_e\left(p\right)\left[1+K_1\alpha_e\left(p\right)\right]\right\}^2},\\ \Lambda_2\left(p\right)&=\frac{\sigma_e\left(p\right)\left[1+K_2\alpha_e\left(p\right)\right]\cdot\sigma_e\left(1-p\right)\left[1+K_2\alpha_e\left(1-p\right)\right]}{\left\{\sigma_e\left(p\right)\left[1+K_2\alpha_e\left(p\right)\right]\right\}^2}. \end{aligned} \tag{30}$$

The expressions f^e will be found in the two-dimensional MAE approximation for a single-flow system

$$\frac{\dfrac{f_e-\mu_1}{f_e+\mu_1}}{1+c(p,\tilde{p}_c)\dfrac{f_e-\mu_1}{f_e+\mu_1}}p+\frac{\dfrac{f_e-\mu_2}{f_e+\mu_2}}{1+c(p,\tilde{p}_c)\dfrac{f_e-\mu_2}{f_e+\mu_2}}(1-p)=0, \tag{31}$$

where in the two-dimensional case the term similar to the Sarychev-Vinogradov term has the form

$$c(p,\tilde{p}_c)=(1-2\tilde{p}_c)U(\mu_1,\mu_2)\left(\frac{p}{\tilde{p}_c}\right)^{\tilde{p}_c}\left(\frac{1-p}{1-\tilde{p}_c}\right)^{1-\tilde{p}_c}, \tag{32}$$

and

$$U(\mu_1,\mu_2)=\begin{cases}1, & \mu_1>\mu_2\\ 0, & \mu_1=\mu_2\\ -1, & \mu_1<\mu_2\end{cases} \tag{33}$$

Substituting the obtained f_1^e and f_2^e in (20), we find $\Lambda_1(p)$ and $\Lambda_2(p)$. Fig.3 shows the concentration behaviour of $\Lambda\sigma(p)$, $\Lambda\alpha(p)$ and $\Lambda_1(p)$ from (10) and (30). Naturally, in (10) there is the effective conductivity from (24). As can be seen from the figure, the functions $\Lambda\sigma(p)$, $\Lambda\alpha(p)$ depend on the concentration, in contrast to $\Lambda_1(p)$, which is practically independent of the concentration, which can be called one of the reciprocity relations for thermoelectric phenomena.

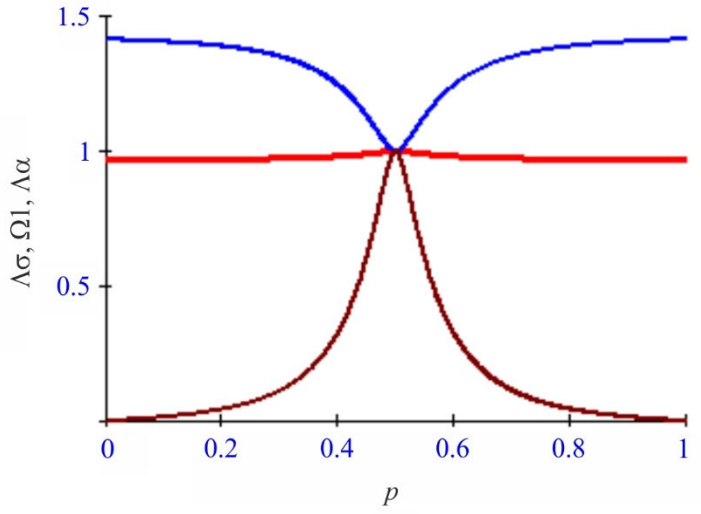

Fig.3 Concentration dependences $\Lambda\sigma(p)$, $\Lambda\alpha(p)$ and $\Lambda_1(p)$ with an unshifted percolation threshold $\tilde{p}_c=1/2$. For example, the following values of local kinetic coefficients were chosen:

$$\sigma_1=5\cdot10^7\,Ohm^{-1}m^{-1},\ \chi_1=0.1\,W/m,\ \alpha_1=0\ V/\mathrm{K},\ \sigma_2=3.207\cdot10^4\ Ohm^{-1}m^{-1},$$

$$\chi_2=3.3\cdot10^{-3}\ W/m,\ \gamma_2=6.414\,V/K,\ T=300\ K$$

Note that when the percolation threshold shifts, that is, even with a small deviation of $\tilde{p}_c$ from 1/2, the expression $\Lambda_1(p)$ (and, of course, $\Lambda_2(p)$), which was constant, begins to significantly depend on the concentration.

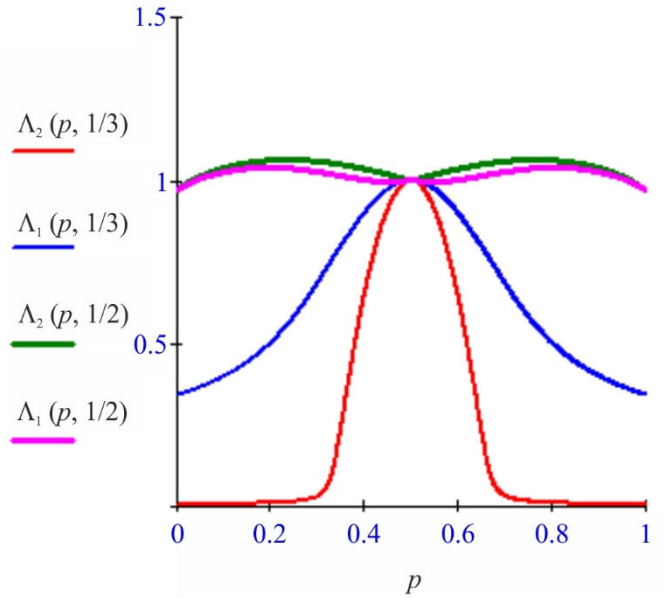

Fig. 4 Concentration dependences $\Lambda_2(p, p_c = 1/2), \Lambda_1(p, p_c = 1/2)$, $\Lambda_1(p, p_c = 1/3), \Lambda_2(p, p_c = 1/3)$ - *top down*

In the three-dimensional case, when (8) and (9) hold, the products (30) for the unshifted percolation threshold, i.e. when $\tilde{p}_c = 1/3$, cease to be independent of the concentration, which is natural in general, since a strong dependence on the concentration is also observed in the single-flow case - Fig. 4. However, when the percolation threshold is shifted, when choosing $\tilde{p}_c = 1/2$ the reciprocity relations are approximately fulfilled. The three-dimensional case deserves a separate detailed analysis.

Conclusions

The reciprocity relations written for the effective conductivity (single-flow system) can be generalized to the case of thermoelectric phenomena in the two-dimensional case. In the three-dimensional form, the canonical mean field theory (Bruggeman-Landauer approximation) shows that there are no such relations. In the case of a shifted percolation threshold, in the three-dimensional case, although approximate, the reciprocity relations take place.

References

1. Torquato S. (2002). *Random heterogeneous materials. Microstructure and macroscopic properties*, Springer Verlag: New York, USA. doi: 10.1115/1.1483342
2. Balagurov B. Ya. (2015). Electrophysical properties in composites. Leland.
3. Andrianov I. V., Awrejcewicz J., Danishevskyy V. V. (2018). *Asymptotical mechanics of composites*, Springer: Cham, Germany. doi: 10.1007/978-3-319-65786-8
4. Choy T. C. (2016). *Effective medium theory: principles and applications*, Oxford University Press: Oxford, UK. doi:10.1093/acprof:oso/9780198705093.001.0001

5. Snarskii A., Bezsudnov I. V., Sevryukov V. A., Morozovskiy A., Malinsky J. (2016). *Transport processes in macroscopically disordered media. From mean field theory to percolation*. Springer Verlag: New York, USA. doi: 10.1007/978-1-4419-8291-9.
6. Bruggeman V. D. (1935). Berechnung verschiedener physikalischer Konstanten von heterogenen Substanzen. I. Dielektrizitätskonstanten und Leitfähigkeiten der Mischkörper aus isotropen Substanzen. *Ann. Phys*. *(Leipzig)*, 1935, *416*, 664. doi: 10.1002/andp.19354160705
7. Landauer R. (1952). The electrical resistance of binary metallic mixtures. *J. Appl. Phys.* 1952, *23*, 784. doi:10.1063/1.1702301
8. Straley J. P. (1981). Thermoelectric properties of inhomogeneous materials. *Journal of Physics D: Applied Physics*, *14* (11), 2101.
9. Halpern V. (1983). *J.Phys.C*, 16, 7, L217.
10. Bergman D. J., & Levy O. (1991). Thermoelectric properties of a composite medium. *Journal of Applied Physics*, *70* (11), 6821 – 6833.
11. Webman I., Jortner J., & Cohen M. H. (1977). Thermoelectric power in inhomogeneous materials. *Physical Review B*, *16* (6), 2959.
12. Snarskii A. A. (2004). Effective conductivity of 2D macroscopic heterogeneous self-dual media. *Laser physics*, *14* (3), 337 – 343.
13. Keller, J. B. (1964). A theorem on the conductivity of a composite medium. *Journal of Mathematical Physics*, *5* (4), 548 – 549.
14. Dykhne A. M. (1971). Conductivity of a two-dimensional two-phase system. *Sov. Phys. JETP*, *32* (1), 63 – 65.
15. Sarychev A. K., Vinogradov A. P. (1983). Effective medium theory for the magnetoconductivity tensor of disordered material. *phys. stat. sol. (b), 117*, K113-K118. doi: 10.1002/pssb.2221170252
16. Snarskii A. A., Shamonin M., & Yuskevich P. (2021). Effect of magnetic-field-induced restructuring on the elastic properties of magnetoactive elastomers. *Journal of Magnetism and Magnetic Materials*, *517*, 167392.
17. Snarskii A. A., Shamonin M., Yuskevich P., Saveliev D. V., & Belyaeva I. A. (2020). Induced anisotropy in composite materials with reconfigurable microstructure: Effective medium model with movable percolation threshold. *Physica A: Statistical Mechanics and its Applications*, *560*, 125170.
18. Snarskii A. A., Zorinets D., Shamonin M., & Kalita V. M. (2019). Theoretical method for calculation of effective properties of composite materials with reconfigurable microstructure: Electric and magnetic phenomena. *Physica A: Statistical Mechanics and its Applications*, *535*, 122467.
19. Bodnaruk A. V., Kalita V. M., Kulyk M. M., Lozenko A. F., Ryabchenko S. M., Snarskii A. A., & Shamonin M. (2019). Temperature blocking and magnetization of magnetoactive elastomers. *Journal of Magnetism and Magnetic Materials*, *471*, 464-467
20. Dykhne A. M. (1971). Private communication 1980.

Submitted: 21.03.2023

Снарський О. А., *док. фіз.- мат. наук, професор*
Іванова І. М., *канд. фіз-мат.наук, доцент*
Федотов В. В., *старший викладач*

Національний технічний університет України "Київський політехнічний інститут імені Ігоря Сікорського", Берестейський проспект, 37, Київ, 03056, Україна
e-mail: asnarskii@gmail.com

ТЕРМОЕЛЕКТРИЧНІ КОМПОЗИТИ ТА СПІВВІДНОШЕННЯ ВЗАЄМНОСТІ

Розглянуто ефективні кінетичні коефіцієнти у макронеоднорідних середовищах, їхня поведінка при зміні концентрації фаз компонентів та завданні порога протікання. Знайдено комбінації ефективних кінетичних коефіцієнтів, за яких виконуються співвідношення взаємності. Бібл. 20, рис. 4.

Ключові слова: кінетичні коефіцієнти, двофазне середовище, однопотокові системи, термоЕРС.

References

1. Torquato S. (2002). *Random heterogeneous materials. Microstructure and macroscopic properties*, Springer Verlag: New York, USA. doi: 10.1115/1.1483342
2. Balagurov B. Ya. (2015). Electrophysical properties in composites. Leland.
3. Andrianov I. V., Awrejcewicz J., Danishevskyy V. V. (2018). *Asymptotical mechanics of composites*, Springer: Cham, Germany. doi: 10.1007/978-3-319-65786-8
4. Choy T. C. (2016). *Effective medium theory: principles and applications*, Oxford University Press: Oxford, UK. doi:10.1093/acprof:oso/9780198705093.001.0001
5. Snarskii A., Bezsudnov I. V., Sevryukov V. A., Morozovskiy A., Malinsky J. (2016). *Transport processes in macroscopically disordered media. From mean field theory to percolation.* Springer Verlag: New York, USA. doi: 10.1007/978-1-4419-8291-9.
6. Bruggeman V. D. (1935). Berechnung verschiedener physikalischer Konstanten von heterogenen Substanzen. I. Dielektrizitätskonstanten und Leitfähigkeiten der Mischkörper aus isotropen Substanzen. *Ann. Phys. (Leipzig)*, 1935, *416*, 664. doi: 10.1002/andp.19354160705
7. Landauer R. (1952). The electrical resistance of binary metallic mixtures. *J. Appl. Phys.* 1952, *23*, 784. doi:10.1063/1.1702301
8. Straley J. P. (1981). Thermoelectric properties of inhomogeneous materials. *Journal of Physics D: Applied Physics*, *14* (11), 2101.
9. Halpern V. (1983). *J.Phys.C*, 16, 7, L217.
10. Bergman D. J., & Levy O. (1991). Thermoelectric properties of a composite medium. *Journal of Applied Physics*, *70* (11), 6821 – 6833.
11. Webman I., Jortner J., & Cohen M. H. (1977). Thermoelectric power in inhomogeneous materials. *Physical Review B*, *16* (6), 2959.
12. Snarskii A. A. (2004). Effective conductivity of 2D macroscopic heterogeneous self-dual media. *Laser physics*, *14* (3), 337 – 343.

13. Keller, J. B. (1964). A theorem on the conductivity of a composite medium. *Journal of Mathematical Physics*, *5* (4), 548 – 549.
14. Dykhne A. M. (1971). Conductivity of a two-dimensional two-phase system. *Sov. Phys. JETP*, *32* (1), 63 – 65.
15. Sarychev A. K., Vinogradov A. P. (1983). Effective medium theory for the magnetoconductivity tensor of disordered material. *phys. stat. sol. (b), 117*, K113-K118. doi: 10.1002/pssb.2221170252
16. Snarskii A. A., Shamonin M., & Yuskevich P. (2021). Effect of magnetic-field-induced restructuring on the elastic properties of magnetoactive elastomers. *Journal of Magnetism and Magnetic Materials*, *517*, 167392.
17. Snarskii A. A., Shamonin M., Yuskevich P., Saveliev D. V., & Belyaeva I. A. (2020). Induced anisotropy in composite materials with reconfigurable microstructure: Effective medium model with movable percolation threshold. *Physica A: Statistical Mechanics and its Applications*, *560*, 125170.
18. Snarskii A. A., Zorinets D., Shamonin M., & Kalita V. M. (2019). Theoretical method for calculation of effective properties of composite materials with reconfigurable microstructure: Electric and magnetic phenomena. *Physica A: Statistical Mechanics and its Applications*, *535*, 122467.
19. Bodnaruk A. V., Kalita V. M., Kulyk M. M., Lozenko A. F., Ryabchenko S. M., Snarskii A. A., & Shamonin M. (2019). Temperature blocking and magnetization of magnetoactive elastomers. *Journal of Magnetism and Magnetic Materials*, *471*, 464-467
20. Dykhne A. M. (1971). Private communication 1980.

Submitted: 21.03.2023

P. V. Gorskiy

P. V. Gorskyi *dok. phys.– mat. sciences*[1,2]

[1]Institute of Thermoelectricity of the NAS
and MES of Ukraine,
1, Nauky str., Chernivtsi, 58029, Ukraine,
e-mail: gena.grim@gmail.com
[2]Yu.Fedkovych Chernivtsi National University,
2, Kotsiubynskyi str., Chernivtsi, 58012, Ukraine

PROBABILITY THEORY OF DEGRADATION OF THERMOELECTRTIC ENERGY CONVERTERS AND ITS USE TO DETERMINE THE RELIABILITY OF THERMOELECTRIC MATERIALS

A probabilistic theory of degradation of thermoelectric energy converters has been developed, which describes such stages of their life cycle as the run-in period, which is described by the Weibull function, the period of stable operation, during which the failure rate is not necessarily constant, and the period of mass failures. To correctly describe these stages, the theory introduced the limit resource of a thermoelectric energy converter, which is consumed over time according to a nonlinear law and is precisely determined by the limit capabilities of thermoelectric and other materials, as well as contact structures. But this limit resource is a generalized integral characteristic of the limit resource capabilities of all materials used to create a thermoelectric energy converter and cannot be unambiguously "distributed" between them. After its complete consumption, there is a complete loss of performance of the thermoelectric energy converter. The parameters of the theory are determined by the least squares method based on processing the results of life tests. By combining the results obtained with a diffusion-nonmonotonic distribution of failure times, the parameters of which are also determined by the least squares method, it is possible to obtain such integral indicators of the reliability of materials as the average limit resource, 95 % limit resource, the minimum achievable equivalent failure rate and relative errors, in this case – with a confidence probability of 0.95.). Bibl. 7, Fig. 2, Tabl. 2.

Key words: probability theory of degradation of thermoelectric energy converters; limit resource of thermoelectric energy converter as the average limit resource of thermoelectric materials; 95 % limit resource of thermoelectric materials; minimum achievable equivalent failure rate, relative errors in their determination

Introduction

The theory of degradation of thermoelectric energy converters outlined in this article, suitable for determining their reliability indicators, can be exclusively probabilistic, since justified procedures and techniques for introducing random factors into a purely deterministic description of physical phenomena and processes that determine failures do not exist today [1]. The purpose of the article is the development of this theory and its application to the calculation of reliability indicators of thermoelectric materials and thermoelectric energy converters.

The simplest form of such a theory is the currently widely used linear theory of relative

parameter degradation, which is widely used in microelectronics [2].

Description and mathematical form of the theory

In its most general form, the developed generalized probabilistic theory of degradation of thermoelectric energy converters takes into account the following aspects of the physics of their failures.

1. There is such a threshold time τ, prior to which failures do not occur.
2. Gross technological defects in the manufacture of thermoelectric energy converters are rejected the fastest, that is, there is a "run-in period", during which degradation of the thermoelectric energy converter occurs according to Weibull's law.
3. There is a limit resource of a thermoelectric energy converter, which is consumed over time according to a nonlinear law.
4. Therefore, the mathematical form of the developed theory is as follows:

$$V(t) = V_0 \exp\left(- \frac{\left(\frac{t-\tau}{t_0} \right)^{\alpha}}{\gamma \left(1 - \frac{t}{t_0} \right)^{\beta}} \right) \tag{1}$$

where $V(t)$ is time-dependent parameter – suitability criterion of thermoelectric energy converter (most often output power or efficiency), t_0 is limit resource, α is parameter of Weibull's – distribution shape, γ is scale parameter β is indicator of nonlinearity of limit resource consumption, τ is threshold time.

However, in a partial case $-\tau = 0$ $t_0 \to \infty$ we will get the simplest partial modification of the developed theory, which is based on Weibull's law, namely:

$$V(t) = V_0 \exp\left(- \left(\frac{t}{t_s} \right)^{\alpha} \right) \tag{2}$$

where

$$t_s = t_0 \gamma^{1/\alpha} \tag{3}$$

This is the simplest modification of the developed theory which turns into a linear one at $\alpha = 1$ and $t << t_s$.

This is the simplest modification of the developed theory, which does not take into account the presence of a finite limit resource of thermoelectric energy converters, and was used to predict the results of life tests of thermoelectric energy converters in the absence of their obvious failures when they lose 20 % and 90 % of the output power [3 – 5]. Based on the results of this forecasting, a function of the probability of failure-free operation was first built in tabular form for a selected

sample of thermoelectric energy converters relative to their loss of 20 % of the output power. And after that, the obtained data were smoothed by the least squares method, following which the most plausible estimates of the parameters of the diffusion-nonmonotonic law of failure times distribution were determined and then - reliability indicators and relative errors of their determination. This law was developed by the Institute of Mathematical Machine Problems of the National Academy of Sciences of Ukraine and standardized in the DSTU project 300495 “Reliability of equipment. Methods of estimating reliability indicators based on experimental data”. Therefore, with the use of the simplest modification of the developed probabilistic theory of degradation of thermoelectric energy converters, the following indicators of their reliability and relative errors of their determination with a confidence probability of 0.99 were obtained: mean time between failures (MTBF) 11770 h with a relative error of 11.9 %, 95 % resource 9170 h with a relative error of 26.5 %. Therefore, with the use of the simplest modification of the developed probabilistic theory of degradation of thermoelectric energy converters, the following indicators of their reliability and relative errors of their determination with a confidence probability of 0.99 were obtained: mean time between failures (MTBF) 11770 h with a relative error of 11.9 %, 95 % resource 9170 h with a relative error 26.5 %. The equivalent failure rate constant was $\lambda = 8.172 \cdot 10^{-5}$ h^{-1} with a relative error of 10.5 %.

At first glance, this failure rate may seem significant, but it should be taken into account that each of the tested thermoelectric energy converters consists of 127 series connected thermoelements. And from this it follows that the equivalent failure rate of one thermoelement in the mode of electrical energy generation is $6.435 \cdot 10^{-7}$ h^{-1}, which is approximately 3.1 times less than the minimum value given in [6], which is equal to $2 \cdot 10^{-6}$ h^{-1}

On the other hand, the calculation of the reliability indicators of thermoelectric energy converters relative to their loss of 90 % of power or efficiency was necessary because the initial modification of the developed generalized probabilistic theory of degradation of thermoelectric energy converters did not assume the presence of their limit resource. And among others, we were faced with the task of comparing the reliability of thermoelectric energy converters with different electrical connection circuits for thermoelements. And the formulation of such a problem itself is relevant and meaningful when, in the case of a purely series circuit for connection of thermoelements, loss of integrity of at least one thermoelectric leg is possible. In this case, if we do not consider options for shunting or special protection of thermoelectric legs or transition from a purely series circuit of their connection to a parallel, series-in-parallel or parallel-in-series circuit, then it turns out that the loss of the integrity of at least one leg leads to a complete failure of the thermoelectric energy converter as a whole. In this case, the breakdown of the electrical circuit of a leg can be either instantaneous and caused by its destruction as a whole due to the action of thermomechanical stresses caused by cyclic temperature effects or purely mechanical stresses caused by accelerations or shock loads. The specific values of these stresses and their distribution in the bulk of the thermoelectric leg are determined by one or another method of material resistance within the framework of the corresponding physical models. After that, with the use of certain modifications of the Weibull approach, the established stress distribution is associated with the probability of destruction of the thermoelectric leg. Further, it is assumed that all thermoelectric legs, without exception, which are part of the thermoelectric energy converter, are considered to be the same and to fail with equal probability. Without such an assumption, calculations are dramatically complicated.

But the destruction of the electrical circuit of one or more legs can occur gradually during the functioning of the thermoelectric energy converter in the operating mode. The main factor of such destruction can be, for example, the gradual accumulation of cavities and cracks in the transient contact layer due to the formation of intermetallic compounds. In particular, such processes can determine the limit resource of the thermoelectric energy converter, which appears in formula (1).

Determination of theory parameters

The parameters of the theory are determined for each of the thermoelectric energy converters subjected to life tests using the least squares method based on experimental data on the time change in the output power of each of them.

Determination of the predicted time of failures of thermoelectric energy converters

The advantage of the developed probabilistic theory of degradation of thermoelectric energy converters is that given one or another sign of failure, determined by the scientific and technical documentation for products or by agreement with the customer, we can determine the standardized reliability indicators of thermoelectric energy converters even in the absence of their obvious failures during operation. In this case, we considered a loss of 20 % of the initial power of each of the tested thermoelectric energy converters as a failure. Therefore, determining the failure time of each module from formula (1) and ordering the obtained times in ascending order, we obtained the following table of the probability of failure-free operation of the tested thermoelectric energy converters:

Table 1

Table of the probability of failure-free operation of thermoelectric energy converters, when a loss of 20 % of their output power is considered a failure

t, *h*	9390	10020	11160	11250	15600
$P(t)$	0.8	0.6	0.4	0.2	0

Reliability models for determining reliability indicators of thermoelectric materials and energy converters

«"Diffusion-nonmonotonic" reliability model for determining standardized reliability indicators of thermoelectric energy converters

Then, based on the diffusion-nonmonotonic distribution of failure times, the most plausible estimates whose parameters are determined by processing table (1) by the least squares method, the following estimates of the standardized reliability indicators of the tested energy converters with respect to a 20 % loss of generated power are obtained: mean time between failures (MTBF) 11480 h with a relative error of 15.3 % at a confidence probability of 0.95, 95 % resource 7702 h with a relative error of 33.5 % at the same confidence probability and an equivalent constant failure rate $\lambda = 7.716 \cdot 10^{-5}$ h^{-1} with relative error of 15.1 % for the same confidence probability. Hence, the equivalent constant failure rate of one thermoelement is equal to $6.03 \cdot 10^{-7}$ h^{-1}, which is approximately 3 times greater than the experimental value given in [6].

Determination of the limit resource of thermoelectric energy converters and integral indicators of the reliability of thermoelectric materials

Now we will consider the complete loss of functionality of the module as a sign of failure. In this case, we will get the following table of the probability of trouble-free operation:

Table 2

Table of the probability of failure-free operation of thermoelectric energy converters for the case when the failure is considered to be a drop in the output power to zero

t, h	$2.624 \cdot 10^6$	$2.934 \cdot 10^6$	$2.992 \cdot 10^6$	$3.335 \cdot 10^6$
$P(t)$	0.75	0.5	0.25	0

And in this case, based on the diffusion-nonmonotonic distribution of failure times, the most plausible estimates of whose parameters are determined by the least squares method, the following estimates of the standardized reliability indicators of the tested energy converters relative to complete failure are obtained: average limit resource (MTBF) $2.91 \cdot 10^6$ h with a relative error of 5.3 % at a confidence probability of 0.95, 95 %, a limit resource of $2.61 \cdot 10^6$ h with a relative error of 12.9 % at the same trust probability and the minimum achievable failure rate $\lambda = 3.38 \cdot 10^{-6}$ h^{-1} with a relative error of 15.1 % for the same confidence probability. Hence, the equivalent constant failure rate of one thermoelement is equal to $2.64 \cdot 10^{-8}$ h^{-1}

But failures during a significant period of operation which consist in the complete loss of efficiency of thermoelectric converters and resource indicators determined on their basis can be interpreted as indicators of resource stability of least stable materials, or integral indicators of resource stability of materials that are part of a thermoelectric energy converter. But based only on the results of life tests, it is impossible to "separate" the mentioned indicators by individual materials. That is why they are called integral.

However, such an interpretation is at least qualitatively consistent with the results of work [7], which shows that, for example, the processes of diffusion of nickel into the thermoelectric material do not lead to a significant change in the efficiency of thermoelements in the mode of generating electrical energy even for 50 years, i.e. 438300 h, if they are not accompanied by the formation of intermetallic compounds.

It is also consistent with the results of work [8], which shows that if thermoelectric legs based on bismuth telluride are protected so that the flow of sublimated tellurium atoms through their surface does not exceed $7.5 \cdot 10^{15} m^{-2} s^{-1}$, then the complete depletion of a thermoelectric leg with a length of 1.5 mm based on bismuth telluride doped with an excess of tellurium will occur no earlier than in 100 years, i.e. 876,600 hours.

In this way, it is possible to introduce the following integral indicators of resource stability of materials that are part of thermoelectric energy converters: the average limit resource, which is equal to $2.91 \cdot 10^6$ h with a relative error of 5.3 % with a confidence probability of 0.95, 95 %, the limit resource, which is equal to $2.61 \cdot 10^6$ h with a relative error of 12.9% for the same confidence probability and the equivalent minimally achievable constant failure rate, which is equal to $\lambda = 3.38 \cdot 10^{-6}$ h^{-1} with a relative error of 15.1 % for the same confidence probability.

The results of these calculations are illustrated in Figs.1, 2

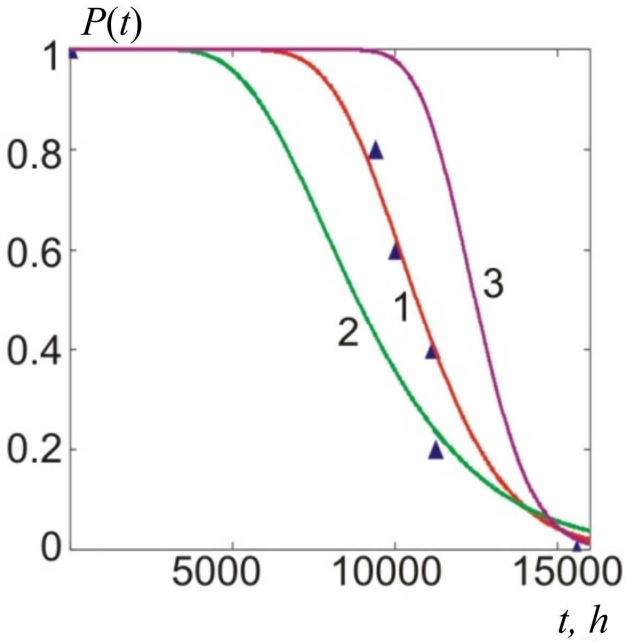

Fig. 1. Dependences of the probability of saving 80% of the output power of thermoelectric energy converters on the time of operation: 1 – the most probable in accordance with the diffusion-nonmonotonic of the distribution of failure times, 2, 3 – limit at a confidence probability of 0.95, triangles –the result of predicting the time of saving 80 % of the output power according to the probabilistic theory of degradation

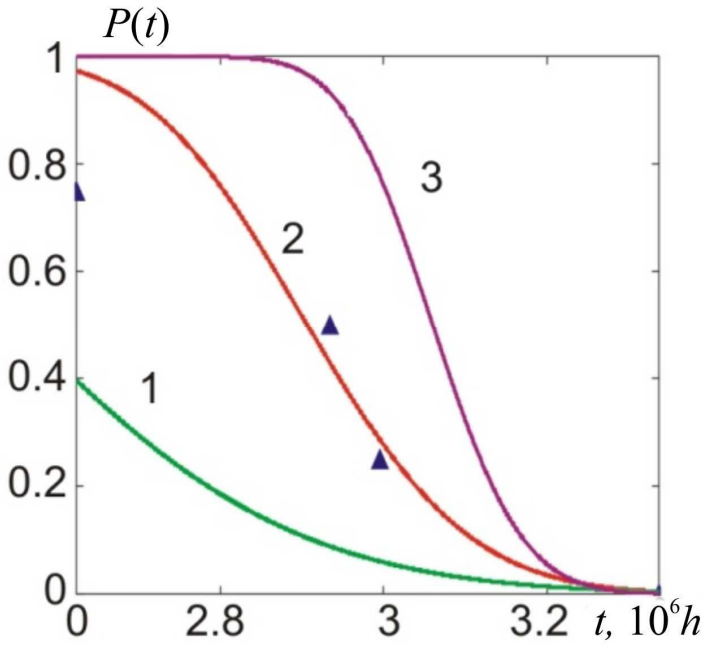

Fig. 2. Dependences of the probability of realization of a certain limit resource of thermoelectric energy converters on the value of this resource: 1 – the most probable in accordance with the diffusion-monotonic law of the distribution of failure time, 2, 3 – limit with a confidence probability of 0.95, triangles– the results of predicting the limit resource according to the probabilistic theory of degradation

Conclusions and recommendations

1. A generalized probabilistic theory of degradation of thermoelectric energy converters has been developed, which covers such periods of their operation as the run-in period, the period of stable operation, and the period of mass failures.
2. Run-in within the framework of the developed theory is described by Weibull's law.
3. The theory explicitly takes into account the limit resource of thermoelectric energy converters, which is consumed over time according to a non-linear law and is determined by the resource capabilities of the least resource-resistant materials.
4. The theory also predicts the existence of a threshold time prior to which failures do not occur.
5. The developed theory, being combined with the diffusion-nonmonotonic law of failure time distribution, allows, based on the results of life tests with acceptable accuracy and an acceptable confidence level, to calculate reliability indicators of thermoelectric energy converters even with a small volume of the test sample and even in the case when there are no obvious failures during testing.
6. As a result of applying the developed theory to processing the results of resource tests of thermoelectric energy converters, the following indicators of their reliability were obtained:
   - average run-in with preservation of 80 % of output power (MTBF) 11.480 h with a relative error of 15.3 % at a confidence level of 0.95; 95 % resource of preservation of 80 % of output power 7702 h with a relative error of 33.5 % for the same confidence probability; and the equivalent constant failure rate $\lambda = 7.716 \cdot 10\text{-}5$ h-1 with a relative error of 15.1 % for the same confidence probability. Hence, the equivalent constant failure rate of one thermoelement is equal to $6.03 \cdot 10^{-7}$ h.$^{-1}$;
   - average run-in to complete failure (MTBF) or the average limit resource $2.91 \cdot 10^{6}$ h with a relative error of 5.3 % at a confidence probability of 0.95, a 95 % resource of $2.57 \cdot 10^{6}$ h with a relative error of 12.9 % at the same confidence probability and the minimum achievable failure rate $\lambda = 3.38 \cdot 10^{-6}$ h^{-1} with a relative error of 15.1 % for the same confidence probability. Hence, the equivalent constant failure rate of one thermoelement is equal to $2.64 \cdot 10^{-8}$ h^{-1}.
7. The obtained results can be used for the research of accelerated tests.

References

1. Anatychuk L. I., Luste O. (2017). Model studies of degradation mechanisms of thermoelectric materials and contact structures. *J.Thermoelectricity*, 4, 62 – 88.
2. Gorskyi P. V. (2022). Peculiarities of determining reliability indicators of thermoelectric generator modules based on experimental data. *Technology and Design in Electronic Equipment*, 1-3, 50 – 56. http://dx.doi.org/10.15222/TKEA2022.1-3.50.
3. Gorskyi P. V. (2022). Comparison of the reliability of thermoelectric generator modules with different circuits of electric connection of thermoelements. *Technology and Design in Electronic Equipment,* 1 – 3, 59 – 64. http://dx.doi.org/10.15222/TKEA2022.4-6.59.
4. Gorskyi P. V. Peculiarities of determining reliability indicators of thermoelectric generator modules. In: *Proceedings of the XXII International Scientific and Practical Conference of the ISPC CIET-XXII Odesa – 2022, May 23 – 27. – P. 38 – 39.*
5. G. K. Kotyrlo (1980). *Raschiot i konstruirovaniie termoelektricheskikh generatorov i teplovykh nasosov. Spravochnik. [Calculation and design of thermoelectric generators and heat pumps. Handbook]*. Kyiv: Naukova dumka.

6. Gorskyi P. V. (2023). Do thermoelectric generator modules degrade due to nickel diffusion. *Technology and Design in Electronic Equipment*, 3-3-4, 59 – 64. http://dx.doi.org/10.15222/TKEA2023.3-4-.59.
7. Sublimation of volatile component as a possible mechanism of thermoelectric material degradation. (2022). *Physics and Chemistry of the Solid State*, 23, 204 – 209. DOI:1015330/pcss23.2.204-209

Submitted: 18.04.2023

Горський П. В., *док. фіз.-мат. наук*[1,2]

[1] Інститут термоелектрики НАН та МОН України,
вул. Науки 1, Чернівці, 58029, Україна;
[2] Чернівецький національний університет імені Юрія Федьковича,
вул. Коцюбинського 2, Чернівці, 58012, Україна
e-mail: gena.grim@gmail.com

ІМОВІРНІСНА ТЕОРІЯ ДЕГРАДАЦІЇ ТЕРМОЕЛЕКТРИЧНИХ ПЕРЕТВОРЮВАЧІВ ЕНЕРГІЇ ТА ЇЇ ВИКОРИСТАННЯ ДЛЯ ВИЗНАЧЕННЯ НАДІЙНОСТІ ТЕРМОЕЛЕКТРИЧНИХ МАТЕРІАЛІВ

Розроблено імовірнісну теорію деградації термоелектричних перетворювачів енергії яка описує такі етапи їх життєвого циклу, як період припрацювання, який описується функцією Вейбула, період стабільного функціонування, на якому інтенсивність відмов не обов'язково є сталою та період масових відмов. Для коректного опису вказаних етапів у теорію введено граничний ресурс термоелектричного перетворювача енергії,який витрачається з часом за нелінійним законом і якраз і визначається граничними можливостями термоелектричних та інших матеріалів а також контактних структур. Але цей граничний ресурс є узагальненою інтегральною характеристикою граничних ресурсних можливостей всіх матеріалів, використаних при створенні термоелектричного перетворювача енергії і не може бути однозначно «розподілений» між ними. Після його повної витрати настає повна втрата працездатності термоелектричного перетворювача енергії. Параметри теорії визначаються методом найменших квадратів на основі обробки результатів ресурсних випробувань. Об'єднуючи отримані результати з дифіузійно-немонотонним розподілом часу відмов,параметри якого також визначаються методом найменших квадратів, можна отримати такі інтегральні показники надійності матеріалів, як середній граничний ресурс, 95 % граничний ресурс мінімальну досяжну еквівалентну інтенсивність відмов та відносні похибки їх визначення (у даному випадку – за довірчої ймовірності 0.95). Бібл. 7, рис. 2, табл. 2.

Ключові слова: ймовірнісна теорія деградації термоелектричних перетворювачів енергії, Граничний ресурс термоелектричного перетворювача енергії, як середній граничний ресурс термоелектричних матеріалів, 95 % граничний ресурс термоелектричних матеріалів, мінімальна досяжна еквівалентна інтенсивність відмов, відносні похибки їх визначення.

References

1. Anatychuk L.I., Luste O. (2017). Model studies of degradation mechanisms of thermoelectric materials and contact structures. *J.Thermoelectricity*, 4, 62 – 88.
2. Gorskyi P.V. (2022). Peculiarities of determining reliability indicators of thermoelectric generator modules based on experimental data. *Technology and Design in Electronic Equipment*, 1-3, 50 – 56. http://dx.doi.org/10.15222/TKEA2022.1-3.50.
3. Gorskyi P.V. (2022). Comparison of the reliability of thermoelectric generator modules with different circuits of electric connection of thermoelements. *Technology and Design in Electronic Equipment,* 1 – 3, 59 – 64. http://dx.doi.org/10.15222/TKEA2022.4-6.59.
4. Gorskyi P.V. Peculiarities of determining reliability indicators of thermoelectric generator modules. In: *Proceedings of the XXII International Scientific and Practical Conference of the ISPC CIET-XXII Odesa – 2022, May 23 – 27. – P. 38 – 39.*
5. G.K. Kotyrlo (1980). *Raschiot i konstruirovaniie termoelektricheskikh generatorov i teplovykh nasosov. Spravochnik. [Calculation and design of thermoelectric generators and heat pumps. Handbook]*. Kyiv: Naukova dumka.
6. Gorskyi P.V. (2023). Do thermoelectric generator modules degrade due to nickel diffusion. *Technology and Design in Electronic Equipment*, 3-3-4, 59 – 64. http://dx.doi.org/10.15222/TKEA2023.3-4-.59.
7. Sublimation of volatile component as a possible mechanism of thermoelectric material degradation. (2022). *Physics and Chemistry of the Solid State*, 23, 204 – 209. DOI:1015330/pcss23.2.204-209

Submitted: 18.04.2023

Anatychuk L. I.

L. I. Anatychuk, *acad. National Academy of Sciences of Ukraine*[1,2]
M. M. Korop [1]

[1] Institute of Thermoelectricity of the NAS and MES of Ukraine,
1 Nauky str., Chernivtsi, 58029, Ukraine;
e-mail: anatych@gmail.com, mykola.korop@chnu.edu.ua
[2] Yuriy Fedkovych Chernivtsi National University, 2 Kotsiubynskyi str., Chernivtsi, 58000, Ukraine
e-mail: anatych@gmail.com

Korop M. M.

APPLICATION OF MACHINE LEARNING TO PREDICT THE PROPERTIES OF Bi_2Te_3-BASED THERMOELECTRIC MATERIALS

The paper provides examples of assessing the effectiveness of machine learning for predicting the properties of Bi_2Te_3-based thermoelectric materials. The results of their application and methods for selecting optimal input data parameters are considered, the differences and features of choosing algorithms, the stages of work and training machine models, as well as the criteria for assessing the effectiveness and validation of the obtained forecasts are described. Bibl. 18, Fig. 1, Tabl. 3.
Key words: machine learning methods, thermoelectric materials science.

Introduction

General characterization of the problem. Thermoelectric materials, which serve as the basis for machine-free thermal energy into electrical energy conversion, are gaining more and more popularity and practical application. One of the main criteria for evaluating promising materials is the quality factor Z proposed by Joffe, which can be expressed using formula 1:

$$ZT = \alpha^2 \frac{\sigma T}{\chi}, \quad (1)$$

where α is the Seebeck coefficient, σ is electrical conductivity, T is temperature, χ is thermal conductivity.

One of the most popular thermoelectric materials is Bi_2Te_3, the high figure of merit of which was achieved based on physical observations and an empirical approach. The increase in Z for this material occurred through the use of isovalent impurities, owing to which a decrease in χ (thermal conductivity) is achieved without a significant change in σ (electrical conductivity). During the following decades, further significant increase in the figure of merit did not occur, so the search for new methods and approaches is important.

In materials science, machine methods of optimizing materials and achieving their extreme values are of increasing interest. Machine learning is considered a subspecies of artificial intelligence that allows generalization, interpolation and extrapolation of input data, search for patterns and operating information in a more intelligent way. The main task of machine learning in predicting the properties of thermoelectric materials is to find the most accurate values with the smallest error, based on a limited amount of input data, which serve as a source of information obtained using both theoretical calculations and experimental measurements. Therefore, the question was raised to study how effective machine learning is for its application in thermoelectric materials science and to consider a number of works on its application.

The purpose of the work is to study the efficiency of machine learning methods in the task of predicting and optimizing the properties of Bi_2Te_3-based thermoelectric materials.

Supervised machine learning methods for Bi_2Te_3

Supervised machine learning methods are one of the main types of machine learning, where "supervised" means that the learning process is based on data with labels (absolute values) of the desired variable. Such methods are often used to solve problems of regression (predicting a numerical value) or classification (assigning data to their category). The accuracy and efficiency of such methods heavily depends on the quality of the training data and avoiding the risk of overtraining the model (having adapted to the input data, the model stops generalizing the information received and making accurate predictions for new data that the model has not previously received).

The following controlled machine learning algorithms have been used in scientific works devoted to solving problems of materials science: linear regression, logistic regression, decision trees, random forest, support vector machines, neural networks. Each of the algorithms has its own advantages and areas of application, and one of the main factors of choosing among them is the achievement of the highest accuracy under the given conditions [2].

Regression algorithms of machine learning

In the field of machine learning, regression algorithms are statistical methods that make a numerical prediction for a dependent variable based on its dependence on one or more independent variables.

For example, when predicting the *ZT* (thermoelectric figure of merit) value, it (the *ZT* value) will act as a dependent variable, and the input data of temperature, electrical conductivity, and Seebeck coefficient will act as independent variables.

There are a number of approaches to solving regression problems: linear regression, logistic regression, polynomial, Ridge regression, and Lasso regression [15]. Such models are relatively easy to learn, do not require large computing power, but contain limitations in the ability to generalize only simple dependences.

Linear regression models detect a linear relationship between *x* and *y* based on an input statistical data set. The mathematical representation of such a model can be described using formula 2.

$$y = b + \sum_{i=1}^{n} w_i * x_i, \tag{2}$$

where *y* is the predicted value of the dependent variable;
b (bias) is an absolute value that allows the model to account for bias in the output values that cannot

be explained by the independent variables; *w* is the weighting factor, which indicates how much the change in the independent variable *x* explains the change in the dependent variable *y*.

Polynomial regression models are designed to find non-linear relationships between input and output values. Such models are able to generalize more complex cases and are described using formula 3.

$$y = b + \sum_{i=0}^{n} w_i * x_i^i, \tag{3}$$

The risk of using polynomial regression is that the model will overtrain with high values of *n*, high prediction accuracy on training data, and low accuracy with new data and difficulty in explaining the trained model.

One of the main reasons for overtraining the model is too large values of the coefficients in equations 2 and 3 for the input parameters (weights) and a small amount of training data. To solve the problem of insufficient training data, data expansion methods can be used, namely: introducing noise for numerical values, changing the size, brightness for images, etc. Here, the term "noise" should be understood as random errors or variations to the original data - they allow providing training data to the input of the model that are as close as possible to real values. In the case of retraining the model, as a precautionary measure, regularization is used, which is a control method and adds additional constraints on the model weights. This includes L_1 (Lasso), L_2 (Ridge), or a combination of these regularizations.

At each stage of model training, cost functions are applied to achieve maximum accuracy. Their main task is to estimate the model error during training to adjust the coefficients (weights) so that this error is minimal. For regression problems, the root mean square error is often used, which is described by formula 4. Based on the values of the cost function, gradients are calculated to calculate new weights for each training step.

$$\sigma = \frac{\sum_{i=1}^{n}(x_i - y_i)^2}{n}, \tag{4}$$

where *x* is the exact value, *y* is the value predicted by the model.

Thus, the L_1 and L_2 regularizations mentioned above act as additional terms that are added to the cost function during model training. L_1 regularization adds absolute values of weights for certain descriptors, thereby changing them to 0 for parameters that are insignificant. L_2 regularization adds squared weights to the cost function, thereby "penalizing" the model for large weight values.

A practical way to apply supervised machine learning methods

The organization of the learning process of an artificial intelligence model can be represented as the following list of actions.

1. **Collection of training data:** at this stage, primary data (independent variables) are collected, which can be expressed by numerical values (crystal structure, chemical formula, average atomic number, etc.) or categorical values [3]. Dependent values (labels) that represent the outcome or class to be predicted are obtained from theoretical calculations or experimental measurements.
2. **Pre-processing of data:** aims to improve the quality of collected data, find and remove noise, missing or incorrect data. Categorization and coding of data or their normalization is carried out [4].
3. **Selection of the model algorithm:** is carried out on the basis of prepared data in such a way as to achieve the set goals and obtain the highest accuracy. The selection process is highly dependent on the task at hand and the input data set. Evaluation of input data, presence of noise, number of

functions, degree of linearity between variables, trade-off between complexity and efficiency of the model, minimizing the possibility of retraining the model.

4. **Training of the selected model and optimization**: adjustments (weights, thresholds, etc.) to achieve accuracy targets and minimize errors.
5. **Evaluation of the performance of trained model:** the goal is to identify and correct problems that arose during the training process, for example, accurate work with training data and incorrect work with new sets of input data.
6. **Testing of the resulting model**: carried out to determine its accuracy and efficiency.

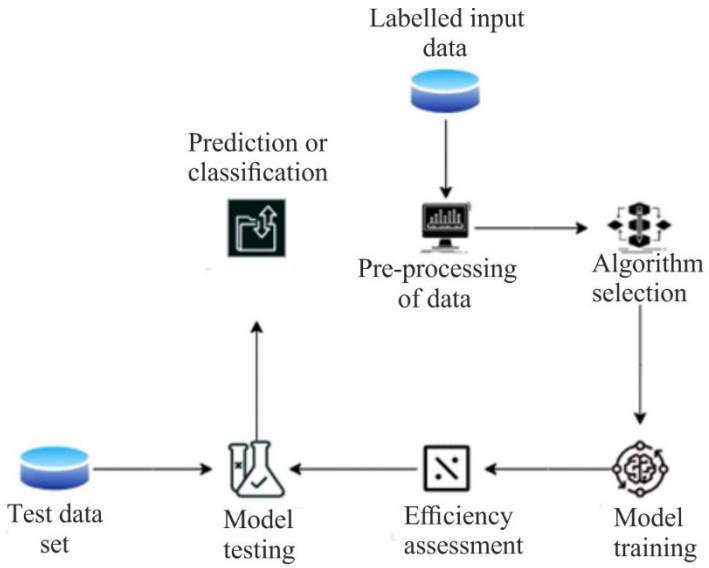

Fig. 1. Scheme of application of a supervised machine learning method

Wudil, Y. et al. [1] carried out work on predicting the quality factor of Bi_2Te_3-based materials using the lattice structure constants (a and c) and the electrical properties of the materials as predictors. The input data was generated based on a number of experimental works, from which the transport properties and crystal lattice parameters were taken. Also, to generalize the model, the results were formed both for the pure material and for the material with impurities. Two intensively researched compounds of *n*-type $Bi_2Te_{2.7}Se_{0.3}$ and *p*-type $Bi_{1.5}Sb_{0.5}Te_3$ were taken into account. The final data set contained 280 data points.

5 parameters were selected as descriptors: Seebeck coefficient, electrical conductivity, temperature, lattice dimensions (a, c). These parameters were selected by finding the interdependence of the target value and the input data, determined using the Pearson correlation coefficient. The choice of lattice parameters is expedient due to the dependence of the structural parameters of the lattice on the methods of manufacturing the material.

Parv Katyal, et al.[5] in their study set themselves the goal of determining algorithms and methods of machine learning that can work with a limited set of input data to establish interdependences between the *ZT* coefficient and the chemical and physical properties of compounds Bi_2Te_3, $CoSb_3$, $Ba_8Ga_{16}Ge_{30}$. To train the artificial intelligence, a data set of 1098 calculated points was used, in this set the *ZT* values were obtained at different temperatures. The descriptors chosen were: temperature, Seebeck coefficient, power factor, cell volume, resistance, total mass of one cell, average atomic volume, space group,

symmetry elements. The data set was divided randomly in the proportion of 80 % training data and 20 % testing data. For machine learning, the random forest method was selected, which is an ensemble method that consists of constructing several decision trees during training and as a result of calculating the average prediction of individual trees [6]. The authors of [5] divided the data set into 500 decision trees and calculated the average value of the results of all trees.

Zhi-Lei Wang, et al. [7] conducted a study to predict the properties of extruded $Cu_xBi_2Te_{2.85}Se_{0.15}$ samples using machine learning. A data set of seven experimental data sets and 12 characteristics were used: composition, relative density, orientation factor, average grain size, microstructural feature, grain boundary characteristics, charge carrier concentration, mobility, Seebeck coefficient, electrical resistance, thermal conductivity. An artificial neural network with one hidden layer was selected as the modeling algorithm, the sigmoid function was applied as the activation function, and the hyperparameters hidden layer node size and weight reduction were optimized using Bayesian optimization at a learning rate of 0.01. To avoid overtraining of the model, the input data was divided in the proportion of 60 % - training and 40 % - test using 4-fold cross-validation [8]. Cross-validation helps reduce the risk of model overtraining by dividing the data set into several equal or nearly equal parts. After this, the model is trained on all parts of the data, and the last part is left for testing. This process is repeated several times, each time selecting a different part as the test set. As a result, average indicators are calculated and an overall performance rating is found.

Qu, R. [16] investigates the thermal conductivity properties of $MnBi_2Te_4$ and $Bi_2Te_3/MnBi_2Te_4$ superlattice by applying a deep neural network (DNNP) using data obtained using density functional theory. Using DFT calculations, datasets containing atomic configurations, corresponding energies and forces, and temperatures (ranging from 200 K to 500 K) were prepared for model training. For training reliability, 1200 configurations were prepared, divided evenly across the specified temperature range, providing a comprehensive representation of the class space of the system. The DNNP model was structured with an embedded layer followed by three hidden layers, each with 160 nodes. This architecture was chosen to effectively capture the complexity of atomic interactions in the materials being studied. The training process was carefully configured, optimizing loss functions and hyperparameters to minimize the error between DNNP predictions and DFT calculations.

Research by Agarwal A. et al. [17] discusses a method for predicting the thermoelectric power factor for Bi_2Te_3 material during a powder bed laser melting (PBF-LB) process using machine learning techniques for additive manufacturing (AM). Additive manufacturing (AM) refers to a group of technologies that create objects by adding material layer by layer, based on digital 3D models. Unlike traditional subtractive manufacturing methods, which start with a solid stock and then cut away the excess to create the part, AM builds parts directly from the raw material layer by layer, which minimizes waste and allows the creation of complex geometries that would be difficult or impossible to achieve with conventional production methods. Ensemble machine learning methods are used to predict the power factor of Bi_2Te_3. Using specialized equipment, processing parameters and sensor data such as laser power, speed, layout spacing, layer thickness, and focus were collected. For image processing, the OpenCV Python library was applied to transform the acquired sensor images into meaningful features, including texture, surface roughness, and pixel intensity statistics. Feature scaling and data partitioning (80 % for training, 20 % for testing) were performed to ensure model reliability and generalization.

Headley, C.V. et al. [18] in his work describes an innovative combination of machine learning (ML) techniques with additive manufacturing (AM) processes to optimize the production of thermoelectric materials. In particular, the work draws attention to the production of parts from *n*-type

$Bi_2Te_{2.7}Se_{0.3}$ using a laser for melting and fusion of powder material into solid 3D objects. The study uses support vector regression (SVR) within ensemble learning. A bootstrap method was used to build an ensemble of SVR models, a technique that involves resampling from the training data set with replacement to train multiple models. The main descriptors for these models are LPBF process parameters such as laser power (which varied from 10 W to 40 W) and scan speed (which varied from 250 mm/s to 550 mm/s), which directly affect the width and depth of the molten of the "pool" area. To evaluate the model, the mean and standard deviation of forecasts from the ensemble of SVR models were used. These metrics are important for understanding the accuracy and reliability of ML predictions for the size of the molten "pool" that forms during the LPBF process.

Unsupervised machine learning methods for Bi_2Te_3

Unsupervised machine learning methods are a separate category of algorithms capable of learning from input data without direct control and defined labels [9]. Such methods find patterns of behaviour in data and their relationships in an offline mode, which allows one to effectively solve the tasks of clustering or finding associations. Unsupervised learning is a universal method, as it can find non-obvious connections of data in complex structures. Popular algorithms include: κ-means, hierarchical clustering, principal component algorithm, neural networks. Table 1 presents a visual comparison of supervised and unsupervised machine learning methods.

Table 1

Comparison of supervised and unsupervised machine learning methods

Supervised machine learning methods	**Unsupervised machine learning methods**
Prediction of a numerical value or classification of input data with labels.	Finding patterns and relationships in data based on data without any associated labels.
It requires input data processing, normalization, possible label encoding, feature selection, or development of specific features for the prediction task.	The main emphasis is on the selection of features to determine the more fundamental qualities of the data; there is no implementation of labels and their processing.
The model is selected depending on the task (regression or clustering), key parameters of the model are adjusted to minimize the difference between the actual and predicted labels.	Based on the type of pattern recognition (association, clustering, dimensionality reduction), the desired algorithm is selected without reference to labelled input data.
Absolute and relative error, precision, root mean square error are used as parameters for evaluating the efficiency of learning models. Input data is divided into educational and training data.	Silhouette index and Davis-Boldin index for clustering problems, as well as a subjective assessment of the membership of each selected instance with other objects in the class.
The obtained results are interpreted in the context of the given task and possible re-calibration of the model based on the performance evaluation.	There is a need to visualize the obtained results for better interpretation and focus on understanding the identified groupings and patterns.

Summarizing the table above, supervised machine learning methods can be characterized as such that work with labelled input data and allow solving prediction and clustering problems. In turn, unsupervised machine learning methods guide the research process to identify patterns and hidden structures of interdependences in unlabelled input data.

At the moment, no works have been found that use unsupervised machine learning methods to study the Bi_2Te_3 thermoelectric material, but there are several interesting areas of their application:

1. Formulation of the clustering problem for grouping samples of Bi_2Te_3 materials according to their similarity to a certain class, which will allow to reveal regularities and correlations in large data sets regarding the influence of synthesis methods, addition of impurities or nanostructure on the performance of such samples. Such a study would help to develop a methodology and recommendations for improving the process of synthesis and processing of material to solve the problems [10].
2. Application of unsupervised learning algorithms to extract features from microscopic images or crystallographic data of Bi_2Te_3 to find and cluster defects or crystal structures. The results of the work can be used as a way to improve the quality of control over the production of thermoelectric material and assess the effect of defects on the efficiency of samples [11].
3. Collection and preparation of a data set of impurities that are used and traditionally unexplored with Bi_2Te_3 to search for promising combinations. Due to the high performance of machine learning and the specific use of unsupervised methods, it is possible to develop a significant number of possible compounds [12].

Results of application of machine learning Bi_2Te_3

In the article by Wudil et al. [1] there were developed five weak regression models (Lasso regression, linear regression, decision tree regression, support vector regression) and one strong model combining the previous five using an ensemble technique using AdaBoost [13]. To evaluate the performance of these models, correlation coefficients, mean absolute error, coefficient of determination R2 and root mean square error were used. As a result, decision tree regression and support vector regression models showed high correlation coefficients of 99 % and 90.8 %, respectively. Enhanced models, using the AdaBoost algorithm, showed even higher indicators of 99.5 % and 94 %. During the validation, it was emphasized that the decision tree regression and support vector regression models with reduced mean absolute error and root mean square error are effective in assessing material quality. On the basis of this study, it is concluded that the implementation of enhanced weak regression algorithms significantly improves the accuracy of forecasting Bi_2Te_3 based thermoelectric semiconductors.

Another paper by Wudil [14] presents a scientific study using machine learning to estimate the thermal conductivity of materials based on $Bi_2Te_{2.7}Se_{0.3}$. Decision tree regression and support vector regression algorithms boosted with adaptive AdaBoost boost were also used in this work. For the selection of descriptors, a correlation was found between the input parameters of the data set and the sought value, presented in Table 2.

Table 2

Correlation coefficients between the input parameters and the target variable

	σ (S/m)	S (μV/K)	a (A)	c (A)	K (W/mK)	T (K)
σ (S/m)	1	–0.71	–0.15	–0.57	0.62	–0.36

Continue of table 2

S (μV/K)	–0.71	1	–0.22	0.33	–0.74	–0.088
a (A)	–0.15	–0.22	1	0.4	–0.11	0.076
c (A)	–0.57	0.33	0.4	1	–0.31	0.25
K (W/mK)	0.62	–0.74	–0.11	–0.31	1	0.29
T (K)	–0.36	–0.088	0.076	0.25	0.29	1

The model uses electrical properties and structural parameters of material lattices as input characteristics. The efficiency of the developed models is evaluated on the basis of such parameters as the correlation coefficient, the average absolute error, and the root mean square error. The decision tree model with AdaBoost enhancement showed a correlation coefficient of 99.4 % and a coefficient of determination R2 of 98.8 % in the test phase. These models have also been used to predict thermal conductivity for various physical specimens, such as transition metal compounds. The influence of substrate temperature during pulsed laser deposition was studied.

In the work of Parv Katyal et al. [5] the results of the study confirmed the high efficiency of predicting the *ZT* value for various compounds (Bi_2Te_3, $CoSb_3$, $Ba_8Ga_{16}Ge_{30}$, $Ba_8Ga_{18}Ge_{28}$) using the decision tree random forest algorithm. The evaluation of the efficiency of the model showed a low discrepancy with the expected result and an average absolute error of 0.0734, which shows the promise of this method in the processes of thermoelectric material evaluation. Table 3 presents the results of the proposed model for predicting *ZT* at different temperatures for a group of compounds.

Table 3

Experimental and predicted ZT values at different temperatures for the lead telluride family, the cobalt antimonide family, and the germanium-based clathrates

Temperature (K)	Experimental *ZT* value	ZT value predicted by the model	Chemical formula of material
400	0.5025	0.5923415	Bi_2Te_3
700	1.392715388	1.4253434	Bi_2Te_3
1000	1.636067789	1.5812441	Bi_2Te_3
600	0.871875767	0.938096442	Bi_2Te_3
300	0.316428584	0.384607488	Bi_2Te_3
300	0.424000225	0.502502554	$CoSb_3$
400	0.668512792	0.578206119	$CoSb_3$
700	1.181566055	1.16347007	$CoSb_3$
700	0.668168	0.7181711	$Ba_8Ga_{16}Ge_{30}$
300	0.01603609	0.067494695	$Ba_8Ga_{18}Ge_{28}$
1000	0.962666667	1.1242445	$Ba_8Ga_{18}Ge_{28}$

In the work of Wang Z. et al. [7] the study showed that the addition of copper impurities to *Bi-Te-Se* materials improves their thermoelectric characteristics. Copper atoms are introduced into interstitial spaces, changing the microstructure of the material and reducing the concentration of charge carriers. This leads to an increase in the Seebeck coefficient, electrical resistance and a decrease in the thermal conductivity of the media. The paper uses machine learning methods, including artificial neural network (ANN) and Bayesian optimization models, to predict and optimize the thermoelectric properties of these materials. Although the machine learning model is promising, problems related to retraining due to the small sample size have been noted.

In the work of Qu, R. [16], the model achieved high accuracy, as evidenced by low rms error values of 0.15 meV per atom for superlattice configurations for energy and force predictions. Predictions of thermal conductivity for $MnBi_2Te_4$ coincided well with experimental values, confirming the high efficiency of the DNNP model. The small discrepancies that were noted were within acceptable limits, highlighting the difficulties in excluding lattice from electronic thermal conductivity in experimental measurements. The $Bi_2Te_3/MnBi_2Te_4$ superlattice showed significantly reduced transverse thermal conductivity, which may be important for potential thermoelectric applications. In particular, the transverse thermal conductivity at 300 K was predicted to be 0.15 W $m^{-1}K^{-1}$, significantly lower than pure $MnBi_2Te_4$ or Bi_2Te_3, demonstrating the higher thermoelectric potential of the superlattice. Further analysis of the results showed that the decrease in transverse thermal conductivity in the superlattice can be explained by the dispersion relations of phonons, in particular, the appearance of bandgaps and a decrease in the speed of phonons. These phonon behaviours are key to understanding the mechanisms governing heat transfer in these complex materials.

Agarwal, A. et al. [17]. The classifier model based on bagging aggregation showed a high accuracy of 90 %, indicating a significant correlation between the selected features and the power factor of the thermoelectric material. Laser focus, power, and speed were among the main processing parameters affecting the power factor. Features associated with polarimetry data, especially post-distribution and post-melting angle of polarization (AoP) and degree of linear polarization (DoLP), were critical for power factor prediction. A total of 220 samples were produced and 117 were used for analysis, resulting in 3.157 data points for building machine learning models.

Headley, C. V. et al. [18] initially used 13 scan lines, which later expanded to 93 parameter combinations after six rounds of training, demonstrating the efficiency of an iterative, data-driven approach for refining process parameters. machine method, revealed the LPBF process parameters that resulted in the production of $Bi_2Te_{2.7}Se_{0.3}$ parts with a density greater than 99% and no cracks, demonstrating the high precision and quality that can be achieved. One notable advancement was the ability to produce thermoelectric parts with atypical geometries, such as hollow rectangles and trapezoids, with a relative density of 98.6 % (±1 %) and increased thermoelectric efficiency. The above shapes are difficult to produce using traditional manufacturing methods, but can be achieved through LPBF due to precise control over process parameters.

Conclusions

1. The efficiency of machine learning methods for predicting the properties of thermoelectric material Bi_2Te_3 was assessed.
2. Supervised machine learning algorithms, namely AdaBoost boosted weak models, decision tree regression, and support vector regression, are well suited for ZT factor prediction and thermal conductivity estimation of Bi_2Te_3-based thermoelectric materials.

3. Estimation of the efficiency of using the ensemble method, a random forest of decision trees, showed a low divergence with the expected result and an average absolute error of 0.0734 for compounds (Bi_2Te_3, $CoSb_3$, $Ba_8Ga_{16}Ge_{30}$, $Ba_8Ga_{18}Ge_{28}$).
4. There is considerable complexity in the amount of existing experimentally measured information about thermoelectric materials, which forces researchers to work with a limited set of information, which in turn leads to a decrease in the accuracy of forecasts.
5. With the help of machine learning, it is possible to determine a number of parameters for the efficient production of thermoelectric parts using additive manufacturing methods.

References

1. Wudil, Y. & Gondal, M. A. (2022). Predicting the thermoelectric energy figure of merit of Bi_2Te_3-based semiconducting materials: A machine learning approach. *SSRN Electronic Journal. Elsevier BV.* https://doi.org/10.2139/ssrn.4215166
2. Burkart, N. & Huber, M. F. (2021). A survey on the explainability of supervised machine learning. *Journal of Artificial Intelligence Research*, 70, 245 – 317. AI Access Foundation. https://doi.org/10.1613/jair.1.12228
3. Gaultois, M. W., Oliynyk, A. O., Mar, A., Sparks, T. D., Mulholland, G. J. & Meredig, B. (2016). Perspective: Web-based machine learning models for real-time screening of thermoelectric materials properties. *APL Materials*, 4 (5). AIP Publishing. https://doi.org/10.1063/1.4952607
4. Gonzalez Zelaya, C. V. (2019). Towards explaining the effects of data preprocessing on machine learning. *IEEE 35th International Conference on Data Engineering (ICDE).* IEEE. https://doi.org/10.1109/icde.2019.00245
5. Parv Katyal, Madhav Rathi, Piyush Mehra and Amrish K. Panwar (2020). Evaluation of figure of merit of thermoelectric materials using machine learning. *International Journal of Advanced Science and Technology*, 29(11s), 2858-2863. Retrieved from http://sersc.org/journals/index.php /IJAST/article/view/23766
6. Liu, Y., Wang, Y., & Zhang, J. (2012). New machine learning algorithm: random forest. In *Information Computing and Applications* (pp. 246 – 252). Springer Berlin Heidelberg. https://doi.org/10.1007/978-3-642-34062-8_32
7. Wang, Z., Yokoyama, Y., Onda, T., Adachi, Y., & Chen, Z. (2019). Improved thermoelectric properties of hot-extruded Bi–Te–Se bulk materials with Cu doping and property predictions via machine learning. *Advanced Electronic Materials*, 5 (6). Wiley. https://doi.org/10.1002/aelm.201900079
8. A. Ramezan, C., A. Warner, T., & E. Maxwell, A. (2019). Evaluation of sampling and cross-validation tuning strategies for regional-scale machine learning classification. *Remote Sensing*, 11(2), 185. MDPI AG. https://doi.org/10.3390/rs11020185
9. Alloghani, M., Al-Jumeily, D., Mustafina, J., Hussain, A., & Aljaaf, A. J. (2019). A systematic review on supervised and unsupervised machine learning algorithms for data science. *Unsupervised and Semi-Supervised Learning* (pp. 3 – 21). Springer International Publishing. https://doi.org/10.1007/978-3-030-22475-2_1
10. Na, G. S. (2023). Artificial intelligence for learning material synthesis processes of thermoelectric materials. *Chemistry of Materials*, 35(19), 8272 – 8280). American Chemical Society (ACS). https://doi.org/10.1021/acs.chemmater.3c01834
11. Sheng, Y., Deng, T., Qiu, P., Shi, X., Xi, J., Han, Y., & Yang, J. (2021). Accelerating the discovery

of *Cu – Sn – S* thermoelectric compounds via high-throughput synthesis, characterization, and machine learning-assisted image analysis. *Chemistry of Materials,* 33(17), 6918 – 6924. American Chemical Society (ACS). https://doi.org/10.1021/acs.chemmater.1c01856

12. Jia, X., Deng, Y., Bao, X., Yao, H., Li, S., Li, Z., Chen, C., Wang, X., Mao, J., Cao, F., Sui, J., Wu, J., Wang, C., Zhang, Q., & Liu, X. (2022). Unsupervised machine learning for discovery of promising half-Heusler thermoelectric materials. *Computational Materials*, 8(1). Springer Science and Business Media LLC. https://doi.org/10.1038/s41524-022-00723-9
13. CAO, Y., MIAO, Q.-G., LIU, J.-C., & GAO, L. (2013). Advance and prospects of AdaBoost algorithm. *Acta Automatica Sinica,* 39 (6), 745–758. Elsevier BV. https://doi.org/10.1016/s1874-1029(13)60052-x
14. Wudil, Y. S. (2023). Ensemble learning-based investigation of thermal conductivity of Bi_2Te_2.7Se0.3-based thermoelectric clean energy materials. *Results in Engineering,* 18, 101203. Elsevier BV. https://doi.org/10.1016/j.rineng.2023.101203
15. Wang, T., Zhang, C., Snoussi, H., & Zhang, G. (2019). Machine learning approaches for thermoelectric materials research. *Advanced Functional Materials,* 30(5). Wiley. https://doi.org/10.1002/adfm.201906041
16. Qu, R., Lv, Y., & Lu, Z. (2023). A deep neural network potential to study the thermal conductivity of MnBi2Te4 and Bi2Te3/MnBi2Te4 superlattice, *Journal of Electronic Materials*, 52(7), 4475 – 4483). Springer Science and Business Media LLC. https://doi.org/10.1007/s11664-023-10403-z
17. Agarwal, A., Banerjee, T., Gockel, J., LeBlanc, S., Walker, J., & Middendorf, J. (2023). *Predicting thermoelectric power factor of bismuth telluride during laser powder bed fusion additive manufacturing (Version 1).* arXiv. https://doi.org/10.48550/ARXIV.2303.15663
18. Headley, C. V., Herrera del Valle, R. J., Ma, J., Balachandran, P., Ponnambalam, V., LeBlanc, S., Kirsch, D., & Martin, J. B. (2024). The development of an augmented machine learning approach for the additive manufacturing of thermoelectric materials. *Journal of Manufacturing Processes*, 116, 165 – 175). Elsevier BV. https://doi.org/10.1016/j.jmapro.2024.02.045

Submitted: 12.04.2023

Анатичук Л. І., *акад. НАН України* [1,2]
Короп М. М. [1]

[1] Інститут термоелектрики НАН та МОН України,
вул. Науки, 1, Чернівці, 58029, Україна;
e-mail: anatych@gmail.com, mykola.korop@chnu.edu.ua
[2] Чернівецький національний університет
імені Юрія Федьковича,
вул. Коцюбинського 2, Чернівці, 58012, Україна
e-mail: anatych@gmail.com

ЗАСТОСУВАННЯ МАШИННОГО НАВЧАННЯ ДЛЯ ПРОГНОЗУВАННЯ ВЛАСТИВОСТЕЙ ТЕРМОЕЛЕКТРИЧНИХ МАТЕРІАЛІВ НА ОСНОВІ Bi_2Te_3

У роботі наводяться приклади оцінки ефективності застосування машинного навчання для прогнозування властивостей термоелектричних матеріалів на основі Bi_2Te_3. Оглянуто результати їх застосування та способи вибору оптимальних параметрів вхідних даних, описано відмінності та особливості вибору алгоритмів, етапи роботи та навчання машинних моделей, а також критерії оцінки ефективності та валідації отриманих прогнозів. Бібл. 18, рис. 1, табл. 3.

Ключові слова: методи машинного навчання, термоелектричне матеріалознавство.

References

1. Wudil, Y. & Gondal, M. A. (2022). Predicting the thermoelectric energy figure of merit of Bi_2Te_3-based semiconducting materials: A machine learning approach. *SSRN Electronic Journal. Elsevier BV.* https://doi.org/10.2139/ssrn.4215166
2. Burkart, N. & Huber, M. F. (2021). A survey on the explainability of supervised machine learning. *Journal of Artificial Intelligence Research*, 70, 245 – 317. AI Access Foundation. https://doi.org/10.1613/jair.1.12228
3. Gaultois, M. W., Oliynyk, A. O., Mar, A., Sparks, T. D., Mulholland, G. J. & Meredig, B. (2016). Perspective: Web-based machine learning models for real-time screening of thermoelectric materials properties. *APL Materials*, 4 (5). AIP Publishing. https://doi.org/10.1063/1.4952607
4. Gonzalez Zelaya, C. V. (2019). Towards explaining the effects of data preprocessing on machine learning. *IEEE 35th International Conference on Data Engineering (ICDE).* IEEE. https://doi.org/10.1109/icde.2019.00245
5. Parv Katyal, Madhav Rathi, Piyush Mehra and Amrish K. Panwar (2020). Evaluation of figure of merit of thermoelectric materials using machine learning. *International Journal of Advanced Science and Technology*, 29(11s), 2858-2863. Retrieved from http://sersc.org/journals/index.php /IJAST/article/view/23766
6. Liu, Y., Wang, Y., & Zhang, J. (2012). New machine learning algorithm: random forest. In *Information Computing and Applications* (pp. 246 – 252). Springer Berlin Heidelberg. https://doi.org/10.1007/978-3-642-34062-8_32
7. Wang, Z., Yokoyama, Y., Onda, T., Adachi, Y., & Chen, Z. (2019). Improved thermoelectric properties of hot-extruded Bi–Te–Se bulk materials with Cu doping and property predictions via machine learning. *Advanced Electronic Materials*, 5 (6). Wiley. https://doi.org/10.1002/aelm.201900079
8. A. Ramezan, C., A. Warner, T., & E. Maxwell, A. (2019). Evaluation of sampling and cross-validation tuning strategies for regional-scale machine learning classification. *Remote Sensing*, 11(2), 185. MDPI AG. https://doi.org/10.3390/rs11020185
9. Alloghani, M., Al-Jumeily, D., Mustafina, J., Hussain, A., & Aljaaf, A. J. (2019). A systematic review on supervised and unsupervised machine learning algorithms for data science. *Unsupervised and Semi-Supervised Learning* (pp. 3 – 21). Springer International Publishing. https://doi.org/10.1007/978-3-030-22475-2_1
10. Na, G. S. (2023). Artificial intelligence for learning material synthesis processes of

thermoelectric materials. *Chemistry of Materials*, 35(19), 8272 – 8280). American Chemical Society (ACS). https://doi.org/10.1021/acs.chemmater.3c01834

11. Sheng, Y., Deng, T., Qiu, P., Shi, X., Xi, J., Han, Y., & Yang, J. (2021). Accelerating the discovery of *Cu – Sn – S* thermoelectric compounds via high-throughput synthesis, characterization, and machine learning-assisted image analysis. *Chemistry of Materials,* 33(17), 6918 – 6924. American Chemical Society (ACS). https://doi.org/10.1021/acs.chemmater.1c01856
12. Jia, X., Deng, Y., Bao, X., Yao, H., Li, S., Li, Z., Chen, C., Wang, X., Mao, J., Cao, F., Sui, J., Wu, J., Wang, C., Zhang, Q., & Liu, X. (2022). Unsupervised machine learning for discovery of promising half-Heusler thermoelectric materials. *Computational Materials*, 8(1). Springer Science and Business Media LLC. https://doi.org/10.1038/s41524-022-00723-9
13. CAO, Y., MIAO, Q.-G., LIU, J.-C., & GAO, L. (2013). Advance and prospects of AdaBoost algorithm. *Acta Automatica Sinica,* 39 (6), 745–758. Elsevier BV. https://doi.org/10.1016/s1874-1029(13)60052-x
14. Wudil, Y. S. (2023). Ensemble learning-based investigation of thermal conductivity of Bi_2Te_2.7Se0.3-based thermoelectric clean energy materials. *Results in Engineering,* 18, 101203. Elsevier BV. https://doi.org/10.1016/j.rineng.2023.101203
15. Wang, T., Zhang, C., Snoussi, H., & Zhang, G. (2019). Machine learning approaches for thermoelectric materials research. *Advanced Functional Materials,* 30(5). Wiley. https://doi.org/10.1002/adfm.201906041
16. Qu, R., Lv, Y., & Lu, Z. (2023). A deep neural network potential to study the thermal conductivity of MnBi2Te4 and Bi2Te3/MnBi2Te4 superlattice, *Journal of Electronic Materials*, 52(7), 4475 – 4483). Springer Science and Business Media LLC. https://doi.org/10.1007/s11664-023-10403-z
17. Agarwal, A., Banerjee, T., Gockel, J., LeBlanc, S., Walker, J., & Middendorf, J. (2023). *Predicting thermoelectric power factor of bismuth telluride during laser powder bed fusion additive manufacturing (Version 1).* arXiv. https://doi.org/10.48550/ARXIV.2303.15663
18. Headley, C. V., Herrera del Valle, R. J., Ma, J., Balachandran, P., Ponnambalam, V., LeBlanc, S., Kirsch, D., & Martin, J. B. (2024). The development of an augmented machine learning approach for the additive manufacturing of thermoelectric materials. *Journal of Manufacturing Processes*, 116, 165 – 175). Elsevier BV. https://doi.org/10.1016/j.jmapro.2024.02.045

Submitted: 12.04.2023

O. M. Manyk, *cand phys – math sciences*[1]
T. O. Manyk, *cand phys – math sciences*[2]
V. R. Bilynskyi-Slotylo, *cand phys – math sciences*[1]

[1]Yuriy Fedkovych Chernivtsi National University,
2 Kotsiubynskyi str., Chernivtsi, 58012, Ukraine,
e-mail: o.manyk@chnu.edu.ua,
e-mail: slotulo@gmail.com
[2] Military University of Technology Jaroslaw Dombrowski,
str. gene Sylwester Kaliskiego, 2,
Warsaw 46, 00-908, Poland,
e-mail: tetjana.manyk@wat.edu.pl

THEORETICAL MODELS OF ORDERED ALLOYS OF TERNARY SYSTEMS OF THERMOELECTRIC MATERIALS. 4. CHEMICAL BOND AND STATE DIAGRAMS OF *Bi-Cd-Sb*

A comprehensive approach has been developed for the construction of theoretical models of ordered alloys of ternary systems based on Bi-Cd-Sb.
A diagram of distribution of phase regions and isothermal sections based on intermediate binary compounds Bi-Cd, Bi-Sb, Cd-Sb in the Bi-Cd-Sb system have been constructed.
Calculations of effective radii, redistribution of electron density and dissociation energy of non-equivalent chemical bonds depending on interatomic distances in the Bi-Cd-Sb ternary system are presented. Bibl. 7, Fig. 4, Tabl. 6.
Key words: theoretical models, chemical bond, effective radii, dissociation energy, state diagrams, non-equivalent hybrid orbitals (NHO).

Introduction

Cadmium antimonide is one of the promising thermoelectric materials [1]. Depending on the mode of heat treatment and the method of cooling, cadmium alloys with antimony can crystallize in accordance with the stable and metastable diagrams of alloys [2]. The nature of the chemical bond in such alloys varies from metallic to ionic, covalent and intermediate.

Considering also that the search for new thermoelectric materials increasingly comes down to the need to study multicomponent systems, the study of ternary systems based on *Bi-Cd-Sb* becomes especially relevant, both from the standpoint of chemical bonding and from the standpoint of state diagrams. This will make it possible not only to establish the limits of phase equilibrium in the liquid-crystal regions (melting diagrams), but also to predict cases of incongruent melting.

In this regard, the choice of bismuth as a constituent component of *Bi-Cd-Sb* was not accidental. Bismuth in compounds can have different degrees of oxidation (from -3 to +5) [3]. In addition, according to the state diagram (*Bi-Sb*), both components (*Bi* and *Sb*) are infinitely soluble in liquid and solid states and do not form chemical compounds. At the same time, the state diagrams of *Cd-Sb* and *Bi-Cd* are eutectic diagrams, where both compounds and solid solutions can be formed [4]. In accordance with the

above, the task was set to calculate the parameters of chemical bonds depending on the interatomic distances and to construct phase distribution schemes in the *Bi-Cd-Sb* system.

Theoretical models of state diagrams

This work is devoted to the construction of theoretical models of ordered alloys of ternary systems based on *Cd-Bi-Sb*. What was new in the study of bismuth and cadmium antimonides was that to solve the problem, the equilibrium method was used based on the geometric properties of a triangle - the triangulation method [5].

When building theoretical models, this approach made it possible to generalize the results of experimental studies of *Cd-Bi*, *Bi-Sb* and *Cd-Sb* binary systems; physico-chemical properties and quantum regularities of the initial components. Next, by constructing conoid triangles, the quantitative ratios and equilibrium limits of phases in the liquid-crystal regions were determined. This made it possible to predict cases of congruent and incongruent melting.

The obtained results are shown in Fig. 1 - 4, where the following designations are entered:

α – solid phase based on *Cd*;
β – solid phase based on *Bi*;
γ – solid phase based on *Sb*;
ε – solid phase based on intermediate *Cd-Bi* binary compounds;
ρ – solid phase based on intermediate *Bi-Sb* binary compounds;
δ – solid phase based on intermediate *Cd-Sb* binary compounds;
σ – solid phase based on *Bi-Cd-Sb* ternary system.
L – liquid.

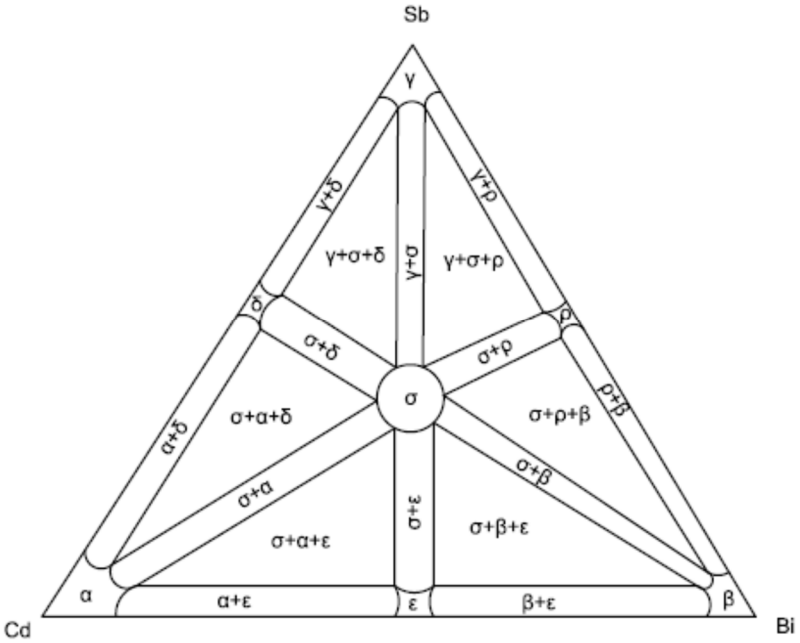

Fig. 1. A diagram of the distribution of Cd-Bi-Sb equilibrium phase regions in the solid state

Fig. 1 shows a diagram of the distribution of *Cd-Sb-Bi* phase regions in the solid state. This made it possible to divide *Cd-Bi-Sb* ternary system into six ordered ternary subsystems and consider interatomic interaction both from the standpoint of state diagrams and chemical bond.

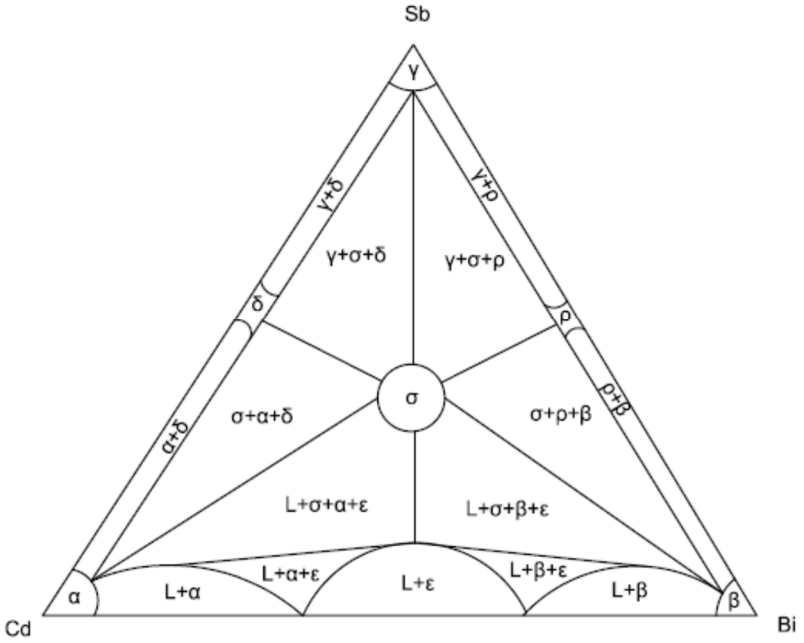

Fig. 2. Cd-Bi-Sb isothermal section at t = 200 °C

Fig. 2 shows an isothermal section at a temperature of t = 200°C. This temperature is lower than the melting temperature of the original components *Bi*, *Cd* and *Sb* and at the same time higher than the temperature of the first eutectic of the *Bi-Cd* system (E_1 = 144°C). Part of the *Cd-Bi* section is occupied by liquid *L*, and the two-phase equilibrium (*L*+α), (*L*+ε), (*L*+β) is carried out by primary crystals α and β, as well as ε-crystals (based on Cd_nBi_m compounds).

In contrast to the previous case, the section contains conoid triangles with equilibrium phases (*L*+α+ε) and (*L*+ε+β), which are formed by primary crystals α, β, ε (based on Cd_nSb_m and Bi_kSb_l compounds) and liquid L. This division of ternary systems into separate sectors of dual state diagrams makes it possible to study the fine structure of cooling and heating of individual elements depending on their environment and the processes of forming the short-range order of chemical bonding.

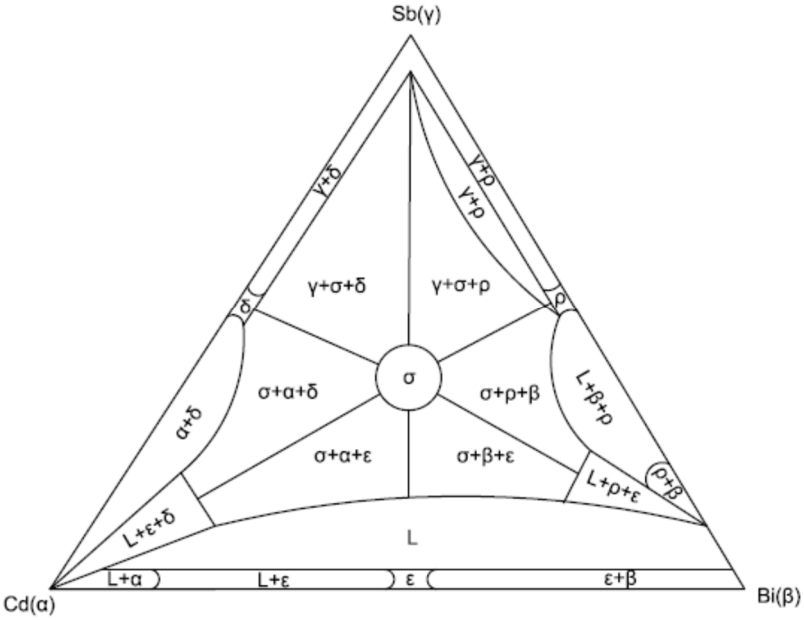

Fig. 3. Cd-Bi-Sb isothermal section at t = 300 °C

Fig. 3 shows an isothermal section at a temperature of t = 300 °C, which is higher than the melting point of bismuth and lower than the melting point of cadmium and antimony. In this case, most of the *Cd-Bi* cross-section is occupied by liquid L, and the equilibrium phases with conoid triangles (L+ε+α) and (L+β+ε) are replaced by phases with conoid triangles (L+ε+δ) and (L+ε+ρ), and this already makes it possible to study the fine structure of cooling and heating using state diagrams of binary alloys.

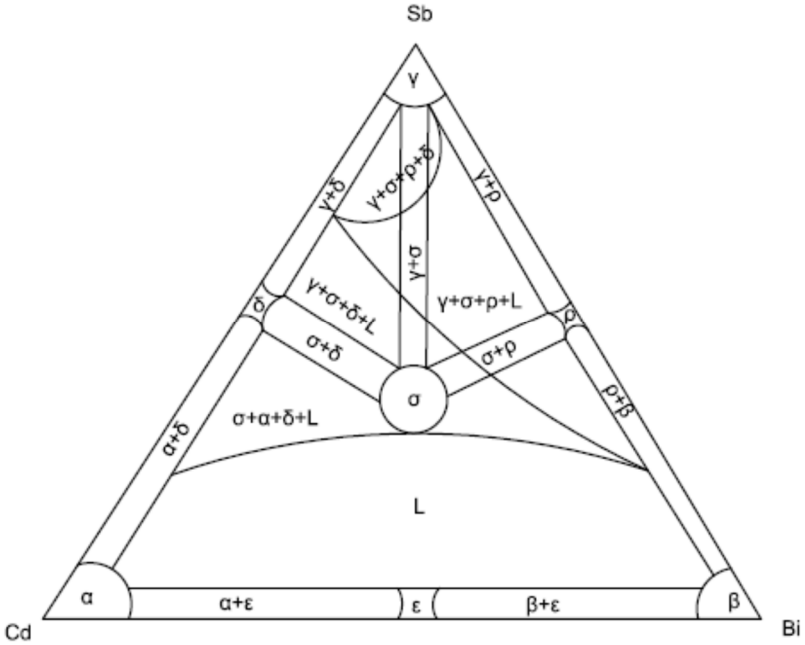

Fig. 4. Cd-Bi-Sb isothermal section at t = 400 °C

Fig. 4 shows an isothermal section at t = 400 °C, which is higher than the melting temperature of the original components of cadmium and bismuth and makes it possible to study the cooling and heating processes of ternary compounds of solid solutions depending on the composition, chemical bond, and technological parameters. Thus, the given isothermal sections make it possible to:

1. Divide the *Cd-Bi-Sb* ternary system into six ordered subsystems and consider the issue of interatomic interaction from the standpoint of state diagrams and chemical bonding.
2. Establish the relationship between phase equilibrium in the liquid-crystal regions and transformations in the solid state.
3. Distinguish between eutectic and peritectic state diagrams.

In this regard, it should be noted that the isothermal sections alone do not yet indicate the numerical values of the temperatures of phase transitions in multicomponent systems. In such cases, the methods of calculating the interatomic interaction from the standpoint of chemical bond are additionally used.

Theoretical models of chemical bonding of ordered *Cd-Bi-Sb* alloys

The combination of experimental and theoretical approaches in the quantitative method for calculating the parameters of the electronic structure of matter is associated with a revision of the system of views on interatomic interaction, with the emergence of qualitatively new, non-standard ideas that are not the result of the development of various directions of existing theories, but also deny some of them. The way to solving the problem lies only through an objective analysis of empirical material [6].

The foundations of such an analysis were laid by Mendeleev when he discovered the periodic law. However, at the current stage, it is impossible to obtain qualitatively new conclusions based on the generalization of experimental data only on the system of neutral unexcited atoms. Further development of the theory of the periodic system is needed, taking into account the quantum nature of atoms, the relationship between the physical and chemical properties of the elements of Mendeleev's table with the structure of their electronic shells, with the properties and electronic structure of the compounds formed by them, depending on the number of electrons n in the orbitals of the interacting atoms.

The analysis of diverse empirical information about the properties of atoms and their ions showed that they can be linked together and generalized by introducing the concept of effective ionic radii R_U. The systems of equations relating the value of R_U to the electron density on atomic orbitals make it possible to calculate the redistribution of electron density depending on interatomic distances and to overcome the difficulties of modern theories of interatomic interaction [7].

The most useful when searching for the form of a graphical solution to the problem of the connection between R_U and n turned out to be the relationship between $tg\alpha = \frac{\Delta log R_U}{\Delta n}$ and electronegativity, fixing the position of the lines in $logR_U = f(n)$ coordinates.

A good agreement of the set of experimental data with the values of R_U and tgα gives the postulated dependence:

$$logR_{UA}^{x} = logR_{UA}^{0} - xtg\alpha, \tag{1}$$

where R_U^0 is radius of atoms in the unexcited state, x is valence.

The usefulness of such equations is determined by the extent to which their use allows obtaining a fairly accurate and physically justified result of interatomic interaction. The existence of a minimum interatomic distance d_{min} during the formation of a chemical bond and two possible values of Z_{eff} for interatomic distances $d_i > d_{min}$ з from the standpoint of the crystal chemical approach is justified by the increase of the internuclear distance when ionicity and covalency change.

The main drawback of this approach is that in many cases the internuclear distances between atoms A and B are smaller than the d_{min} value, and it is impossible to calculate the charge of the ions from the diagrams of the dependence of the effective charges Z_{eff} on the interatomic distances. Difficulties can be overcome by translating the crystal chemical system into the language of quantum chemistry. It should be taken into account that in the zone of binding localized orbitals, the spherical symmetry of the electron density is broken and for $d_i > d_{min}$ the formation of bonds (A-B) is accompanied by the transition of electrons to other directions of interatomic interaction and this bond becomes a donor.

Thus, when $d_i \neq d_{min}$ the effective values of the charges must change. Removal of $(+\Delta e)$ electrons or their localization $(-\Delta e)$ change the values of the charges that a given pair has at $d_i = d_{min}$, i.e. $Z_{eff}A(B) = Z_{min}A(B) + \left(\frac{\Delta e}{Z}\right)$.

With this approach, a system of equations of type (1) makes it possible to match the theoretical part with the experimental part and was solved for all possible values of d_i in the compounds under consideration. Thus, as a result of taking into account the quantum interpretation of empirical material, the expression for the dissociation energy of chemical bonds d_i takes on the form:

$$D_{A-B}^{(i)} = \left(\frac{C_1\left(R_{UA}^0 + R_{UB}^0\right)}{(\mathrm{tg}\,\alpha_A + \mathrm{tg}\,\alpha_B)}\right)\left(\frac{C_2 d_i}{d_i^2 - R_{UA}R_{UB}} - \frac{1}{d_i}\right), \tag{2}$$

where $R^0_{UA(B)}$, R^0_{UB} as before, are the radii of atoms in the unexcited state;

R_{UA}, R_{UB} are effective radii of ions of atoms A, B;

d_i is interatomic distance of i-bond;

i is the number of non-equivalent interatomic distances in the compounds under study;

C_1 is coefficient reflecting the relationship between dimensional and energy characteristics of interatomic interaction (measured in electron volts);

C_2 depends on the type of crystal structure (dimensionless).

With regard to the above remarks, calculations of effective charges, effective radii, dissociation energies for chemical bonds φ_i at different interatomic distances d_i, and various structural modifications of *Bi-Cd-Sb* were carried out in this work. In the tables, the values of the coefficients C_1 and C_2 in the first approximation are chosen to be equal to unity.

Table 1

Effective charges, effective radii, dissociation energies depending on interatomic distances of Bi-Bi NHO

Bi-Bi NHO / Parameters	*Bi-Bi*					
	φ_1	φ_2	φ_3	φ_4	φ_5	φ_6
d_i(Å)	2.8	2.9	3.0	3.1	3.2	3.3
R_U^{Bi}(Å)	1.40	1.45	1.50	1.55	1.60	1.65
$\Delta q_i(\varphi_i)$	+0.85	+0.7	+0.5	+0.3	+0.1	-0.1
$D(\varphi_i)$ ev	2.854	2.755	2.663	2.577	2.497	2.421

Table 2

Effective charges, effective radii, dissociation energies depending on interatomic distances of Cd-Cd NHO

Cd-Cd NHO / Parameters	*Cd-Cd*					
	φ_1	φ_2	φ_3	φ_4	φ_5	φ_6
d_i(Å)	2.8	2.9	3.0	3.1	3.2	3.3
R_U^{Cd}(Å)	1.4	1.45	1.5	1.55	1.6	1.65
$\Delta q_i(\varphi_i)$	+0.33	+0.18	+0.025	-0.05	-0.27	-0.4
$D(\varphi_i)$ ev	1.853	1.789	1.730	1.674	1.622	1.572

Table 3

Effective charges, effective radii, dissociation energies depending on interatomic distances of Sb-Sb NHO

Sb-Sb NHO / Parameters	*Sb-Sb*					
	φ_1	φ_2	φ_3	φ_4	φ_5	φ_6
d_i(Å)	2.8	2.9	3.0	3.1	3.2	3.3
R_U^{Sb}(Å)	1.4	1.45	1.5	1.55	1.6	1.65
$\Delta q_i(\varphi_i)$	0.2	0	-0.2	-0.39	-0.6	-0.75
$D(\varphi_i)$ ev	2.232	2.252	2.177	2.107	2.041	1.980

Table 4

Effective charges, effective radii, dissociation energies depending on interatomic distances of Cd-Bi NHO

Cd-Bi NHO / Parameters	*Cd-Bi*					
	φ_1	φ_2	φ_3	φ_4	φ_5	φ_6
d_i(Å)	2.8	2.9	3.0	3.1	3.2	3.3
R_U^{Cd}(Å)	1.32	1.37	1.43	1.49	1.54	1.60
R_U^{Bi}(Å)	1.48	1.53	1.57	1.61	1.66	1.70
$\Delta q_i(\varphi_i)$	0.62	0.42	0.25	0.07	-0.1	-0.2
$D(\varphi_i)$ ev	2.256	2.179	2.108	2.042	1.979	1.920

Table 5

Effective charges, effective radii, dissociation energies depending on interatomic distances of Bi-Sb NHO

Bi-Sb NHO / Parameters	*Bi-Sb*					
	φ_1	φ_2	φ_3	φ_4	φ_5	φ_6
d_i(Å)	2.8	2.9	3.0	3.1	3.2	3.3
R_U^{Bi}(Å)	1.49	1.54	1.58	1.64	1.69	1.74
R_U^{Sb}(Å)	1.31	1.36	1.42	1.46	1.51	1.56
$\Delta q_i(\varphi_i)$	0.57	0.35	0.2	-0.05	-0.25	-0.45
$D(\varphi_i)$ ev	2.568	2.480	2.396	2.322	2.250	2.182

Table 6

Effective charges, effective radii, dissociation energies depending on interatomic distances of Cd-Sb NHO

Cd-Sb NHO / Parameters	*Cd-Sb*					
	φ_1	φ_2	φ_3	φ_4	φ_5	φ_6
d_i(Å)	2.8	2.9	3.0	3.1	3.2	3.3
R_U^{Cd}(Å)	1.42	1.48	1.53	1.6	1.65	1.71
R_U^{Sb}(Å)	1.38	1.42	1.47	1.5	1.55	1.59
$\Delta q_i(\varphi_i)$	0.27	0.1	-0.06	-0.22	-0.4	-0.55
$D(\varphi_i)$ ev	2.061	1.989	1.922	1.859	1.800	1.746

Discussion of the results

As follows from the results presented in Tables 1-2, with the growth of interatomic distances, the dissociation energy of the corresponding chemical bonds decreases, and the redistribution of electron density in the interval of interatomic distances $3 \leq d_i \leq 3$in the structural varieties of Bi-Sb changes sign The structural varieties of *Bi-Cd* behave similarly, but already in other intervals $3.1 \leq d_i \leq 3.2$.

This means that chemical bonds can be both donor and acceptor under certain conditions. This confirms the experimentally established fact [3] that in compounds bismuth has different degrees of oxidation from -3 to +5.

The use of the obtained research results makes it possible to predict the shape of the liquidus, and therefore the type of melting and rearrangement of atoms in melts [8] of the resulting material.

Conclusions

1. The diagram of the distribution of *Bi-Cd-Sb* phase regions is constructed.
2. Isothermal sections of *Bi-Cd-Sb* at different temperatures were studied, which made it possible to divide the *Cd-Bi-Sb* ternary system into six ordered subsystems and consider the interatomic interaction from the standpoint of state diagrams and chemical bond.
3. The parameters of the chemical bond in the *Bi-Cd-Sb* ternary systems were calculated depending on the interatomic distances for various structural modifications.
4. The results obtained can be used in the development of technological modes of new materials based on *Bi-Cd-Sb*.

References

1. Anatychuk L.I. (2003). *Thermoelectricity. Vol.2. Thermoelectric power converters*. Kyiv, Chernivtsi: Institute of Thermoelectricity.
2. Ashcheulov A.A., Manik O.N., Marenkin S.F. (2003). Cadmium Antimonide: chemical Bonding and Technology. *Inorganic Materials*, 39 (2), 59 – 67.
3. Manik O.M., Manik T.O., Bilynskyi-Slotylo V.R. (2017). Models of Bi_2Te_3 chemical bond. *J. Thermoelectricity*, 3, 13 – 22.
4. Hansen M., Anderko K. (1958). *Constitution of Binary Alloys*, 2nd Ed. New York: McGraw-Hill, p. 118.
5. Barchiy I.E., Peresh E.Yu., Rizak V.M., Khudolii V.O. (2003). *Heterogenni rivnovahy. [Heterogeneous equilibria]. Uzhhorod*: Zakarrpattia Publ. [in Ukrainian].
6. Manik O.M. (1999). *Bahatofactornyi pidhid v teortetychnomu materialoznavstvi [Multi-factor approach in theoretical materials science*]. Chernivtsi: Prut [in Ukrainian].
7. Manik O.M., Manik T.O., Bilynskyi-Slotylo V.R. (2018). Theoretical models of ordered alloys of cadmium antimonide. *J. Thermoelectricity*, 4, 4 – 30.
8. Yeryomenko O.I., Manyk O.M., Raranskyi M.D. (2005). Study of chemical bonding features in solid solution crystals of the *CdSb-ZnSb* system. *Scientific Bulletin of Chernivtsi University. Physics. Electronics*, 268, 109 – 112.

Submitted: 26.04.2023

Маник О. М., *канд. фіз.-мат. наук*[1]
Маник Т. О., *канд. фіз.-мат. наук*[2]
Білинський-Слотило В. Р., *канд. фіз.-мат. наук*[1]

[1] Чернівецький національний університет імені Юрія Федьковича,
вул. Коцюбинського 2, Чернівці, 58012, Україна;
e-mail: o.manyk@chnu.edu.ua, slotulo@gmail.com
[2] Військово-технічний університет ім. Ярослава Домбровського,
вул. ген. Сільвестра Каліського, 2, Варшава 46, 00-908, Польща
e-mail: tetjana.manyk@wat.edu.pl

ТЕОРЕТИЧНІ МОДЕЛІ ВПОРЯДКОВУВАНИХ СПЛАВІВ ПОТРІЙНИХ СИСТЕМ ТЕРМОЕЛЕКТРИЧНИХ МАТЕРІАЛІВ. 4. ХІМІЧНИЙ ЗВ'ЯЗОК ТА ДІАГРАМИ СТАНУ *Bi-Cd-Sb*

Розроблено комплексний підхід для побудови теоретичних моделей упорядковуваних сплавів потрійних систем на основі Bi-Cd-Sb.
Побудовано схему розподілу фазових областей та ізотермічні перерізи на основі проміжних бінарних сполук Bi-Cd, Bi-Sb, Cd-Sb в системі Bi-Cd-Sb.
Представлено розрахунки ефективних радіусів, перерозподілу електронної густини та енергії дисоціації нееквівалентних хімічних зв'язків в залежності від міжатомних віддалей в потрійній системі Bi-Cd-Sb. Бібл. 8, рис.4, табл. 6.
Ключові слова: теоретичні моделі, хімічний зв'язок, ефективні радіуси, енергія дисоціації, діаграми стану, нееквівалентні гібридні орбіталі (НГО).

References

1. Anatychuk L. I. (2003). *Thermoelectricity. Vol.2. Thermoelectric power converters*. Kyiv, Chernivtsi: Institute of Thermoelectricity.
2. Ashcheulov A. A., Manik O. N., Marenkin S. F. (2003). Cadmium Antimonide: chemical Bonding and Technology. *Inorganic Materials*, 39 (2), 59 – 67.
3. Manik O. M., Manik T. O., Bilynskyi-Slotylo V. R. (2017). Models of Bi_2Te_3 chemical bond. *J. Thermoelectricity*, 3, 13 – 22.
4. Hansen M., Anderko K. (1958). *Constitution of Binary Alloys*, 2nd Ed. New York: McGraw-Hill, p. 118.
5. Barchiy I. E., Peresh E. Yu., Rizak V. M., Khudolii V. O. (2003). *Heterogenni rivnovahy. [Heterogeneous equilibria]. Uzhhorod*: Zakarrpattia Publ. [in Ukrainian].
6. Manik O. M. (1999). *Bahatofactornyi pidhid v teortetychnomu materialoznavstvi [Multi-factor approach in theoretical materials science*]. Chernivtsi: Prut [in Ukrainian].
7. Manik O. M., Manik T. O., Bilynskyi-Slotylo V. R. (2018). Theoretical models of ordered alloys of cadmium antimonide. *J. Thermoelectricity*, 4, 4 – 30.
8. Yeryomenko O. I., Manyk O. M., Raranskyi M. D. (2005). Study of chemical bonding features in solid solution crystals of the *CdSb-ZnSb* system. *Scientific Bulletin of Chernivtsi University. Physics. Electronics*, 268, 109 – 112.

Submitted: 26.04.2023

D. E. Rybchakov

D. E. Rybchakov

Institute of Thermoelectricity of the NAS and MES of Ukraine,
1, Nauky str., Chernivtsi, 58029, Ukraine,
e-mail: anatych@gmail.com

USE OF COMPUTER SIMULATION FOR OPTIMIZATION OF TECHNOLOGICAL MODES OF MANUFACTURING THERMOELECTRIC MATERIALS BASED ON *Bi-Te* OBTAINED BY VERTICAL ZONE MELTING METHOD

The article presents the main types of computer models used for the study of thermoelectric materials. A description of physical and mathematical models of crystal growth, and a method of using crystal growth models to optimize the technology of manufacturing thermoelectric material based on Bi-Te, and thermoelectric parameters of manufactured thermoelectric materials are given. Bibl. 5. Fig. 4.

Key words: vertical zone melting, thermoelectric material, computer model.

Introduction

In the age of technological progress and high requirements to production efficiency, computer simulation is becoming an indispensable tool for the development and improvement of new materials and technologies. One of the areas where this is especially relevant is the production of thermoelectric materials by the method of vertical zone melting, since this method is the main one in the mass production of thermoelectric products [1 – 2]. The advantages of using computer simulation in this context are obvious and tangible at every stage of thew process.

The relevance of the work is the introduction of computer methods into the technological modes of manufacturing thermoelectric materials, which will reduce materials costs and time for the process of improving the material.

The purpose of the work is to develop a computer approach for optimizing technological modes for the production of thermoelectric materials

Computer models in thermoelectricity

The main types of models used in the research of thermoelectric materials are:

- Kinetic models: These models describe the dynamics of crystal growth according to the laws of physical chemistry and heat transfer. They take into account diffusion processes, mass transfer, heat transfer, etc.
- Flux models: These models investigate the movement and interaction of atoms or molecules in the melt phase, specifically accounting for the flux of reactants and products.
- Molecular dynamics: In these models, atoms or molecules are considered individually and their motions are modeled using physical laws.

- Computer simulation of mass and heat transfer: These models describe the interaction of reagents with the surface of the crystal, diffusion processes, heat flows, etc.

Crystal growth models: These models study crystal growth by considering various process parameters such as temperature, growth rate, reactant concentration.

Description of the computer model

The use of computer models of crystal growth is the most promising solution for optimizing the technological regime for growing thermoelectric material. These models take into account various parameters and conditions for crystal growth, such as temperature, growth rate, and concentration of reagents. They are based on the physical principles of diffusion, heat transfer and other processes that occur during zone melting. These models can provide information about how the crystallization front moves, what factors affect its shape and speed of formation. The shape of the crystallization front is one of the key parameters that affects the quality of the obtained thermoelectric material. The most favorable for the growth of single crystals with a small number of structural defects is a flat crystallization front, because on the crystallization front convex in the melt or concave in the crystal, random crystal nuclei (impurity nuclei) will grow compatible with the main one, and on the flat crystallization front, uniform and stable crystal growth is formed with a minimum number of defects [3 – 5].

Based on the physical model of vertical zone melting, a computer model was created to study the formation of the shape of the crystallization front in order to find the optimal dimensions of the heater for a specific thermoelectric material based on *Bi-Te*. The physical model of vertical zone melting is presented in Fig. 1.

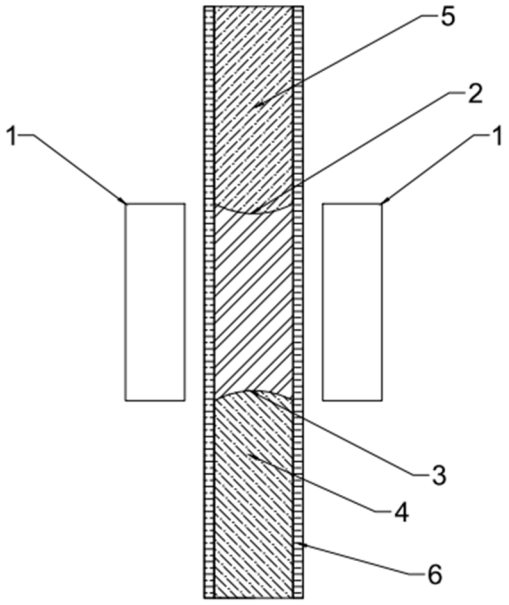

Fig. 1. Physical model: 1 –heaters, 2 – boundary of melt front,
3 – boundary of crystallization front, 4 – material in solid phase (single crystal),
5 – material in solid phase (polycrystal), 6 – quartz ampoule

The computer model was created using Comsol Multiphysics software. It represents a classical system of differential equations of thermal conductivity supplemented by dependences of the physical properties of the material being studied. The constructed computer model makes it possible to change

geometric and temperature parameters and monitor the formation of the crystallization front. The results of modeling the dependence of the shape of the crystallization front, thermoelectric material based on *Bi-Te*, on the height of the cylindrical heater are shown in Fig. 2. This made it possible to determine that the flat front is fully formed at the ratio $h = 2.25d$ for the given composition of the thermoelectric material based on *Bi-Te*. To determine the influence of the shape of the crystallization front on the parameters of this thermoelectric material based on *Bi-Te*, two ingots were made, the first with a ratio of $h = 2.25d$, and the second with $h = 1.5d$. The thermoelectric parameters of the manufactured material are presented in Fig. 3, 4.

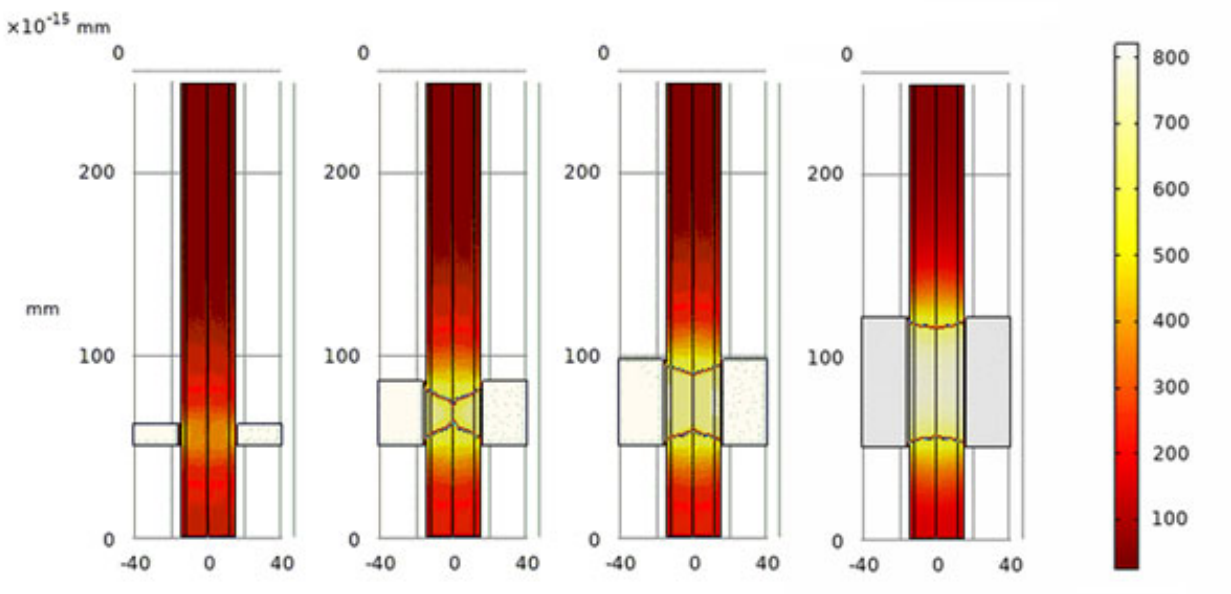

Fig. 2. Computer model of change in the shape of crystallization front

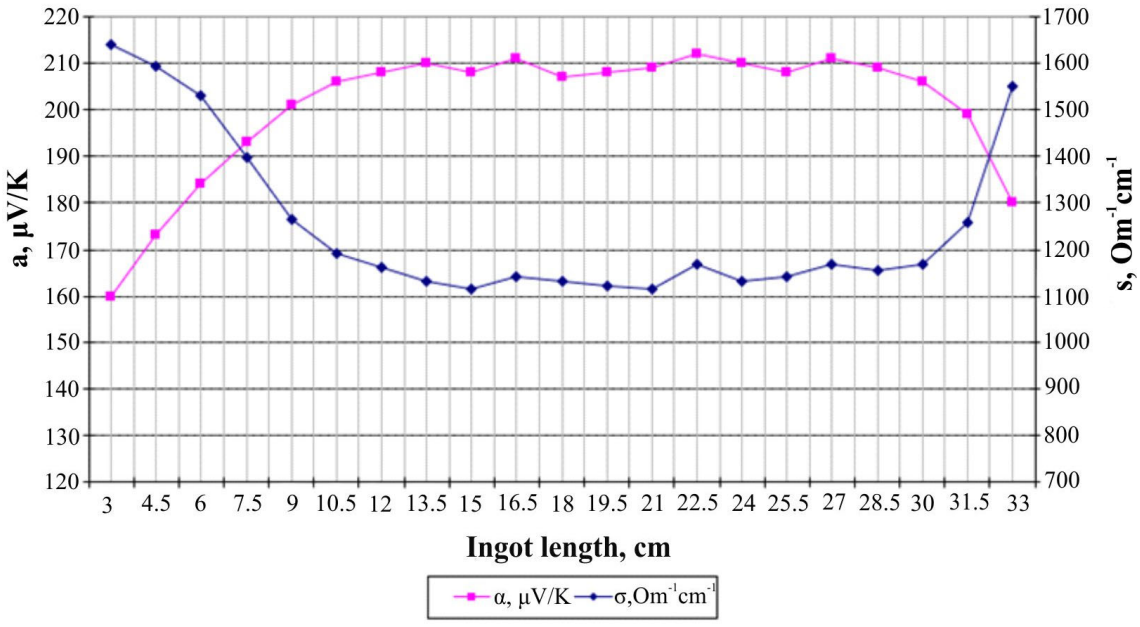

Fig. 3. Thermoelectric parameters, where h=2.25d

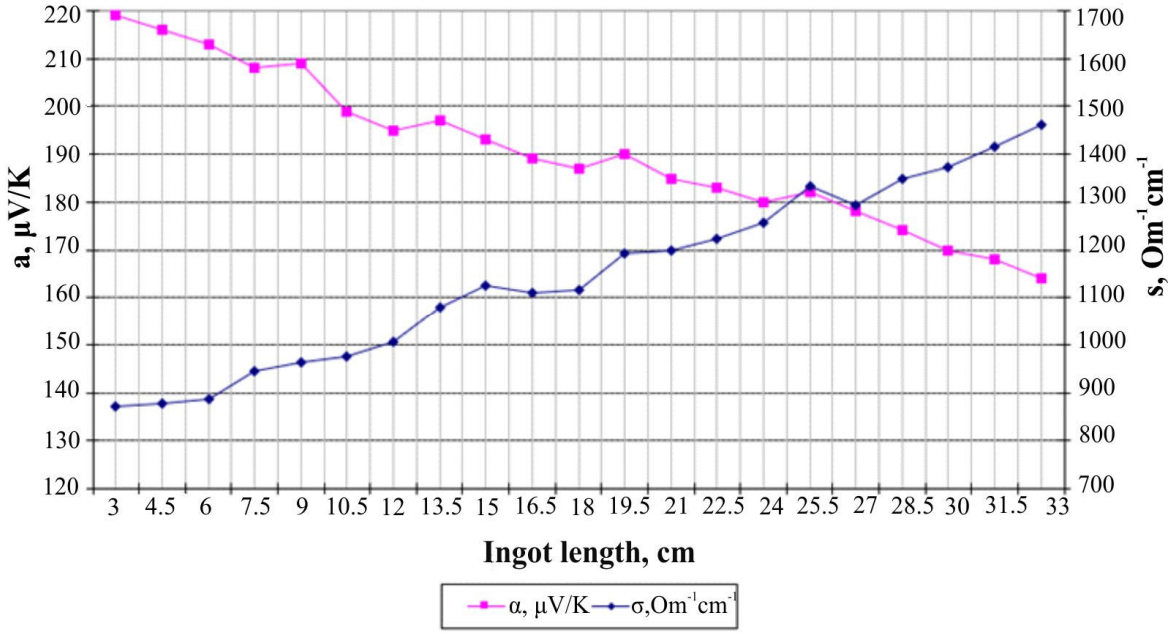

Fig. 4. Thermoelectric parameters, where h=1.5d

As can be seen from the graphs, a flat crystallization front and a relatively large volume of the liquid phase (h = 2.25d) create a homogeneous material with a small number of structural defects along the entire length of the ingot, while the material obtained at a ratio of h = 1.5d, is characterized by heterogeneity of thermoelectric parameters along the length of the ingot. Since nowadays there is a tendency to increase the volume of material production by increasing the diameter of ampoules, the known ratios calculated in other works do not always retain their relevance. That is why it is expedient to study the conditions for the formation of a flat crystallization front, for each composition of components of a thermoelectric material, as a preparatory stage of the technological process, this is especially relevant for the mass production of thermoelectric materials at enterprises.

It should be noted that depending on the composition of the components, or when the technological equipment is changed, the period of formation of the flat crystallization front may also change, which will require additional research to optimize the new technology and maximize the quality of the manufactured thermoelectric material. Such studies usually lead to significant expenditure of time and money for conducting experiments, therefore, the use of such computer models for the optimization of this process allows to significantly reduce the material costs and time required for the optimization of the manufacturing technology.

Conclusions

The use of computer simulation in the production of thermoelectric materials obtained by the method of vertical zone melting allows for a faster, more efficient and innovative development and manufacturing process. This significantly reduces the time and material costs of experiments and opens up new opportunities for the creation of highly efficient materials thar can be widely used in the production of thermoelectric devices and systems that use renewable energy sources and heat flows.

The Author expresses his gratitude to Academician of NASU Anatychuk L.I. for providing the research topic.

References

1. Goltsman B. M., Kudinov V. A., Smirnov I. A. (1972). *Poluprovodnikovyie termoelektricheskiie materialy na osnove Bi_2Te_3 [Semiconductor thermoelectric materials based on Bi_2Te_3]*. B. Ya. Moizhes (Ed.). M: Nauka.
2. Anatychuk L. I. (1979). *Termoelementy i termoelektricheskiie ustroistva [Thermoelements and thermoelectric devices]*. Kyiv: Naukova Dumka.
3. Vilke K.T. (1977). *Metody vyrashchivaniia kristallov [Methods of crystal growth]*. L: Nedra.
4. Nitsovich O. V. (2018). Research on the conditions of forming a flat crystallization front when growing Bi_2Te_3 based thermoelectric material by vertical zone melting method. *J. Thermoelectricity*, 3, 76 – 82.
5. Nitsovich O. V. (2018). Computer simulation of Bi_2Te_3 crystallization process in the presence of electrical current. *J. Thermoelectricity*, 5, 12 – 21.

Submitted: 27.02.2023

Рибчаков Д. Є.

Інститут термоелектрики НАН та МОН України,
вул. Науки, 1, Чернівці, 58029, Україна,
e-mail: anatych@gmail.com

ВИКОРИСТАННЯ КОМП'ЮТЕРНОГО МОДЕЛЮВАННЯ ДЛЯ ОПТИМІЗАЦІЇ ТЕХНОЛОГІЧНИХ РЕЖИМІВ ВИГОТОВЛЕННЯ ТЕРМОЕЛЕКТРИЧНИХ МАТЕРІАЛІВ НА ОСНОВІ *Bi-Te* ОТРИМАНИХ МЕТОДОМ ВЕРТИКАЛЬНОЇ ЗОННОЇ ПЛАВКИ

У статті наводяться основні типи комп'ютерних моделей, які застосовуються для дослідження термоелектричних матеріалів. Наводиться опис фізичної та математичної моделей вирощування кристалів, та метод застосування моделей вирощування кристалів для оптимізації технології виготовлення термоелектричного матеріалу на основі Bi-Te, та термоелектричні параметри виготовлених термоелектричних матеріалів. Бібл. 5. Рис. 4.
Ключові слова: вертикальна зонна плавка, термоелектричний матеріал, комп'ютерна модель.

References

1. Goltsman B. M., Kudinov V. A., Smirnov I. A. (1972). *Poluprovodnikovyie termoelektricheskiie materialy na osnove Bi_2Te_3 [Semiconductor thermoelectric materials based on Bi_2Te_3]*. B. Ya. Moizhes (Ed.). M: Nauka.

2. Anatychuk L. I. (1979). *Termoelementy i termoelektricheskiie ustroistva [Thermoelements and thermoelectric devices]*. Kyiv: Naukova Dumka.
3. Vilke K. T. (1977). *Metody vyrashchivaniia kristallov [Methods of crystal growth]*. L: Nedra.
4. Nitsovich O. V. (2018). Research on the conditions of forming a flat crystallization front when growing Bi_2Te_3 based thermoelectric material by vertical zone melting method. *J. Thermoelectricity*, 3, 76 – 82.
5. Nitsovich O. V. (2018). Computer simulation of Bi_2Te_3 crystallization process in the presence of electrical current. *J. Thermoelectricity*, 5, 12 – 21.

Submitted: 27.02.2023

L. I. Anatychuk, *acad. of the NAS of Ukraine* [1,2]
R. R. Kobylianskyi, *cand. phys.-math. sciences*[1,2]
V. V. Lysko, *cand. phys.-math. sciences*[1,2]

[1]Institute of Thermoelectricity of the NAS and MES of Ukraine,
1, Nauky str., Chernivtsi, 58029, Ukraine,
e–mail: anatych@gmail.com;
[2]Yu.Fedkovych Chernivtsi National University,
2, Kotsiubynskyi str., Chernivtsi, 58012, Ukraine

COMPUTER DESIGN OF A THERMOELECTRIC PULMONARY AIR CONDENSER WITH THERMOSTATING OF COLLECTED CONDENSATE

A new design of a thermoelectric pulmonary air condenser is proposed, in which an additional thermostated chamber is used to collect condensed moisture. This allows maintaining the temperature of the collected condensate at a given permissible level to prevent its hypothermia and standardize the storage conditions. The physical model and computer model of the device are presented, the distribution of temperature and velocity of air movement in the condensate collection tube is determined depending on the temperatures of the working and additional chambers, as well as humidity, temperature and volume of exhaled air. The results of calculations of the cooling efficiency of thermoelectric modules, necessary to ensure the specified modes of operation of the device, are given. Bibl. 7, Fig. 9.
Key words: diagnostics, coronavirus, condensate, exhaled air, thermoelectric cooling.

Introduction

Diagnostic testing plays a crucial role in overcoming the pandemic of the coronavirus disease COVID-19, caused by the severe acute respiratory syndrome coronavirus SARS-CoV-2. Rapid and accurate diagnostic tests are mandatory for identification and treatment of infected individuals, contact tracing, epidemiologic characterization, and healthcare decision-making. Modern diagnostic testing for the coronavirus disease COVID-19 is based on the detection of the SARS-CoV-2 coronavirus in swab samples from the nasopharynx by the reverse transcription polymerase chain reaction (RT-PCR) method. However, this test is associated with an increased risk of viral spread and environmental contamination and shows a relatively low sensitivity due to technical shortcomings of the sampling method. Given that COVID-19 is transmitted through aerosols and droplets exhaled by humans, the detection of SARS-CoV-2 in pulmonary condensate may serve as a promising non-invasive diagnostic method. This method is proposed in the works of scientists from Japan, the USA, Ireland and other countries as a more sensitive and reliable method of detecting COVID-19 [1 – 3]. Generally, special devices, namely condensers, are used to collect condensate, in which vapors from the air exhaled by a person condense at a temperature from 0 to -70 °C and are collected in a container for further research by the RT-PCR method [4]. Lowering the condensation temperature makes it possible to speed up obtaining the amount of biological material required for research. At the same time, the operating temperatures of condensers that use ice at 0°C or compressor cooling down to -20°C are not efficient

enough and do not provide a high condensation rate. In addition, compressor condensers are complex, expensive, with insufficient control and maintenance of operating temperature, as well as the presence of dangerous refrigerants. The temperature of -70 °C, which is achieved using dry ice (solid CO2), is excessive and extremely inconvenient for operation, which drastically reduces the possibilities of using this method. The paper [5] gives the results of computer design of a thermoelectric device for collecting exhaled air condensate with precisely regulated condensation temperatures below -20 °C and close to -70 °C without the use of dry ice

However, in some cases, it is also important that the collected condensate does not freeze and is not supercooled, because this can negatively affect the results of research [6]. For such a case, a device scheme with a separate thermostated chamber, in which condensed moisture is collected, can be used.

The purpose of the work is computer design and development of the design of a thermoelectric pulmonary air condenser with thermostatng of the collected condensate.

Physical and computer models of a thermoelectric pulmonary air condenser

Physical model of a cooling unit for a thermoelectric pulmonary air condenser with a separate thermostated chamber in which condensed moisture is collected, is shown in Fig. 1.

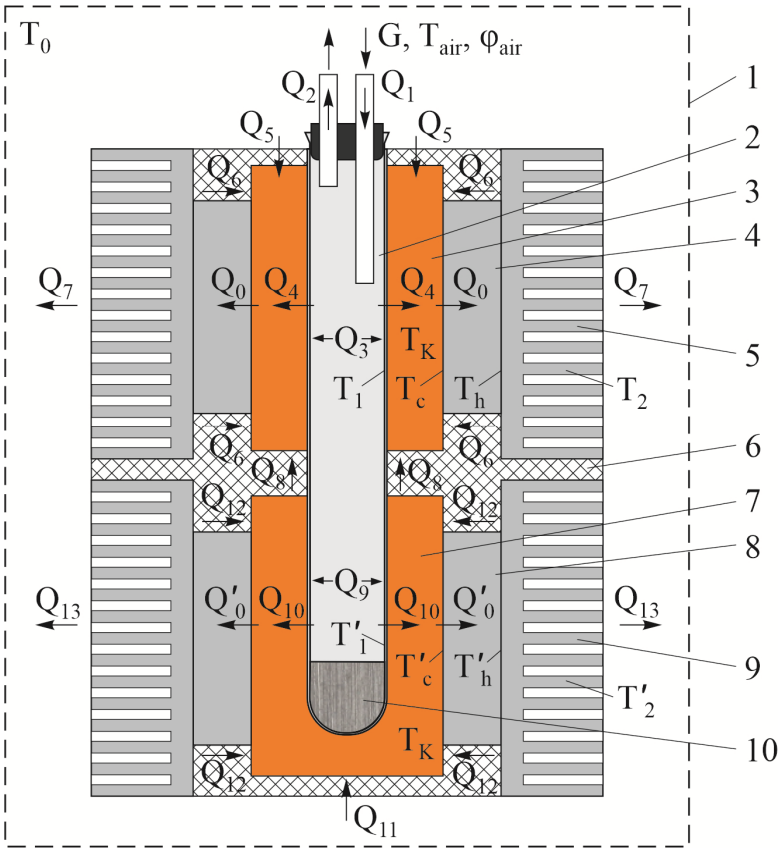

Fig. 1 – Physical model of a cooling unit for a thermoelectric device for collecting condensate from the air exhaled by a person: 1 – thermostat (device body); 2 – test tube for collecting condensate; 3 – working chamber; 4, 8 – thermoelectric modules; 5, 9 – air heat exchangers; 6 – thermal insulation; 7 – additional cooling chamber; 10 – collected moisture

In Fig. 1:

G, T_{air}, φ_{air} – consumption, temperature and relative humidity of air exhaled by the patient;

Q_1 – heat flow entering the tube for collecting condensate together with the air exhaled by the patient;

Q_2 – heat flow removed from the test tube to the environment;

Q_3, Q_9 – heat released in the test tube during the condensation of exhaled air vapours;

Q_4 – heat flow transferred from the walls of the test tube to the working cooling chamber;

Q_5 –inflow of heat to the working cooling chamber from the environment through thermal insulation;

Q_6 –inflow of heat to the working cooling chamber from the air heat exchangers through thermal insulation;

Q_7 – heat flow removed from the air heat exchangers of the working cooling chamber to the environment;

Q_8 – inflow of heat from the additional cooling chamber to the working chamber through thermal insulation;

Q_{10} – heat flow transferred from the test tube walls to additional cooling chamber;

Q_{11} – inflow of heat to the additional cooling chamber from the environment through thermal insulation;

Q_{12} – inflow of heat to the additional cooling chamber from the air heat exchangers through thermal insulation;

Q_{13} – heat flow removed from the air heat exchangers of the additional cooling chamber to the environment;

Q_0, Q'_0 – cooling capacity of thermoelectric modules of the working and additional cooling chambers;

T_1, T'_1 – temperatures of test tube walls in the working and additional cooling chambers;

T_c, T'_c – cold side temperature of thermoelectric modules of the working and additional cooling chambers;

T_h, T'_h – hot side temperature of thermoelectric modules of the working and additional cooling chambers;

T_2, T'_2 – temperature of air heat exchangers of the working and additional cooling chambers;

T_0 – temperature of the environment (device body).

A computer model of the device was built using the Comsol Multiphysics software package. In doing so, the following program modules were used.

1. *Turbulent Flow*. Allows simulating turbulent flow using a wide range of turbulence models, as well as Large Eddy Simulation (LES) and Detached Eddy Simulation (DES). The eight turbulence models differ in how they model flow near walls, the number of additional variables that are calculated, and what these variables represent. All these models supplement the Navier-Stokes equation with an additional eddy viscosity term of turbulence, but they differ in the way it is calculated

2. *Heat Transfer in Solids*. Allows solving equation

$$\rho C_p\left(\frac{\partial T}{\partial t} + \mathbf{u}_{\text{trans}} \cdot \nabla T\right) + \nabla \cdot (\mathbf{q} + \mathbf{q}_r) = -\alpha T : \frac{dS}{dt} + Q$$

where:

- ρ – density (SI unit: kg/m^3);
- C_p – specific heat capacity at constant pressure (SI unit: J/(kg·K));
- T – absolute temperature (SI unit: K);
- $\mathbf{u}_{\text{trans}}$ – vector of translational speed (SI unit: m/s);
- $\mathbf{q}$ – heat flow due to thermal conductivity (SI unit: W/m^2);
- $\mathbf{q}_r$ – heat flow due to radiation (SI unit: W/m^2);
- α – coefficient of thermal expansion (SI unit: 1/K);

• S – the second Piol-Kirchhoff stress tensor (SI unit: Pa);

• Q comprises additional sources of heat (SI unit: W/m^3).

For a stationary problem, the temperature does not change with time and conditions, and derivatives disappear with time.

3. *Moisture Transfer in Air*. Interface of moisture transfer in air solves the equation

$$M_{\mathrm{v}}\frac{\partial c_{\mathrm{v}}}{\partial t}+M_{\mathrm{v}}\mathbf{u}\cdot\nabla c_{\mathrm{v}}+\nabla\cdot\mathbf{g}=G$$

in which the change in moisture content is expressed through the transfer of vapor concentration, which itself can be expressed as the product of the molar mass of water, the relative humidity, and the vapour saturation concentration:

$$\mathbf{g}=-M_{\mathrm{v}}D\nabla c_{\mathrm{v}}$$

$$c_{\mathrm{v}}=\phi c_{\mathrm{sat}}$$

with the following material properties, fields and source:

• M_{v} (SI unit: kg/mole – molar mass of water vapour;

• φ (dimensionless) – relative humidity;

• c_{sat} (SI unit: mole/m^3) – vapour saturation concentration;

• D (SI unit: m^2/s) – coefficient of vapour diffusion in air;

• u (SI unit: m/s) – air velocity field;

• G (SI unit: kg/(m^3·s)) – moisture source (or absorber).

Transfer of vapor concentration occurs by convection and diffusion in moist air. It is assumed that moisture consists only of vapour. In other words, the concentration of the liquid is zero.

4. *Heat Transfer in Moist Air*.. It is used to model heat transfer in moist air by convection and diffusion using thermodynamic properties defined as a function of the amount of vapor in moist air.

5. *Multiphysics. Nonisotermal Flow*. Non-isothermal flow refers to fluid flows with non-constant temperatures. When a liquid undergoes a change in temperature, its material properties, such as density and viscosity, change accordingly. In some situations, these changes are large enough to have a significant effect on the flow field. And since the liquid transfers heat, the temperature field, in turn, is affected by changes in the flow field.

6. *Multiphysics. Moisture Flow.* The Moisture Flow multiphysics coupling is used to model fluid flows where fluid properties (density, viscosity) depend on moisture content. The Moisture Flow interface allows you to maintain vapor concentration, mass and momentum in the air. It synchronizes the functions of the moisture transport and fluid flow interfaces when a turbulent flow regime is defined.

7. *Multiphysics. Heat and Moisture*. This multiphysics relationship is used to model coupled heat and moisture exchange processes in various environments, including moist air by modeling moisture transport by vapor diffusion and convection and heat transfer by conduction and convection. The thermodynamic properties of moist air depend on the moisture content, while the temperature is used to define the saturation conditions for vapor concentration. This module synchronizes the functions of heat transfer and moisture transport interfaces:

• determines the relative humidity ϕw (with appropriate temperature and pressure) to adjust the appropriate input to the Wet Air function of the heat transfer interface;

• determines the temperature to set the model input data in the functions of the moisture transport interface;

• calculates the latent heat source due to evaporation and condensation fluxes on surfaces and adds it to the heat transfer equation.

The created computer model makes it possible to calculate temperature distributions in the working chamber and the tube for collecting condensate from air exhaled by a person, the velocity of air in the tube, and determine the amount of condensate received.

Computer simulation results

The used boundary conditions of the computer model correspond to the physical model shown in Fig. 1. In this case, the average consumption of incoming air is determined by the number of exhalations per minute and the volume of exhaled air. It is known from the literature that the typical number of exhalations per minute is between 12 and 21. In doing so, the volume of exhaled air is equal to 0.3 - 0.7 l. The work [7] shows the results of experimental studies of the temperature and relative humidity of the exhaled air: the temperature range of exhaled air is 31.4-35.4 °C for participants from Haifa and 31.4 - 34.8 °C for participants from Paris, and the exhaled air relative humidity range is 65.0-88.6 % and 41.9-91.0 % for Haifa and Paris. participants respectively. That is, the temperature of air exhaled by people is in the range of 34-35 °C, and the relative humidity of the air is high, 90 % and above, regardless of geographical location.

The above ranges of input parameters were used for calculations. Fig. 3 shows a typical temperature distribution in a condensate collection tube. For this case, the following input parameters were used: working chamber temperature – 223.15 K; the temperature of the additional chamber - 273.15 K; the temperature of the air exhaled by a person - 306.65 K; humidity of exhaled air – 90 %; the average air velocity at the entrance to the test tube is equivalent to 18 exhalations per minute with an air volume of 0.5 l.

The computer model makes it possible to obtain similar distributions for other values of the input parameters, to build the dependences of the amount of collected condensate and its temperature on these parameters, to determine the requirements for thermoelectric modules and to optimize the design and operating modes of the device.

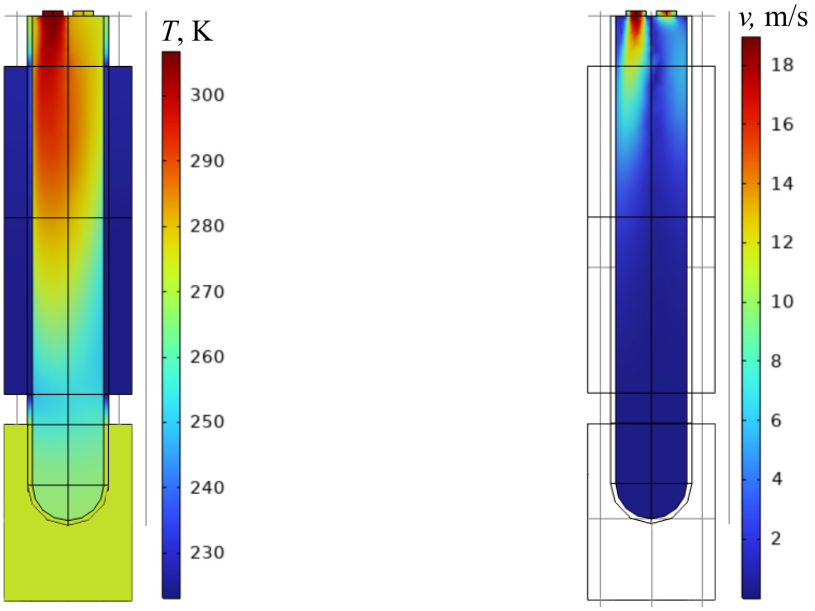

Fig. 3. Typical distributions of temperature (a) and air velocity (b) in the test tube for collecting exhaled air condensate

Figs. 4, 5 give an example of the results of computer calculations of the condensate collection velocity V_K (in ml per minute) and the thermal power Q_0 that must be removed from the working chamber at different values of the working chamber temperature T_K, relative humidity of the exhaled air φ_{air}, temperature and exhaled air consumption.

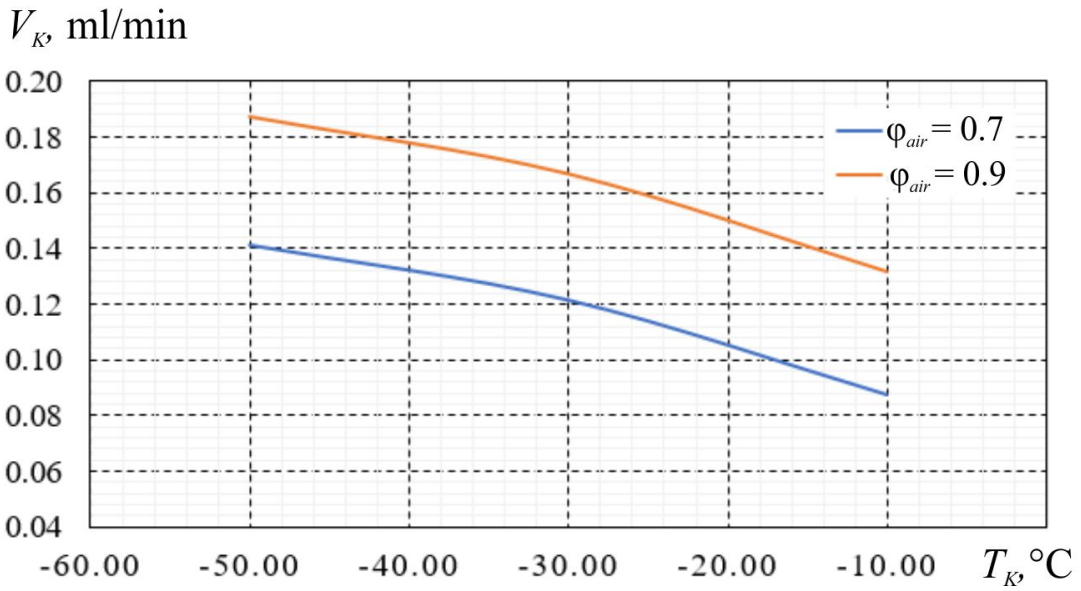

Fig. 4. Dependences of the condensate collection velocity V_K on the temperature in the working chamber T_K for different values of the relative humidity of the exhaled air (the temperature of the additional cooling chamber is 0 °C; the temperature of the exhaled air is 33.5 °C; the air consumption is equivalent to 18 exhalations per minute with an exhalation volume of 0.5 l)

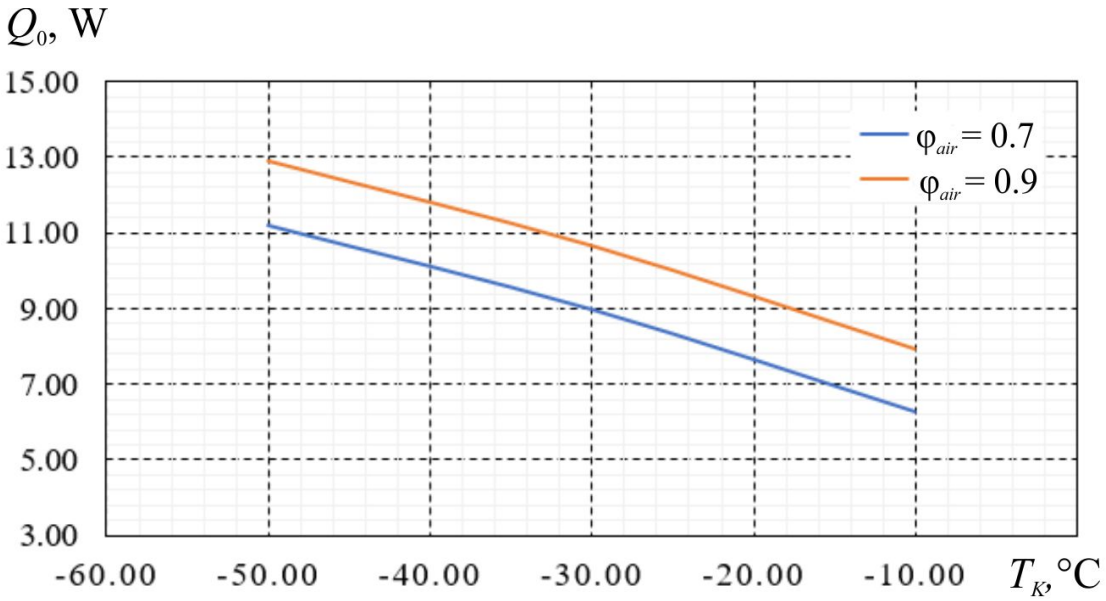

Fig. 5. Dependences of the thermal power Q_0, which must be removed from the working chamber, on the temperature in the working chamber T_K for different values of the relative humidity of the exhaled air (the temperature of the additional cooling chamber is 0 °C; the temperature of the exhaled air is 33.5 °C; the air consumption is equivalent to 18 exhalations per minute with an exhalation volume of 0.5 l)

Fig. 6 shows the dependence of the condensate collection velocity V_K on the exhaled air consumption G for different temperature values of the working chamber T_K (at an exhaled air

temperature of 33.5 °C and its relative humidity of 90%), and Fig. 7 – the corresponding dependence of the thermal power Q_0, which must be removed from the working chamber to ensure such operating modes.

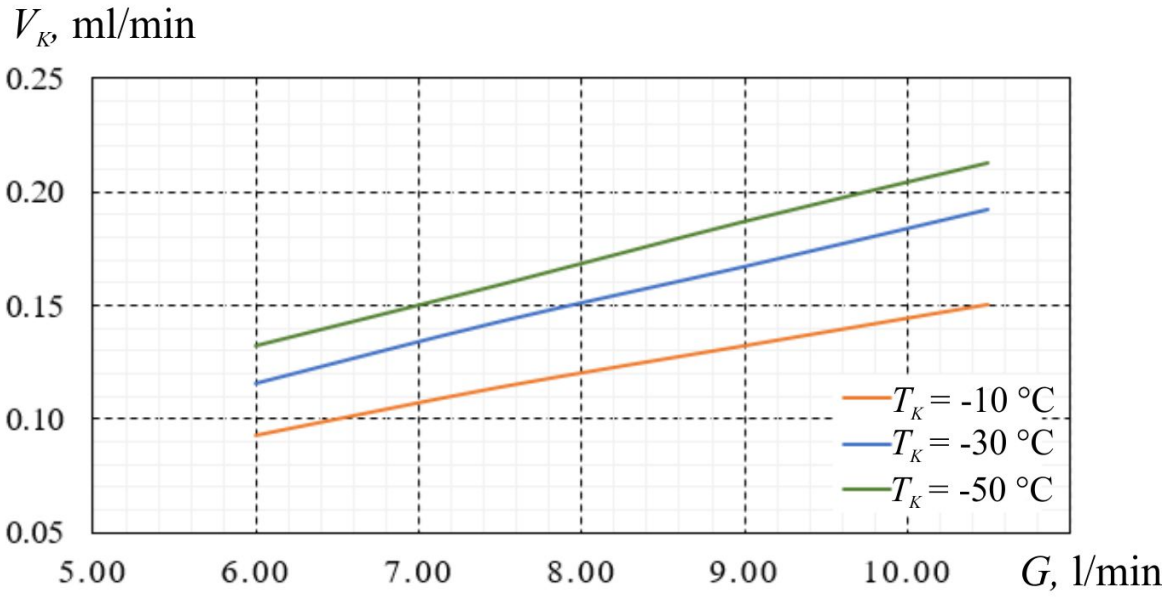

Fig. 6. Dependences of the condensate collection velocity V_K on the exhaled air consumption G for different temperature values of the working chamber T_K (at the temperature of the exhaled air 33.5 °C, its relative humidity 90 % and the temperature of the additional cooling chamber – 0 °C)

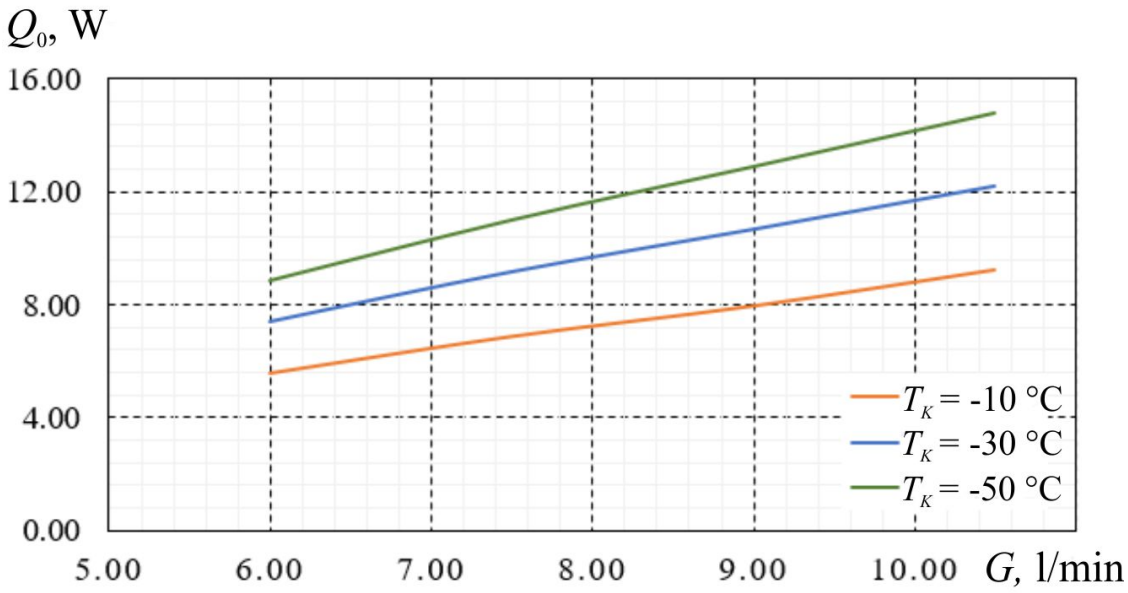

Fig. 7. Dependences of the thermal power Q_0which must be removed from the working chamber, on the exhaled air consumption G for different values of the temperature of the working chamber T_K (at the temperature of the exhaled air 33.5 °C, its relative humidity 90 % and the temperature of the additional cooling chamber – 0 °C)

Based on the results of computer simulation, to ensure the necessary operating modes of a thermoelectric device for collecting condensate from the air exhaled by a person, one module, for example, the Altec-2 type produced by the Institute of Thermoelectricity, is sufficient to maintain the temperature of the working chamber at the specified cooling capacity of the module

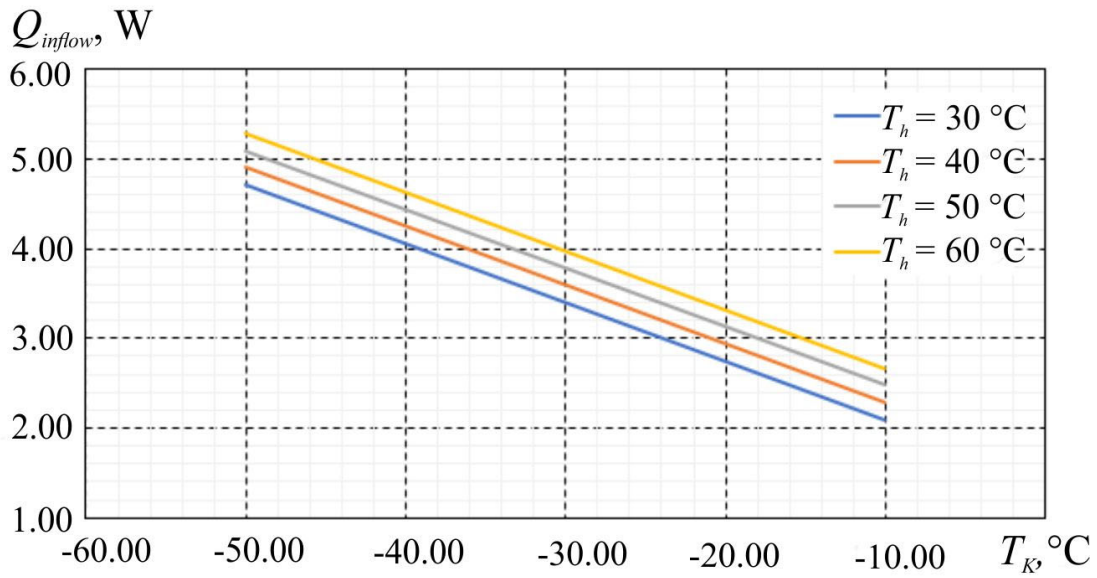

Fig. 8. Dependences of heat inflows from the environment to the working chamber Q_{inflow} on the temperature of the working chamber T_K for different values of the hot side temperature of the thermoelectric module (the temperature of the additional chamber is -0 °C)

Using computer simulation in Comsol Multiphysics for the physical model shown above in Fig. 1, the amounts of heat inflow from the environment Q_{inflow}, are calculated which are composed of heats: Q_5 – heat inflow to the working chamber from the environment through thermal insulation, Q_6 – heat inflow into the working chamber from air heat exchangers through thermal insulation, and Q_8 – heat inflow from additional cooling chamber to the working chamber due to thermal insulation. The results of the calculations are shown in Fig. 8.

Taking into account the maximum values of the thermal power Q_0, which must be removed from the working chamber for different values of its temperature T_K, the dependence of the total cooling capacity of the thermoelectric module of the working chamber Q_{0total} on its temperature was obtained for different values of the hot side temperature of the module (Fig. 9).

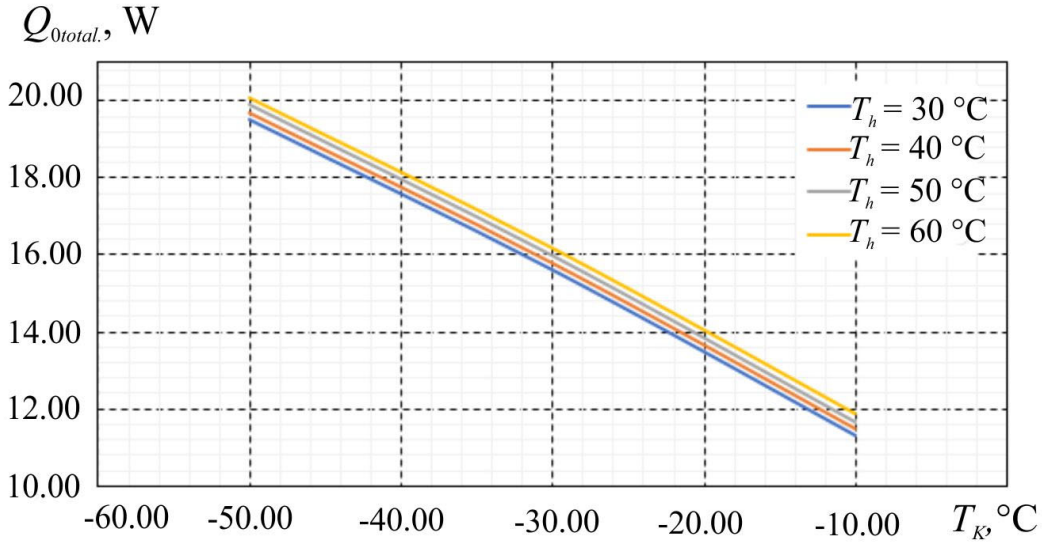

Fig. 9. Dependences of cooling capacity of thermoelectric module of the working chamber $Q_{0total.}$ on its temperature T_K for different hot side temperature values of thermoelectric module (the temperature of additional chamber –0 °C)

Thus, in order to ensure the necessary modes of the working chamber of the device (temperature below -20 ℃) with a power consumption of the Altec-2 thermoelectric module of about 145 W and a cooling capacity of up to 20 W, a heat exchange system is required, which will remove about 165 W of heat with a temperature difference relative to the environment not above 15 ℃. At the same time, additional chamber thermostating does not require such low temperatures and can be performed using standard thermoelectric cooling modules.

The presented results are the basis for the further development of the design of a thermoelectric device for collecting condensate from the air exhaled by a person.

Conclusions

1. A physical and computer model of a thermoelectric pulmonary air condenser was built, in which an additional thermostated chamber was used to collect condensed moisture, which. allows maintaining the temperature of the collected condensate at a given level, different from the temperature in the working cooling chamber.
2. The dependences of temperature distributions and air velocity in a condensate collection tube on the temperatures of the working and additional chambers, as well as the humidity, temperature and volume of exhaled air, and the amount of heat inflow from the environment were calculated.
3. It has been established that reducing the temperature of the working chamber to -50 ℃ (at an additional chamber temperature of 0 ℃) makes it possible to achieve a condensate collection velocity of 0.13 - 0.21 ml/min. At the same time, to ensure the required operating mode, the cooling capacity of the thermoelectric modules of the working chamber should be 19 - 20 W.

References

1. Hunt John (2007). Exhaled breath condensate-an overview. *Immunol Allergy Clin North Am.,* 27 (4), 587 – 596.
2. Hunt J. (2002). Exhaled breath condensate: An evolving tool for noninvasive evaluation of lung disease. *J Allergy Clin Immunol*; 110 (1): 28 – 34.
3. Horvath I., Hunt J. and Barnes P. J. (2005). Exhaled breath condensate: methodological recommendations and unresolved questions. *Eur Respir J*, 26: 523 – 548.
4. Konstantinidi Efstathia M., Lappas Andreas S, Tzortzi Anna S. and Behrakis Panagiotis K. (2015). Exhaled breath condensate: technical and diagnostic aspects. *Scientific World Journal*, V. 2015, Article ID 435160, 25 pages.
5. Anatychuk L. I., Kobylianskyi R. R., Lysko V. V. (2022). Computer design of a thermoelectric pulmonary air condenser for diagnostics of coronavirus and other diseases. *J. Thermoelectricity*, 1, 65 – 72.
6. Zamuruyev K. O., Borras E., Pettit D. R., Aksenov A. A., Simmons J. D., Weimer B. C., Schivo M., Kenyon N. J., Delplanque J. P., Davis C. E. (2018). Effect of temperature control on the metabolite content in exhaled breath condensate. *Anal Chim Acta.* May 2; 1006: 49 – 60. doi: 10.1016/j.aca.2017.12.025.
7. Mansour, Elias & Vishinkin, Rotem & Rihet, Stéphane & Saliba, Walaa & Fish, Falk & Sarfati, Patrice & Haick, Hossam. (2019). Measurement of temperature and relative humidity in exhaled breath. *Sensors and Actuators B Chemical*. 127371. 10.1016/j.snb.2019.127371.

Submitted: 29.03.2023

Анатичук Л. І., *акад. НАН України* [1,2]
Кобилянський Р. Р., *канд. фіз.-мат. наук* [1,2]
Лисько В. В., *канд. фіз.-мат. наук* [1,2]

[1] Інститут термоелектрики НАН та МОН України,
вул. Науки, 1, Чернівці, 58029, Україна;
[2] Чернівецький національний університет імені Юрія Федьковича,
вул. Коцюбинського 2, Чернівці, 58012, Україна
e-mail: anatych@gmail.com

КОМП'ЮТЕРНЕ ПРОЄКТУВАННЯ ТЕРМОЕЛЕКТРИЧНОГО КОНДЕНСАТОРА ЛЕГЕНЕВОГО ПОВІТРЯ З ТЕРМОСТАТУВАННЯМ ЗІБРАНОГО КОНДЕНСАТУ

Запропоновано нову конструкцію термоелектричного конденсатора легеневого повітря, у якій використано додаткову термостатовану камеру для збирання конденсованої вологи. Це дозволяє підтримувати температуру зібраного конденсату на заданому допустимому рівні для запобігання його переохолодженню і стандартизації умов зберігання. Наведено фізичну модель та комп'ютерну моделі приладу, визначено розподіли температури та швидкості руху повітря у пробірці для збирання конденсату в залежності від температур робочої та додаткової камер, а також вологості, температури та об'єму видихуваного повітря. Наведено результати розрахунків холодопродуктивності термоелектричних модулів, необхідної для забезпечення заданих режимів роботи приладу. Бібл. 7, рис. 9.
Ключові слова: діагностика, коронавірус, конденсат, видихуване повітря, термоелектричне охолодження.

References

1. Hunt John (2007). Exhaled breath condensate-an overview. *Immunol Allergy Clin North Am.,* 27 (4), 587 – 596.
2. Hunt J. (2002). Exhaled breath condensate: An evolving tool for noninvasive evaluation of lung disease. *J Allergy Clin Immunol*; 110 (1): 28 – 34.
3. Horvath I., Hunt J. and Barnes P.J.(2005). Exhaled breath condensate: methodological recommendations and unresolved questions*. Eur Respir J*, 26: 523 – 548.
4. Konstantinidi Efstathia M., Lappas Andreas S, Tzortzi Anna S. and Behrakis Panagiotis K. (2015). Exhaled breath condensate: technical and diagnostic aspects.*Scientific World Journal*, V. 2015, Article ID 435160, 25 pages.
5. Anatychuk L. I., Kobylianskyi R. R., Lysko V. V. (2022). Computer design of a thermoelectric pulmonary air condenser for diagnostics of coronavirus and other diseases. *J. Thermoelectricity*, 1, 65 – 72.
6. Zamuruyev K. O., Borras E., Pettit D. R., Aksenov A. A., Simmons J. D., Weimer B. C., Schivo M., Kenyon N. J., Delplanque J. P., Davis C. E. (2018). Effect of temperature control on the metabolite content in exhaled breath condensate. *Anal Chim Acta.* May 2; 1006: 49 – 60. doi: 10.1016/j.aca.2017.12.025.
7. Mansour, Elias & Vishinkin, Rotem & Rihet, Stéphane & Saliba, Walaa & Fish, Falk & Sarfati, Patrice & Haick, Hossam. (2019). Measurement of temperature and relative humidity in exhaled breath. *Sensors and Actuators B Chemical*. 127371. 10.1016/j.snb.2019.127371.

Submitted: 29.03.2023

ARTICLE SUBMISSION GUIDELINES

For publication in a specialized journal, scientific works are accepted that have never been printed before. The article should be written on an actual topic, contain the results of an in-depth scientific study, the novelty and justification of scientific conclusions for the purpose of the article (the task in view).

The materials published in the journal are subject to internal and external review which is carried out by members of the editorial board and international editorial board of the journal or experts of the relevant field. Reviewing is done on the basis of confidentiality. In the event of a negative review or substantial remarks, the article may be rejected or returned to the author(s) for revision. In the case when the author(s) disagrees with the opinion of the reviewer, an additional independent review may be done by the editorial board. After the author makes changes in accordance with the comments of the reviewer, the article is signed to print.

The editorial board has the right to refuse to publish manuscripts containing previously published data, as well as materials that do not fit the profile of the journal or materials of research pursued in violation of ethical norms (for instance, conflicts between authors or between authors and organization, plagiarism, etc.). The editorial board of the journal reserves the right to edit and reduce the manuscripts without violating the author's content. Rejected manuscripts are not returned to the authors.

Submission of manuscript to the journal

The manuscript is submitted to the editorial office of the journal in paper form in duplicate and in electronic form on an electronic medium (disc, memory stick). The electronic version of the article shall fully correspond to the paper version. The manuscript must be signed by all co-authors or a responsible representative.

In some cases it is allowed to send an article by e-mail instead of an electronic medium (disc, memory stick).

English-speaking authors submit their manuscripts in English. Russian-speaking and Ukrainian-speaking authors submit their manuscripts in English and in Russian or Ukrainian, respectively. Page format is A4. The number of pages shall not exceed 15 (together with References and extended abstracts). By agreement with the editorial board, the number of pages can be increased.

To the manuscript is added:

1. Official recommendation letter, signed by the head of the institution where the work was carried out.

2. License agreement on the transfer of copyright (the form of the agreement can be obtained from the editorial office of the journal or downloaded from the journal website – Dohovir.pdf). The license agreement comes into force after the acceptance of the article for publication. Signing of the license agreement by the author(s) means that they are acquainted and agree with the terms of the agreement.

3. Information about each of the authors – full name, position, place of work, academic title, academic degree, contact information (phone number, e-mail address), ORCID code (if available). Information about the authors is submitted as follows:

authors from Ukraine - in three languages, namely Ukrainian, Russian and English;

authors from the CIS countries - in two languages, namely Russian and English;

authors from foreign countries – in English.

4. Medium with the text of the article, figures, tables, information about the authors in electronic form.

5. Colored photo of the author(s). Black-and-white photos are not accepted by the editorial staff. With the number of authors more than two, their photos are not shown.

Requirements for article design

The article should be structured according to the following sections:

- *Introduction*. Contains the problem statement, relevance of the chosen topic, analysis of recent research and publications, purpose and objectives.
- *Presentation of the main research material* and the results obtained.
- *Conclusions* summing up the work and the prospects for further research in this direction.
- *References*.

The first page of the article contains information:

1) in the upper left corner – UDC identifier (for authors from Ukraine and the CIS countries);

2) surname(s) and initials, academic degree and scientific title of the author(s);

3) the name of the institution where the author(s) work, the postal address, telephone number, e-mail address of the author(s);

4) article title;

5) abstract to the article – not more than 1 800 characters. The abstract should reflect the consistent logic of describing the results and describe the main objectives of the study, summarize the most significant results;

6) key words – not more than 8 words.

The text of the article is printed in Times New Roman, font size 11 pt, line spacing 1.2 on A4 size paper, justified alignment. There should be no hyphenation in the article.

Page setup: "mirror margins" – top margin – 2.5 cm, bottom margin – 2.0 cm, inside – 2.0 cm, outside – 3.0 cm, from the edge to page header and page footer – 1.27 cm.

Graphic materials, pictures shall be submitted in color or, as an exception, black and white, in .opj or .cdr formats, .jpg or .tif formats being also permissible. According to author's choice, the tables and partially the text can be also in color.

Figures are printed on separate pages. The text in the figures must be in the font size 10 pt. On the charts, the units of measure are separated by commas. Figures are numbered in the order of their arrangement in the text, parts of the figures are numbered with letters – a, b, .. On the back of the figure, the title of the article, the author (authors) and the figure number are written in pencil. Scanned images and graphs are not allowed to be inserted.

Tables are provided on separate pages and must be executed using the MSWord table editor. Using pseudo-graph characters to design tables is inadmissible.

Formulae shall be typed in Equation or MatType formula editors. Articles with formulae written by hand are not accepted for printing. It is necessary to give definitions of quantities that are first used in the text, and then use the appropriate term.

Captions to figures and tables are printed in the manuscript after the references.

Reference list shall appear at the end of the article. References are numbered consecutively in the order in which they are quoted in the text of the article. References to unpublished and unfinished works are inadmissible.

Attention! In connection with the inclusion of the journal in the international bibliographic abstract database, the reference list should consist of two blocks: CITED LITERATURE and REFERENCES (this requirement also applies to English articles):

CITED LITERATURE – sources in the original language, executed in accordance with the

Ukrainian standard of bibliographic description DSTU 8302:2015. With the aid of VAK.in.ua (http://vak.in.ua) you can automatically, quickly and easily execute your "Cited literature" list in conformity with the requirements of State Certification Commission of Ukraine and prepare references to scientific sources in Ukraine in understandable and unified manner. This portal facilitates the processing of scientific sources when writing your publications, dissertations and other scientific papers.

REFERENCES – the same cited literature list transliterated in Roman alphabet (recommendations according to international bibliographic standard APA-2010, guidelines for drawing up a transliterated reference list "References" are on the site http//www.dse.org.ua, section for authors).

To speed up the publication of the article, please adhere to the following rules:

- in the upper left corner of the first page of the article – the UDC identifier;
- family name and initials of the author(s);
- academic degree, scientific title;

begin a new line, Times New Roman font, size 12 pt, line spacing 1.2, center alignment;

- name of organization, address (street, city, zip code, country), e-mail of the author(s);

begin a new line 1 cm below the name and initials of the author(s), Times New Roman font, size 11 pt, line spacing 1.2, center alignment;

- the title of the article is arranged 1 cm below the name of organization, in capital letters, semi-bold, font Times New Roman, size 12 pt, line spacing 1.2, center alignment. The title of the article shall be concrete and possibly concise;
- the abstract is arranged 1 cm below the title of the article, font Times New Roman, size 10 pt, in italics, line spacing 1.2, justified alignment in Ukrainian or Russian (for Ukrainian-speaking and Russian-speaking authors, respectively);
- key words are arranged below the abstract, font Times New Roman, size 10 pt, line spacing 1.2, justified alignment. The language of the key words corresponds to that of the abstract. Heading "Key words" - font Times New Roman, size 10 pt, semi-bold;
- the main text of the article is arranged 1 cm below the abstract, indent 1 cm, font Times New Roman, size 11 pt, line space spacing 1.2, justified alignment;
- formulae are typed in formula editor, fonts Symbol, Times New Roman. Font size is "normal" – 12 pt, "large index" – 7 pt, "small index" – 5 pt, "large symbol" – 18 pt, "small symbol" – 12 pt. The formula is arranged in the text, center aligned and shall not occupy more than 5/6 of the line width, formulae are numbered in parentheses on the right;
- dimensions of all quantities used in the article are represented in the International System of Units (SI) with the explication of the symbols employed;
- figures are arranged in the text. The figures and pictures shall be clear and contrast; the plot axes – parallel to sheet edges, thus eliminating possible displacement of angles in scaling; figures are submitted in color, black-and-white figures are not accepted by the editorial staff of the journal;
- tables are arranged in the text. The width of the table shall be 1 cm less than the line width. Above the table its ordinary number is indicated, right alignment. Continuous table numbering throughout the text. The title of the table is arranged below its number, center alignment;

• references should appear at the end of the article. References within the text should be enclosed in square brackets behind the text. References should be numbered in order of first appearance in the text. Examples of various reference types are given below.

Examples of LITERATURE CITED

Journal articles

Anatychuk L.I., Mykhailovsky V.Ya., Maksymuk M.V., Andrusiak I.S. Experimental research on thermoelectric automobile starting pre-heater operated with diesel fuel. *J.Thermoelectricity*. 2016. №4. P.84–94.

Books

Anatychuk L.I. *Thermoelements and thermoelectric devices. Handbook.* Kyiv, Naukova dumka, 1979. 768 p.

Patents

Patent of Ukraine № 85293. Anatychuk L.I., Luste O.J., Nitsovych O.V. Thermoelement.

Conference proceedings

Lysko V.V. *State of the art and expected progress in metrology of thermoelectric materials.* Proceedings of the XVII International Forum on Thermoelectricity (May 14-18, 2017, Belfast). Chernivtsi, 2017. 64 p.

Authors' abstracts

Kobylianskyi R.R. *Thermoelectric devices for treatment of skin diseases*: extended abstract of candidate's thesis. Chernivtsi, 2011. 20 p.

Examples of REFERENCES

Journal articles

Gorskiy P.V. (2015). Ob usloviakh vysokoi dobrotnosti i metodikakh poiska perspektivnykh sverhreshetochnykh termoelektricheskikh materialov [On the conditions of high figure of merit and methods of search for promising superlattice thermoelectric materials]. *Termoelektrichestvo - J.Thermoelectricity,* 3, 5 – 14 [in Russian].

Books

Anatychuk L.I. (2003). *Thermoelectricity. Vol.2. Thermoelectric power converters*. Kyiv, Chernivtsi: Institute of Thermoelectricity.

Patents

Patent of Ukraine № 85293. Anatychuk L. I., Luste O.Ya., Nitsovych O.V. Thermoelements [In Ukrainian].

Conference proceedings

Rifert V.G. Intensification of heat exchange at condensation and evaporation of liquid in 5 flowing-down films. In: *Proc. of the 9th International Conference Heat Transfer.* May 20-25, 1990, Israel.

Authors'abstracts

Mashukov A.O. *Efficiency hospital state of rehabilitation of patients with color carcer.* PhD (Med.) Odesa, 2011 [In Ukrainian].